AN EXPLORATION OF PLANAR LIPID BILAYER PROPERTIES CONTRIBUTING TO LIPID FLIP-FLOP USING SUM-FREQUENCY SPECTROSCOPY

by

John Samuel Allhusen

A dissertation submitted to the faculty of
The University of Utah
in partial fulfillment of the requirements for the degree of

Doctor of Philosophy

Department of Chemistry

The University of Utah

May 2018

The University of Utah Graduate School

STATEMENT OF DISSERTATION APPROVAL

The dissertation of **John Samuel Allhusen**

has been approved by the following supervisory committee members:

John C. Conboy	, Chair	**1/10/2018** Date Approved
Joel Mark Harris	, Member	**1/10/2018** Date Approved
Jennifer Shumaker-Parry	, Member	**1/10/2018** Date Approved
Bethany Buck Koehntop	, Member	**1/12/2018** Date Approved
Markus Babst	, Member	**1/10/2018** Date Approved

and by **Cynthia Burrows** , Chair/Dean of

the Department/College/School of **Chemistry**

and by David B. Kieda, Dean of The Graduate School.

ABSTRACT

The focus of this dissertation is on the investigation of the physical parameters impacting phospholipid membrane structure and dynamics. Sum-frequency spectroscopy (SFVS) was used to investigate the structural organization of planar supported lipid membranes. Specifically, the structural characteristics of cholesterol influencing the kinetic and thermodynamics of 1,2-distearoyl-*sn*-glycero-3-phosphocholine (DSPC) flip-flop was examined by incorporating cholestanol or cholestene into a DSPC membrane. Cholestanol lacks the double bond in the sterol ring and cholestene is without the hydroxyl group on carbon 3. These studies found that the structural modifications to cholesterol altered the thermodynamics of lipid flip-flop by changing the physical compressibility of the membranes. The impact of membrane physical parameters was further explored by developing a biologically compatible thin conductive oxide material.

Conductive metal oxide materials are attractive substrates for the analysis of membrane electrochemical properties as model lipid membranes are more easily created on oxides compared to metal surface electrodes. The widely used material of indium tin oxide has a limited functional pH range and is easily removed from a surface. A new, robust thin conductive oxide was created out of ruthenium dioxide (RuO_2) using simplistic colloidal solution-gelation (sol-gel) chemistry that has widely been established for synthesizing amorphous silica glass films. These electrodes demonstrated unique stability under harsh physical and chemical conditions making them suitable for long

term use in studying planar membrane models.

The structure of membranes formed by vesicle fusion on planar substrates was investigated using SFVS, fluorescence microscopy and electrochemical impedance spectroscopy (EIS). This methodology is widely used in model membranes to study the interactions plasma membrane components. Previously implemented techniques studying the mechanism of vesicle fusion are incapable of investigating possible population differences between leaflets that may arise during bilayer formation. SFVS is capable of distinguishing the interleaflet structure of vesicle fused membranes resulting in increased comprehension of vesicle fusion. These experiments were coupled with epifluorescence microscopy and EIS of membranes on RuO_2 electrodes to examine the integrity of vesicle fused membranes.

This dissertation demonstrates the capabilities of SFVS for use in the investigation of the chemical interactions between lipid components within planar supported model membranes.

TABLE OF CONTENTS

LIST OF FIGURES

LIST OF TABLES

ACKNOWLEDGEMENTS

I would like to acknowledge all the individuals within the chemistry department at the University of Utah who help make the high caliber of research possible. Without their efforts we would all be tinkering away in our garages.

I want to express my deepest gratitude towards my mentor and advisor Dr. John Conboy. His teaching efforts, support and guidance have been unwavering and are sincerely appreciated. His passion towards scientific integrity and the pursuit of the truest scientific answer pushed me to exceed my own expectations of my ability.

I would like to thank the members of my dissertation committee, Drs. Joel Harris, Jennifer Shumaker-Parry, Bethany Buck-Koehntop, and Markus Babst. I am grateful for the thought provoking discussions and encouragement you have provided over the past five years.

To all past members of the Conboy group, I would like to express my thanks. Your efforts provided the scientific foundation of the current research in our lab. I would especially like to think Krystal Brown, who introduced me to a life of lasers and Krystal Sly, who set an exemplary model for how to conduct great research while maintaining a grounded perspective that helped me push through some very difficult moments. To the current members of the Conboy group, Aaron and Renee, thank you for everything; from diligently editing my jumbled words, to sharing enlightening conversations and dancing to Adele, thank you for making the efforts enjoyable.

None of the work described in this dissertation would have been possible without the support and love of my family. Mom and Dad, you instilled a desire for knowledge in me from a young age and have never stopped encouraging me to fulfill my dreams. Thank you. I love both of you. To Marcia and Darrell, thank you for your love and support from the beginning of this journey. Finally, I would like to express my loving gratitude to my wife, Erikka. Your strength, compassion and love have never faltered and have been something that I could always rely upon. I love you, Forever and Always.

CHAPTER 1

INTRODUCTION

Ever since Robert Hooke first looked at a slice of cork under a microscope and coined the term "cell" in the 17th century,[1] human beings have been fascinated with the world beyond the perceptions of the unaided eye. However, it was not until the early 20th century that scientists began thoroughly examining the barrier containing all of the cellular components. The pioneering work of Gorter, Grendel and Fricke in the 1920s on red blood cells first described the bimolecular structure of the cell envelope which is composed of molecules called lipids.[2,3] The structure of these lipid molecules is unique as they possess a hydrophilic group attached to a hydrophobic carbon chain. In aqueous environments, these molecules self-assemble into organized structures where the hydrophilic groups face solution, thereby protecting the carbon chains on the interior of the structure. These structures can consist of single lipid layers (micelles) or bilayer structures (vesicles or liposomes) as is the case for the plasma membrane of eukaryotic organisms.

The complexity of the plasma membrane was most famously described by the fluid mosaic model in 1972 by Singer and Nicolson.[4,5] The intricate structure of the plasma membrane and its components necessitates simpler models be designed and tested in order to unravel the chemical interplay between individual membrane components.

Two of the most widely studied model membrane systems are planar supported lipid bilayers (PSLBs) and vesicles or liposomes. These models provide use as either a means to reconstitute membrane proteins into a bilayer or to examine the physical properties of the lipid components themselves. The latter application of these model membrane systems is the main focus of this dissertation.

In the plasma membrane of eukaryotic organisms, the majority of lipids are phospholipids, where the hydrophilic group is comprised of a phosphate molecule attached to two hydrophobic acyl chains of varying lengths and saturations. Other moieties can be attached to the phosphate group that render the lipid zwitterionic or charged. In nature, there exists an asymmetric distribution of the lipid molecules between the two layers (leaflets) of the plasma membrane[6] where negatively charged lipid molecules phosphoserine (PS) and phosphoethanolamine (PE) are on the interior side of the plasma membrane and the zwitterionic lipids phosphocholine (PC) and sphingomyelin (SM) are on the exterior leaflet of the plasma membrane.[7] The asymmetric lipid matrix also contains proteins, cholesterol, fatty acids and saccharide molecules, creating a complex, protective structure.

Phospholipid synthesis occurs in the endoplasmic reticulum on the interior of the cell, meaning that in order to create and maintain the asymmetry of the plasma membrane, lipid components must traverse between leaflets of the membrane. Initial reports of lipid translocation were presented by McConnell and Kornberg in the 1970s where they studied lipid translocation using the spin labeled lipid 1,2-dipalmitoyl-*sn*-glycero-3-phosphoethanolamine-*n,n*-Dimethyl-*n*-(2',2',6',6'-tetramethyl-4'-piperidyl) (TEMPO-DPPC) dispersed in a matrix of egg PC.[8] The initial rates of phospholipid flip-

flop for these studies were on the order of hours to days. Subsequent studies of lipid translocation conducted by Homan and Pownall using acyl chain pyrene labeled lipids found that their measured rates corresponded well with those previously reported by McConnell.[9] These two influential studies were among the first to report a slow measured rate of phospholipid translocation. These results led investigators to search for an alternative method for facilitating the necessary process of lipid translocation in the plasma membrane. What transpired was the description of a protein facilitated mechanism where proteins classified as flippases, floppases and scramblases were believed to moderate the translocation of lipids between leaflets.[6] Flippase proteins belong to a class of adenosine triphosphate (ATP) dependent ion channel proteins called P_4-ATPases[10,11] and are believed to mediate lipid translocation from the exterior of the cell to the interior. Floppases are a different class of ATP dependent proteins called ATP binding cassette (ABC) transport proteins that move molecules in and out of the cell. These proteins are believed to catalyze the transport of lipids from the interior to the exterior leaflets of the cell.[10,11] Scramblases are a unique type of calcium ion channel protein that facilitates bidirectional translocation of lipid molecules within the plasma membrane.[10,11] However, the measurements of the protein mediated pathways for lipid flip-flop were obtained using labeled lipid components. Devaux and others described the merits of labeled lipids and the information that can be garnered by implementing them to study lipid translocation, while at the same time acknowledging the drawbacks of perturbing the system from its native state due to the addition of exogenous molecules.[12] Based on the previously mentioned studies, it is critical to develop a method that allows for the label free measurement of phospholipid components in bilayer structures to

investigate translocation and membrane properties without the use of exogenous labels.

Recent advances in instrumentation have allowed for sophisticated techniques to emerge enabling the study of lipid membranes without the use of labeling molecules. Sum-frequency vibrational spectroscopy (SFVS) is a coherent, nonlinear optical technique that has been exquisitely implemented to study lipid components in a variety of bilayer compositions. SFVS is ideally suited for use in studying model bilayer systems because signal can only be generated from anisotropic interfaces due to the coherent properties of the technique. Previous work within our research group has characterized the structure and phase transition temperature (T_m) for lipid bilayers composed of saturated lipids with different chain length and bilayers containing cholesterol.[13-15] Kinetic rates and thermodynamic values for lipid translocation have also been previously determined with SFVS.[16-20] Protein incorporation and corresponding effects on flip-flop kinetics and thermodynamics has been previously described.[21,22] The impact of lateral packing and charged headgroups on lipid flip-flop has also been investigated.[16,17,23,24] Cholesterol has been incorporated into saturated gel-phase membranes and was found to increase the rate of phospholipid flip-flop of saturated lipids in the gel phase.[25] All of these prior investigations have provided a foundation to continue to explore the physical parameters and behavior of phospholipids in model membrane systems. The work of this dissertation aims to expand on the previous studies by investigating how the chemical structure of cholesterol affects lipid flip-flop, developing a material that allows for the electrochemical properties of model membranes to be examined, and finally describing the physical characteristics of model membranes formed by vesicle fusion using SFVS and the newly synthesized thin film electrode.

1.1 Cholesterol Structural Contributions to Phospholipid Flip-Flop

Cholesterol is a major constituent within the cell membranes of eukaryotic organisms and comprises up to 40 mol % of the total lipid content with the plasma membrane. As mentioned above, we have previously demonstrated that cholesterol incorporation into a gel-phase lipid membrane increases the rate of lipid flip-flop.[25] In Chapter 2, this work is expanded upon by exploring how the structural characteristics of cholesterol contribute to lipid flip-flop. The molecules cholestanol and cholestene were incorporated into lipid bilayers to examine the effect that the hydroxyl group and the sterol ring of cholesterol have on lipid flip-flop. SFVS was implemented to monitor the vibrational mode of the terminal CH_3 ν_s, at 2875 cm^{-1}, as a function of time and temperature allowing for the kinetic rate of lipid flip-flop to be extracted from the collected data. An expanded discussion of SFVS for the analysis of flip-flop kinetics is included in Chapter 2. The main findings from studies with cholesterol, cholestanol and cholestene were that the rate of lipid flip-flop and therefore the activation energy for lipid translocation was dependent on the physical elasticity of the membrane as described by the molar compression modulus (K*). This study represents the first description and correlation between the activation energy of lipid flip-flop and the elastic compression modulus of the membrane.

A brief investigation of the effect of deuterium labeled lipids in model membranes is provided, due to the inherent symmetry constraints of the system, the use of deuterium labeled lipids is required to create an asymmetric membrane for SFVS measurement. Measurements of deuterium labeled lipids required an additional modification to the existing spectrometer experimental setup and are also included.

Observing a correlation between the physical elastic properties of lipid bilayers and lipid flip-flop led to further investigations into the physical structure of planar membrane systems. One way to characterize the structure of lipid bilayers is by measuring the electrical properties of the supported membranes, which is expanded upon in the following chapters.

1.2 Synthesis of a Biologically Compatible Metal Oxide Material

The plasma membranes of eukaryotic organisms inherently have a potential gradient from the external leaflet to the internal leaflet due to the asymmetric distribution of charged lipids within the membrane. The electrical properties of plasma membranes have long interested scientists ever since Fricke measured the capacitance of red blood cells to be ~ 0.8 $\mu F/cm^2$.[2] This value is within the measured capacitance range for diverse membrane compositions collected in the subsequent decades following Fricke's first measurements.[26] The bulk of these measurements were conducted on free floating "black" lipid membranes or on membranes supported on a conductive metal film. Deposition of lipid membranes on metal films usually requires the use of a pre-functionalized surface to render the metal compatible with the lipid membrane. However, thin conductive oxide (TCO) films like indium tin oxide (ITO) have been used to measure bilayer electrochemical properties without surface modifications but are limited to certain pH ranges due to the stability of the electrode.[27] Chapter 3 describes the synthesis of a chemically and mechanically robust metal oxide film containing ruthenium dioxide (RuO_2) for lipid membrane analysis. The synthesis procedure for this new material was done using the relatively simple conditions of the colloidal solution and

gelation (sol-gel) technique. Creating materials in this manner allows for easy tuning of the characteristics in terms of conductivity, optical transparency and thickness of deposited films simply by tailoring the solution conditions.

Films were deposited by dip coating and were characterized by ultraviolet-visible (UV-Vis) and Fourier transform infrared (FTIR) spectroscopy, X-ray photoelectron spectroscopy (XPS), multiwavelength spectroscopic ellipsometry, atomic force microscopy (AFM), and electrochemical cyclic voltammetry. The unique optical and electrochemical properties of the synthesized films were demonstrated through the simultaneous implementation of UV-Vis spectroscopy and cyclic voltammetry of the aqueous redox active molecule ferrocene methanol. The chemical robustness of the synthesized films was demonstrated by repeated exposures to a highly acidic, highly oxidative environment followed by cyclic voltammetry. This procedure is similar to the standard cleaning procedure for preparing substrates for lipid bilayer deposition. This material is unique in its chemical structure and stability and is appealing for use in biological applications to study the electrochemical properties of supported lipid membranes.

1.3 Characterizing Planar Supported Bilayers Formed by Vesicle Fusion

There are traditionally two methods used to form planar supported lipid membranes; Langmuir Blodgett/Langmuir Schaefer (LB/LS) deposition and vesicle fusion. The former affords control over each leaflet composition and packing density of lipid molecules. Although vesicle fusion does not allow for such precise control, it is

faster and simpler to implement for creating supported lipid membranes. The method of vesicle fusion has been widely used since the 1980s. However, the mechanism of bilayer formation is still not well understood.[28] Chapter 4 describes studies that provide more substantial evidence towards deciphering the mechanism of bilayer formation from vesicles in solution. SFVS measurements resulted in a measureable signal due to a population difference between leaflets of the formed membranes, which is correlated to the geometrical size differences between two layers for spherical vesicles in solution. The origin of the measured response was experimentally determined to stem from the outer leaflet of the vesicle as it fused to the support. Using LB/LS deposition it was then possible to test if the population difference persisted after an asymmetric bilayer was made symmetric by heating indicating that the leaflet with the greater number of lipids remains after heating.

The previously synthesized conductive material was used to measure the capacitance values of membranes formed via sonicated and extruded vesicles of differing sizes. These experiments demonstrate the ability of the conductive RuO_2 material to be used in conjunction with lipid bilayers allowing for further studies of bilayer electrochemistry to be coupled with SFVS. Epifluorescence microscopy was used to determine the structural integrity of lipid bilayers prepared via vesicle fusion along with any remaining unfused vesicles.

These studies detail a more comprehensive view of bilayer formation via vesicle fusion utilizing sum-frequency spectroscopy, electrochemical impedance spectroscopy and fluorescence imaging.

1.4 Concluding Remarks

Chapter 5 contains a summary of the results obtained from the studies described within this dissertation. The information contained in this dissertation further contributes to the exploration of cell membranes and the ways in which they are formed and studied.

1.5 References

1. Tien, H. T.; Ottova, A. L. The Lipid Bilayer Concept and Its Experimental Realization: From Soap Bubbles, Kitchen Sink, to Bilayer Lipid Membranes. *J. Membr. Sci.* **2001**, *189*, 83-117.

2. Fricke, H.; Morse, S. The Electric Resistance and Capacity of Blood for Frequencies Between 800 and 4.5 Million Cycles. *J. Gen. Physiol.* **1925**, *9*, 153-167.

3. Gorter, E.; Grendel, F. On Bimolecular Layers of Lipoids on the Chromocytes of the Blood. *J. Exp. Med.* **1925**, *41*, 439-443.

4. Nicolson, G. L. The Fluid—Mosaic Model of Membrane Structure: Still Relevant to Understanding the Structure, Function and Dynamics of Biological Membranes After More Than 40 Years. *Biochimica et Biophysica Acta (BBA) - Biomembranes* **2014**, *1838*, 1451-1466.

5. Singer, S. J.; Nicolson, G. L. The Fluid Mosaic Model of the Structure of Cell Membranes. *Science* **1972**, *175*, 720-731.

6. van Meer, G.; Voelker, D. R.; Feigenson, G. W. Membrane Lipids: Where They Are and How They Behave. *Nat. Rev. Mol. Cell Biol.* **2008**, *9*, 112-124.

7. Fadeel, B.; Xue, D. The Ins and Outs of Phospholipid Asymmetry in the Plasma Membrane: Roles in Health and Disease. *Crit. Rev. Biochem. Mol. Biol.* **2009**, *44*, 264-277.

8. McConnell, H. M.; Kornberg, R. D. Inside-Outside Transitions of Phospholipids in Vesicle Membranes. *Biochemistry* **1971**, *10*, 1111-1120.

9. Homan, R.; Pownall, H. J. Transbilayer Diffusion of Phospholipids: Dependence on Headgroup Structure and Acyl Chain Length. *Biochim. Biophys. Acta, Biomembr.* **1988**, *938*, 155-166.

10. Sprong, H.; van der Sluijs, P.; van Meer, G. How Proteins Move Lipids and Lipids Move Proteins. *Nature Reviews Molecular Cell Biology* **2001**, *2*, 504-513.

11. Daleke, D. L. Phospholipid Flippases. *J. Biol. Chem.* **2007**, *282*, 821-825.

12. Devaux, P. F.; Fellmann, P.; Herve, P. Investigation on Lipid Asymmetry Using Lipid Probes. Comparison Between Spin-Labeled Lipids and Fluorescent Lipids. *Chem. Phys. Lipids* **2002**, *116*, 115-134.

13. Liu, J.; Conboy, J. C. Asymmetric Distribution of Lipids in a Phase Segregated Phospholipid Bilayer Observed by Sum-Frequency Vibrational Spectroscopy. *J. Phys. Chem. C* **2007**, *111*, 8988-8999.

14. Liu, J.; Conboy, J. C. Phase Behavior of Planar Supported Lipid Membranes Composed of Cholesterol and 1,2-distearoyl-sn-glycerol-3-phosphocholine Examined by Sum-Frequency Vibrational Spectroscopy. *Vib. Spectrosc.* **2009**, *50*, 106-115.

15. Liu, J.; Conboy, J. C. Phase Transition of a Single Lipid Bilayer Measured by Sum-Frequency Vibrational Spectroscopy. *J. Am. Chem. Soc.* **2004**, *126*, 8894-8895.

16. Anglin, T. C.; Conboy, J. C. Lateral Pressure Dependence of the Phospholipid Transmembrane Diffusion Rate in Planar-Supported Lipid Bilayers. *Biophys. J.* **2008**, *95*, 186-193.

17. Anglin, T. C.; Conboy, J. C. Kinetics and Thermodynamics of Flip-Flop in Binary Phospholipid Membranes Measured by Sum-Frequency Vibrational Spectroscopy. *Biochemistry* **2009**, *48*, 10220-10234.

18. Liu, J.; Conboy, J. C. Direct Measurement of the Transbilayer Movement of Phospholipids by Sum-Frequency Vibrational Spectroscopy. *J. Am. Chem. Soc.* **2004**, *126*, 8376-8377.

19. Liu, J.; Conboy, J. C. 1,2-Diacyl-phosphatidylcholine Flip-Flop Measured Directly by Sum-Frequency Vibrational Spectroscopy. *Biophys. J.* **2005**, *89*, 2522-2532.

20. Anglin, T. C.; Cooper, M. P.; Li, H.; Chandler, K.; Conboy, J. C. Free Energy and Entropy of Activation for Phospholipid Flip-Flop in Planar Supported Lipid Bilayers. *J. Phys. Chem. B* **2010**, *114*, 1903-1914.

21. Anglin, T. C.; Brown, K. L.; Conboy, J. C. Phospholipid Flip-Flop Modulated by Transmembrane Peptides WALP and Melittin. *J. Struct. Biol.* **2009**, *168*, 37-52.

22. Anglin, T. C.; Liu, J.; Conboy, J. C. Facile Lipid Flip-Flop in a Phospholipid Bilayer Induced by Gramicidin A Measured by Sum-Frequency Vibrational Spectroscopy. *Biophys. J.* **2007**, *92*, L01-L03.

23. Brown, K. L.; Conboy, J. C. Lipid Flip-Flop in Binary Membranes Composed of Phosphatidylserine and Phosphatidylcholine. *J. Phys. Chem. B* **2013**, *117*, 15041-15050.

24. Brown, K. L.; Conboy, J. C. Phosphatidylglycerol Flip-Flop Suppression due to Headgroup Charge Repulsion. *J. Phys. Chem. B* **2015**, *119,* 10252-10260.

25. Liu, J.; Brown, K. L.; Conboy, J. C. The Effect of Cholesterol on the Intrinsic Rate of Lipid Flip-Flop as Measured by Sum-Frequency Vibrational Spectroscopy. *Faraday Discuss.* **2013**, *161*, 45-61.

26. Lin, J.; Merzlyakov, M.; Hristova, K.; Searson, P. C. Impedance Spectroscopy of Bilayer Membranes on Single Crystal Silicon. *Biointerphases* **2008**, *3*, FA33-FA40.

27. Granqvist, C. G. Transparent Conductors as Solar Energy Materials: A Panoramic Review. *Sol. Energy Mater. Sol. Cells* **2007**, *91*, 1529-1598.

28. Jackman, J. A.; Kim, M. C.; Zhdanov, V. P.; Cho, N.-J. Relationship Between Vesicle Size and Steric Hindrance Influences Vesicle Rupture on Solid Supports. *Phys. Chem. Chem. Phys.* **2016**, *18*, 3065-3072.

CHAPTER 2

THE STRUCTURAL ORIGINS OF CHOLESTEROL ACCELERATED LIPID FLIP-FLOP STUDIED BY SUM-FREQUENCY VIBRATIONAL SPECTROSCOPY

2.1 Introduction

Cholesterol is an integral component of the plasma membrane in eukaryotic organisms, accounting for 25 – 40 mol % of the total lipid content. Cholesterol stabilizes the membrane and is a vital component for proper cell growth.[1-8] Deficiencies in cholesterol can lead to a variety of diseases including Smith-Lemli-Opitz Syndrome, Alzheimer's and desmosterolosis.[1, 3, 9-12] Due to its critical importance within cells, cholesterol and its subsequent influence on the plasma membrane has been studied by a variety of techniques, such as fluorescence,[1, 8-9, 13-16] differential scanning calorimetry (DSC),[17-18] nuclear magnetic resonance spectroscopy (NMR),[19-23] micropipette aspiration,[24-27] X-ray scattering,[28] Brewster angle microscopy[29] and sum-frequency vibrational spectroscopy (SFVS).[30-37] These techniques have been used to investigate the impact of cholesterol on various physical properties of the plasma membrane including

the lateral diffusion of lipid components, formation of segregated membrane domains, alteration of the native lipid phase transition, membrane elasticity or stiffness and orientation and association of cholesterol within the membrane. However, there is relatively little knowledge on the role cholesterol has on native phospholipid flip-flop (or translocation).

Phospholipid translocation is a process involving the migration of lipid components between the opposing leaflets of a lipid bilayer. The dynamics of phospholipid translocation have puzzled scientists for decades. Several methods have been developed to track the movement of spin- and fluorescently-labeled lipids in vesicles and planar supported lipid bilayers.[38-39] Kinetic rates for labeled lipid flip-flop were measured to be on the order of hours or days using these techniques. Techniques that do not require lipid probes, such as SFVS, atomic force microscopy (AFM), and small-angle neutron scattering (SANS) have also been used to measure lipid translocation.[40-43] These label free techniques have reported values for lipid flip-flop on the order of minutes to hours. Measuring the rate of native (or unlabeled) lipid flip-flop is essential in developing an understanding of the complex molecular interactions between components of the plasma membrane like phospholipids and sterols.

A handful of investigations have examined the influence of cholesterol on phospholipid flip-flop using lipid probes and found that the addition of cholesterol into the membrane decreased the kinetic rate of lipid translocation when cholesterol concentrations exceeded 30 mol %.[44-46] Nakano and coworkers have measured the rate of fluid phase phospholipid flip-flop in the presence of concentrations of cholesterol exceeding 20 mol % using SANS on 100 nm vesicles.[43] They have reported that

cholesterol impedes the rate of lipid translocation in these systems. Recently, Liu *et al.* investigated the influence of cholesterol on unmodified or native DSPC flip-flop in the gel-phase using SFVS.[34] Their findings showed that incorporation of cholesterol into a phospholipid membrane below 15 mol % increased the kinetic rate of flip-flop of gel-phase DSPC due to a decrease in the thermodynamic free energy barrier of lipid translocation.[34] However, the structural characteristics of cholesterol contributing to the observed rate increase have not been investigated.

The current study aims to investigate how the unique structure of cholesterol modulates lipid flip-flop in gel-phase lipid membranes. Two important characteristics of cholesterol are the rigidity created by the double bond on ring B, and its amphiphilic character due to the presence of the hydroxyl group on carbon 3.[9, 47] The role these key structural aspects of cholesterol play in altering DSPC flip-flop was examined by investigating DSPC flip-flop in the presence of 5α-cholestan-3β-ol (cholestanol) which lacks the double bond on ring B, shown in red in Figure 2.1 and 5-cholestene (cholestene) which lacks the C3 hydroxyl group, shown in blue in Figure 2.1. The presence of cholestanol within the human body is relatively low but becomes more pronounced within the plasma membrane in people afflicted with cerebrotendineous xanthomatosis (CTX)[48-49] and is believed to stiffen the membrane, which prevents calcium channels from operating properly. Cholestene, although not found in living cells, is hypothesized to have a faster rate of translocation across the membrane[50] and has been used to examine the binding pathways of the cholesterol degradation enzyme Cytochrome P450 27A1[51] and oxytocin receptor protein.[52] Measuring the rates of DSPC flip-flop in the presence of cholesterol, cholestanol, and cholestene allows for the determination of the influence of

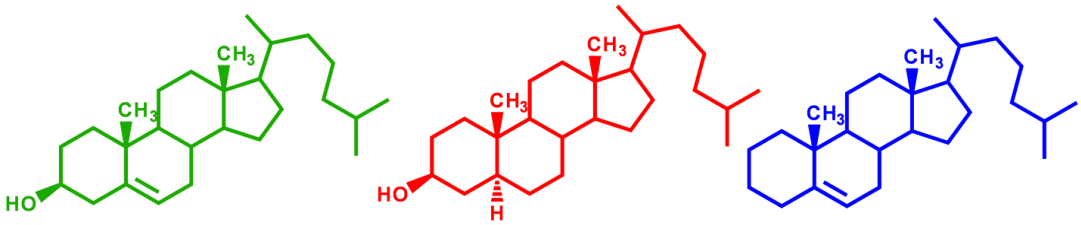

Figure 2.1: Chemical structures for cholesterol (green), cholestanol (red) and cholestene (blue).

sterol ring rigidity and amphiphilicity on lipid translocation.

2.2 Sum-Frequency Vibrational Spectroscopy Theory

SFVS is an appealing technique to investigate the influence of cholesterol structure on lipid flip-flop because of its capability to discern discrete changes in native lipid translocation in a bilayer. We have previously used SFVS to characterize flip-flop processes for pure DSPC lipid membranes,[53-56] the negatively charged lipids phosphoserine and phosphoglycerol,[57-58] bilayers containing transmembrane peptides,[59-60] the effect of lipid packing density[61] and incorporation of cholesterol into gel-phase lipid membranes.[34] The inimitable properties of SFVS have allowed for the measurement of saturated lipid flip-flop with and without a spin label.[56] These measurements demonstrated that attachment of a bulky moiety to saturated phospholipids decreases the rate of lipid flip-flop by an order of magnitude.[56] Since the majority of lipid components within the plasma membrane are unsaturated and in a fluid state, the rate of native flip-flop of unsaturated lipids proceeds on a timescale faster than can be experimentally measured by the SFVS spectrometer described below. Choosing the saturated lipid DSPC allows for native lipid flip-flop to be examined in a reasonable experimental time frame allowing for the influence of various lipid components and membrane environments to be examined.

The theory of SFVS has been described in detail elsewhere.[62-64] However, an explanation of the salient aspects of SFVS is provided. SFVS is a second-order, nonlinear optical technique that uses a coherent, fixed frequency, visible (532 nm) and a coherent, tunable mid-infrared (IR) light source. The two laser beams are overlapped in

space and time at an interface, producing a signal at the sum of the two input frequencies given by the equation:

$$\omega_{SF} = \omega_{vis} + \omega_{IR} \tag{2.1}$$

where the output SFVS signal intensity is defined as:

$$I_{sum} = \left|\tilde{f}_{SF} f_{vis} f_{ir} \chi^{(2)}\right|^2 \tag{2.2}$$

where $\tilde{f}_{SF}$, f_{vis}, and f_{ir} are the Fresnel coefficients describing the electric field intensities of the sum-frequency, visible and IR beams, respectively. $\chi^{(2)}$ is the second order nonlinear susceptibility tensor and contains both a resonant ($\chi_R^{(2)}$) and nonresonant ($\chi_{NR}^{(2)}$) contributions and is described by:

$$\chi^{(2)} = N \sum_{x=1}^{m} \frac{\langle A_k M_{ij} \rangle_x}{\omega_{\upsilon_x} - \omega_{IR} - i\Gamma_{\upsilon_x}} + \chi_{NR}^{(2)} \tag{2.3}$$

where N is the number of molecules probed at the interface, A_k and M_{ij} describe the IR and Raman transition probabilities, ω_υ is the molecular vibration being probed, ω_{IR} is the incident infrared frequency, Γ_υ is the line width of the vibrational transitions at the interface and the *bra-ket* notation denotes that the intensity is sensitive to ensemble orientation of molecules at an interface. In order to observe a vibrational transition using SFVS, it must be IR and Raman active. The coherent SFVS process only occurs when a net orientation of the transition dipole moments for a particular vibrational resonance exists; otherwise oppositely oriented vibrational modes will destructively interfere with each other resulting in no measureable response.

Lipid membranes are an appealing system to study using SFVS as the inherent bilayer structure results in the vibrational resonances of the acyl chains oriented antiparallel with respect to one another. Using the Langmuir Blodgett/Langmuir

Schaefer (LB/LS) method, membranes can be made asymmetric with one leaflet composed of proteated lipids and the other composed of isotopically substituted deuterated lipids. In this configuration, the ensemble vibrations of either the CH or CD modes originating from the acyl chains can be monitored. The SFVS response of the terminal methyl symmetric vibrational mode, CH_3 ν_s, at a frequency of 2875 cm^{-1}, can be described using the effective nonlinear susceptibility tensor $\chi_{eff}^{(2)}$ in terms of the molecular hyperpolarizability (β) defined as:

$$\chi_{eff}^{(2)} = \frac{N_{distal}}{\epsilon_0}\langle\beta_{ijk}^{CH_3\nu_s}\rangle - \frac{N_{proximal}}{\epsilon_0}\langle\beta_{ijk}^{CH_3\nu_s}\rangle + \chi_{NR}^{(2)} \tag{2.4}$$

where (N_{distal}) and ($N_{proximal}$) describe the fraction of proteated lipids in the distal and proximal leaflets, and ε_0 is the permittivity constant. The measured intensity of the SFVS response is proportional to the square of the population difference defined as:

$$I_{CH_3vs} \propto (N_{distal} - N_{proximal})^2 \tag{2.5}$$

For an initially asymmetric bilayer in which one leaflet is proteated and the other deuterated, the intensity of the CH_3 vibrational symmetric stretch (ν_s) can be monitored over time to measure the unimolecular exchange of proteated lipids between leaflets described by:[55-56]

$$N_{distal} \underset{k_-}{\overset{k_+}{\rightleftharpoons}} N_{proximal} \tag{2.6}$$

where k_+ and k_- represent the forward and backwards rates constants for flip-flop, respectively. Initially, the population of proteated lipids for an asymmetric bilayer is $N_{distal} = 1$ and $N_{proximal} = 0$ and the change in N_{distal} as a function of time is:

$$\frac{dN_{distal}}{dt} = k_+N_{distal} - k_-N_{proximal} \tag{2.7}$$

It has been previously experimentally shown that the rates for the forward and backwards

rate constants are equal within error,[56, 65] resulting in the time dependent change of N_{distal} defined by:

$$\frac{dN_{distal}}{dt} = -k(2N_{distal} - 1) \tag{2.8}$$

leading to an integrated form of the rate equation of:

$$2N_{distal} - 1 = e^{-2kt} \tag{2.9}$$

where $2N_{distal} - 1$ is equal to the population difference of proteated components between two leaflets. The effective nonlinear susceptibility tensor is related to the population difference between leaflets as detailed in Equation 2.4 and the time dependent version of $\chi^{(2)}_{eff}$ can be described by:

$$\chi^{(2)}_{eff} = |\chi_R|e^{i\varphi_1}e^{-2kt} + |\chi_{NR}|e^{i\varphi_2} \tag{2.10}$$

where $|\chi_R|$ and $|\chi_{NR}|$ are the complex resonant and nonresonant susceptibility tensors, respectively. The symbol (φ) indicates the phase angle of these tensors. The phase difference (Δφ) can be taken to be 0, describing when the resonant tensor is in phase with the nonresonant background or π for when the resonant tensor element is out of phase with the nonresonant contribution. Equation 2.10 can be substituted into Equation 2.2 yielding the resulting equation:

$$I_{CH_3\,\upsilon_s}(t) = I_{R,max}e^{-4kt} + 2\sqrt{I_r}\sqrt{I_{NR}}e^{-2kt}\cos(\Delta\varphi) + I_{NR} + I_{R,min} \tag{2.11}$$

where $I_{R,max}$ and $I_{R,min}$ are the maximum and minimum intensities of the CH_3 ν_s vibrational mode, respectively. The nonresonant background intensity is I_{NR}. For a lipid bilayer on SiO_2, the nonresonant background measured at a frequency absent of CH vibrational modes in D_2O is minimal and can be neglected from the above equation. Equation 2.11 then simplifies to:

$$I_{CH_3 vs}(t) = I_{max} \exp(-4kt) + I_{min} \quad (2.12)$$

where I_{max} is the maximum signal intensity obtained when $|N_B - N_T| = 1$ for a completely asymmetric bilayer and I_{min} is the signal when $N_B - N_T = 0$, or a completely symmetric bilayer. I_{min} accounts for scattering of the visible beam into the detector and electronic offsets associated with the measurement. The rate obtained from Equation 2.12 can then be used to determine the half-life for lipid flip-flop by:

$$t_{1/2} = \ln(2)/2k \quad (2.13)$$

This approach has been widely used to study lipid flip-flop for a variety of lipid membranes as mentioned above, and has also been used to investigate the mode of action of various drugs and antimicrobial peptides on lipid membranes.[66-69]

This chapter addresses the unique structural and chemical aspects of cholesterol which lead to enhanced phospholipid flip-flop in membranes composed of gel-phase saturated lipids. Both the contributions from sterol ring rigidity and amphiphilicity were analyzed by measuring the rate of DSPC flip-flop when cholesterol, cholestanol and cholestene were present within a membrane. From these data, the transition state energetics were calculated, lending a greater understanding to the interplay between the structure of cholesterol and its ability to modulate phospholipid flip-flop within a membrane.

2.3 Experimental Section

2.3.1 Materials and Methods

Cholesterol (5-cholesten-3β-ol), cholestene (5-cholestene), and cholestanol (5α-cholestan-3β-ol) were purchased from Steraloids Inc. (Newport, RI). Deuterium oxide

(D_2O) and anhydrous chloroform (≥99% $CHCl_3$ with 0.5-1% ethanol as a stabilizer) were purchased from Sigma-Aldrich (St. Louis, Missouri). 1,2-Distearoyl-sn-glycerol-3-phosphocholine (DSPC) and 1,2-distearoyl-d70-sn-glycerol-3-phosphocholine (DSPCd70) were purchased from Avanti Polar Lipids (Alabaster, Al). Sodium chloride (NaCl) and anhydrous dibasic sodium phosphate (Na_2HPO_4) were purchased from Fisher Scientific (Pittsburgh, PA). Monobasic sodium phosphate monohydrate ($NaH_2PO_4•H_2O$) was obtained from Macron Chemicals (Center Valley, PA). All water used throughout this study was purified by a Nanopure Infinity Ultrapure water system (Barnstead Thermolyne, Dubuque, IA) with a minimum resistivity of 18.2 MΩ cm. Phosphate buffered saline (PBS) was prepared from 100 mM NaCl, 10 mM $NaH_2PO_4•H_2O$, and 40 mM NaH_2PO_4 in nanopure water and adjusted to a pH of 7.4 ± 0.1 using 4 M sodium hydroxide (NaOH) and 1 M hydrochloric acid (HCl). The substrates used as lipid bilayer supports were custom fabricated UV grade fused silica prisms and calcium fluoride prisms (CaF_2) coated with silica purchased from Almaz Optics (Marlton, NJ). Prior to bilayer deposition, prisms were thoroughly rinsed with HPLC grade methanol and water before cleaning in an ultraviolet ozone cleaner (Jelight Co., Irvine, CA) for 30 minutes. Following this cleaning, prisms were submerged in a 70% concentrated sulfuric acid (H_2SO_4) and 30% hydrogen peroxide (H_2O_2) v:v solution for a minimum of 30 minutes. *Caution! This solution is highly oxidizing and will react violently with organic materials; care should be taken when handling this solution.* The prisms were then rinsed with water, nitrogen (N_2) dried and argon plasma cleaned (Harrick Scientific, Ithaca, NY) for 2 to 4 minutes prior to bilayer deposition.

2.3.2 Lipid Bilayer Preparation

Initially, stock solutions of DSPC, DSPCd70, cholesterol, cholestene, and cholestanol were individually prepared at a concentration of 1 mg/mL. For the final mixtures, the molar fractions of each component were calculated using the initial stock concentrations. The molar quantities needed to make solutions of 1:50, 1:20, 1:14.28, and 1:10 sterol:lipid (either DSPC or DSPCd70) were combined using the necessary calculated volumes of the initial stock solutions. PBS was used as the subphase for all lipid bilayers prepared using the Langmuir-Blodgett and Langmuir-Schaefer (LB/LS) film deposition method at a temperature ranging from 23 – 25 °C. The proximal leaflet containing the deuterated lipid mixture was spread at the air/buffer interface of a KSV Nima Mini Trough (Helsinki, Finland) and allowed to reach equilibrium for 15 minutes. The monolayer was then compressed to a surface pressure of 30 mN/m[70] at a velocity of 4 mm/min before the substrate was vertically withdrawn at a speed of 3 mm/min via LB deposition. The distal leaflet containing the proteated lipid component was prepared by depositing the appropriate lipid mixture at the air/buffer interface with a 15-minute equilibration time at which point it was compressed to a surface pressure of 30 mN/m. The distal leaflet was deposited using the LS procedure, which involves passing the substrate, with the proximal leaflet, through the air/water interface in a horizontal orientation into the subphase. The substrate with the fully assembled bilayer was then mounted into a custom Teflon flow cell that allows for fluid exchange and temperature measurements using a type K thermocouple. Care was taken to ensure the bilayer was maintained in an aqueous environment at all times after preparation. Prior to the SFVS experiments, the PBS solution was exchanged for one prepared in D_2O in order to avoid

IR spectral overlap from the –OH vibrational modes of water.

2.3.3 Pressure-Area Isotherms

Pressure-area isotherms were collected for each DSPC monolayer containing cholesterol, cholestene and cholestanol at percentages of 0, 2, 5, 7 and 10 mol % temperatures between 22 – 25 °C. The sterol containing lipid solutions were spread at the air/buffer interface and allowed to equilibrate for a minimum of 15 minutes before compression. Monolayers were compressed at a barrier speed of 4 mm/min until a collapse pressure was reached, indicated by a sudden leveling off of the surface pressure. Isotherm experiments were repeated three times and the average is reported. Calculations of the mean molecular area and compression modulus were done at a surface pressure of 30 mN/m. Reported errors in the measured values for the compression modulus were calculated from the multiple replicates and are indicative of the experimental error within the current instrumental setup.

2.3.4 SFVS Measurements

The SFVS setup used in this study has been previously described elsewhere.[55, 65, 71] To collect data in the frequency region from 1950 cm^{-1} to 2150 cm^{-1} the pre-existing spectrometer set up had to be modified and is described in Figure 2.2. A 1064 nm, 10 Hz, 7 ns pulsed laser (Continuum, Santa Clara, CA) was used to pump an optical parametric oscillator (OPO) and optical parametric amplifier (OPA) system (LaserVision, Bellevue, WA) to produce a fixed visible beam at 532 nm and a tunable mid-IR beam. The visible and infrared beams had powers ranging from 5 to 7 mJ/pulse and 2 to 4

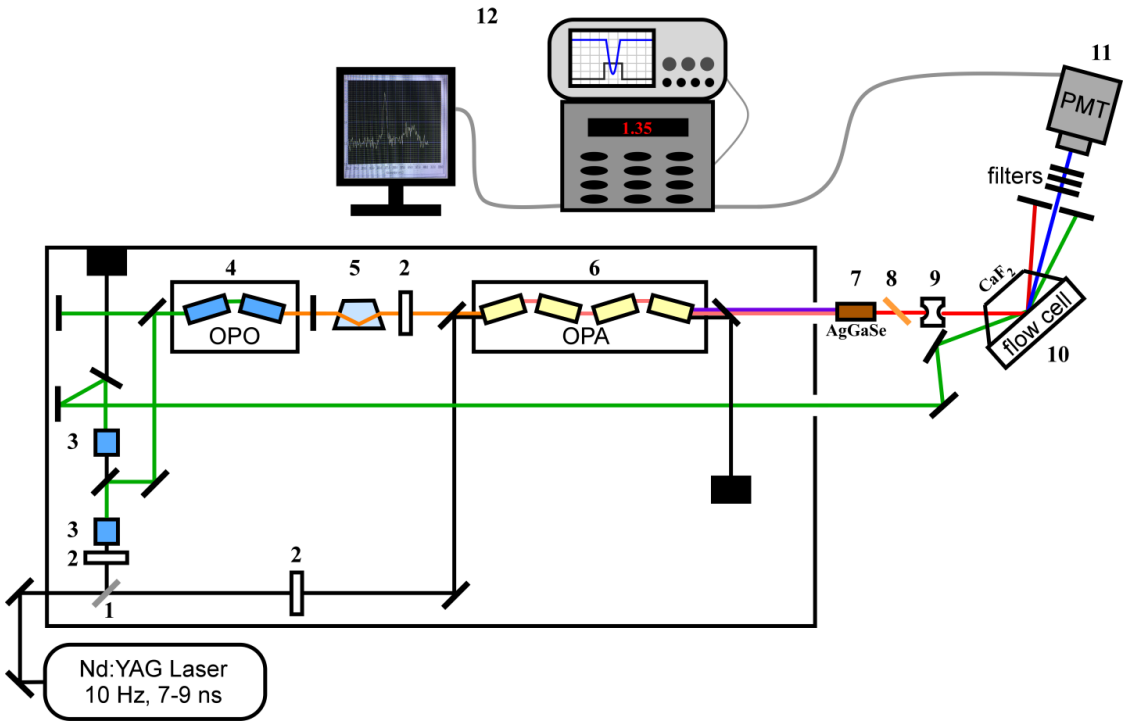

Figure 2.2: Experimental setup for the SFVS spectrometer. An incidental beam at 1064 nm is generated from a Nd:YAG laser at a frequency of 10 Hz with a pulse length between 7-9 ns to seed the SFVS spectrometer. The components of the spectrometer are described below:

1. 50/50 beam splitter
2. λ/2 waveplates
3. Potassium titanyl phosphate (KTP) frequency doubling crystals
4. Optical parametric oscillator (OPO) made of KTP crystals
5. Dove prism
6. Optical parametric amplifier (OPA) made of potassium titanyl arsenate (KTA)
7. Silver gallium selenide (AgGaSe) frequency doubling crystal
8. Zinc selenide (ZnSe) filter
9. Infrared periscope
10. Flow cell containing CaF_2 prism and lipid bilayer
11. Spatial and optical filters and photomultiplier detector
12. Boxcar integrator, oscilloscope and computer for signal collection with LabView

mJ/pulse, respectively. Each beam was collimated to a diameter of ~ 3 to 5 mm. The incident angle for the IR and visible beams was 62° and 67°, respectively. The polarizations of the output sum-frequency beam, input 532 nm beam, and input mid-IR beam were *s, s,* and *p,* respectively. The resulting sum-frequency signal was collected by a photomultiplier tube (Hamamatsu Photonics, Hamamatsu, Japan) and integrated by a Stanford Research Systems boxcar integrator (Sunnyvale, CA).

Initial SFVS spectra of the planar supported lipid bilayers were collected at room temperature (~ 22 – 25 °C) by scanning the tunable IR in 2 cm^{-1} steps from 2750 – 3050 cm^{-1} with a 3-second integration at each step. The flow cell was then attached to a circulating water bath (HAAKE Phoenix II P1 Circulator, Thermo Fisher Scientific) and set to the desired temperature. DSPC flip-flop decay curves were collected only after the bilayer had reached thermal equilibrium indicated by a temperature fluctuation of less than 0.5 °C, typically taking ~ 15 minutes. Signal of the CH_3 ν_s was monitored as a function of time at a fixed temperature using an integration time of 3 seconds. The temperature range chosen for the DSPC flip-flop kinetic studies was dictated by the ability to accurately measure a fast decay at high temperatures (~ 40 minutes) and the stability of the laboratory temperature at long times (~ 16 hours), low temperature limit. A Marquardt-Levenberg algorithm is used to find the parameters of the independent variables in Equation 2.2 that provide the best fit to the data[72] with the aid of SigmaPlot software. The error in the reported k values is within 6% of the described kinetic rates.

2.4 Results and Discussion

2.4.1 SFVS Spectra

Representative spectra for asymmetric bilayers composed of DSPC and DSPCd70 with 0, 2, 5, 7, and 10 mol % of cholesterol, cholestanol or cholestene are shown in Figure 2.3A. Spectral assignments are as follows: the peak at 2848 cm^{-1} is assigned to the CH_2 v_s, the peak at 2875 cm^{-1} is the CH_3 v_s, the shoulder present at ~2900 cm^{-1} is assigned to the CH_2 v_s Fermi resonance (FR), the broad peak at 2949 cm^{-1} is a combination of the CH_3 v_s FR and the CH_3 asymmetric stretch (v_{as}).[34, 54, 71] Figure 2.3B depicts spectra collected after the bilayers have become symmetric due to lipid flip-flop. The absence of any measurable signal indicates a complete randomization, or a symmetric bilayer in which equal numbers of proteated and deuterated lipids reside in each leaflet. It is important to note in Figure 2.3A and 2.3B that there is no measureable amount of signal generated from the presence of the sterols. Resonances from the incorporated sterols are not detected in these studies due to the symmetric distribution of cholesterol, cholestanol or cholestene within the membrane.[34] Cholesterol has also been previously shown to undergo rapid translocation between leaflets, having a kinetic timescale ranging from microseconds to seconds.[45, 50, 73-74] A small amount of signal is detected from the CH_2 v_s at 2848 cm^{-1} of the lipid acyl chains and is attributed to gauche defects. The magnitude of this resonance can be used as a relative determinant of membrane acyl chain ordering, as discussed below.[22, 71, 75-80]

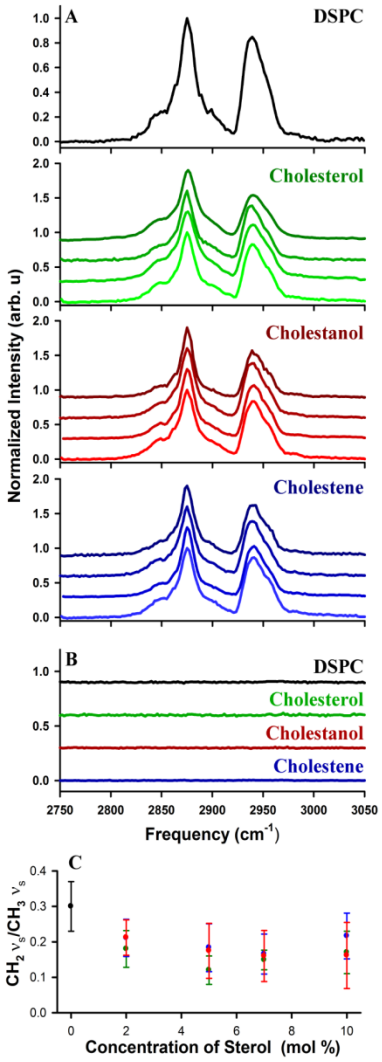

Figure 2.3: SFVS spectra and CH_2/CH_3 ν_s for bilayers containing cholesterol and analogs. A) SFVS spectra for asymmetric bilayers of DSPC:DSPCd70, and bilayers containing cholesterol (green), cholestanol (blue), and cholestene (red). Concentrations of the sterols at 2, 5, 7 and 10 mol % are shown (bottom to top) and have been offset by 0.3 a.u for clarity. B) Representative spectra for bilayers after undergoing complete randomization due to DSPC flip-flop for bilayers containing 7 mol % of cholesterol, cholestene and cholestanol. The spectra have been offset by 0.3 a.u. in all cases for clarity. C) The CH_2 ν_s/ CH_3 ν_s as a function of cholesterol, cholestene and cholestanol concentration with the errors calculated from a minimum of three separate spectra.

2.4.2 Membrane Acyl Chain Structure

From the spectra in Figure 2.3A, the influence of the studied sterols on the relative gauche content in the acyl chains of DSPC can be analyzed by determining the ratio of the integrated peak areas for the CH_2 ν_s to the CH_3 ν_s modes.[22, 71, 75-79, 81] The addition of a sterol molecule like cholesterol is known to create a more ordered membrane structure in fluid phase lipids while decreasing the order of a membrane in gel-phase lipids.[2-3, 8, 17, 20, 30, 37, 82-84] An indicator of increasing membrane order is a decrease in the amount of gauche defects in the lipid acyl chains, which results in a decrease in the CH_2 ν_s intensity. For example, in gel-phase bilayers the CH_2 ν_s/ CH_3 ν_s is expected to be very small due to the all trans-conformation of the acyl chains. The SFVS spectra were fit using a Voigt function for the CH_2 ν_s to the CH_3 ν_s resonances, with the only fixed parameter being the vibrational frequency for each of the resonances which were set to the previously determined vibrational frequencies of the lipid acyl chains.[34, 54, 71] From the spectra in Figure 2.3A, the measured value for the CH_2 ν_s/ CH_3 ν_s was 0.30 ± 0.07 for a pure DSPC bilayer and is consistent with a small number of gauche defects present in a gel-phase membrane below the main phase transition as shown previously by SFVS, IR, Raman and NMR.[22, 71, 78, 85] The average CH_2 ν_s/ CH_3 ν_s ratio is reported for 3-5 independent bilayers and the associated standard deviation. When 2 mol % cholesterol was added into the bilayer, a decrease in the CH_2 ν_s/ CH_3 ν_s to 0.18 ± 0.05 was observed. Continued addition of cholesterol did not cause any further decrease in the CH_2/CH_3 ratio. The same trend was observed for cholestanol and cholestene, as seen in Figure 2.2C which shows the CH_2 ν_s/ CH_3 ν_s as a function of sterol percentage for all studied membrane compositions. The measured CH_2 ν_s/ CH_3 ν_s is independent of concentration

of sterol molecule between 2 and 10 mol %. This observation is consistent with a study by Vist and Davis who examined the phase transition structure of 1,2-dipalmitoyl-sn-glycero-3-phosphocholine (DPPC) with various cholesterol concentrations.[23] The authors found that changes in acyl chain order of DPPC were invariant until 6.5 mol % cholesterol was incorporated.[23] The impact of cholesterol, cholestene and cholestanol on the rate of DSPC flip-flop can be deciphered by measuring the loss of the CH_3 ν_s intensity over time as a function of temperature for asymmetrically prepared bilayers.

2.4.3 Kinetics of DSPC Flip-Flop

Representative DSPC flip-flop decays recorded between 38 and 39 °C for bilayers containing cholesterol, cholestanol or cholestene at concentrations ranging from 2 to 10 mol % are shown in Figure 2.4. The error in the reported kinetic rates arises from the error in the fit of equation 12 to the data for each individual experiment. This error was also propagated in the calculation of the half-lives for lipid flip-flop, listed in Table 2.1. The error in the reported temperatures arises from fluctuations throughout the course of the experiment. The time-dependent sum-frequency response of the CH_3 ν_s decays exponentially. As a reference point, a theoretical decay for a pure DSPC bilayer is shown in each plot and was calculated from the kinetic data in reference 54. It is apparent in Figure 2.3 that increasing concentrations of sterol molecules within the bilayer increases the kinetic rate of DSPC flip-flop. A complete summary of the measured kinetic rates and half-lives for lipid flip-flop as a function of sterol molecule, concentration and temperature is presented in Table 2.1.

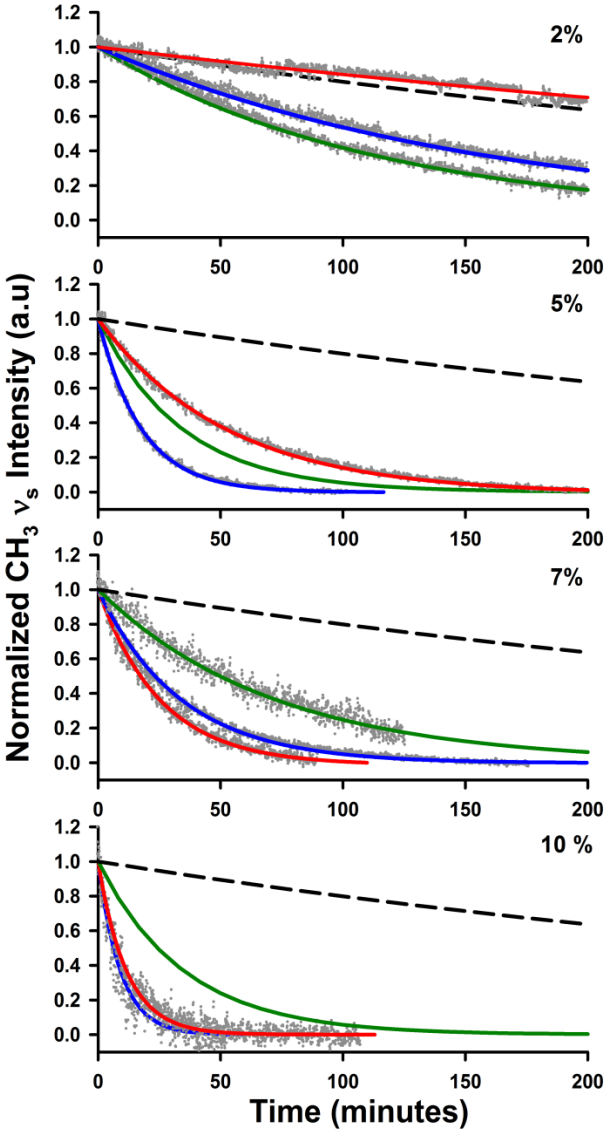

Figure 2.4: Representative DSPC flip-flop decay curves recorded between 38 and 39 °C for bilayers containing cholesterol (green), cholestanol (red), and cholestene (blue) at 2, 5, 7, and 10 mol %. Data were normalized at t = 0, which is when the bilayer reached thermal equilibrium. The solid lines represent the fit to the data using Equation 2.12. Theoretical decays are shown for pure DSPC (dashed line) obtained from the data given in reference 54 along with bilayers containing 5 and 10 mol % cholesterol obtained from data in reference 34.

Table 2.1: Kinetic rates of DSPC flip-flop as a function of cholesterol, cholestanol and cholestene concentration and temperature.

	Cholesterol			Cholestanol			Cholestene		
Sterol	*Temp. (°C)*	*k (s^{-1}) x 10^5*	*$t_{(1/2)}$ (min)*	*Temp. (°C)*	*k (s^{-1}) x 10^5*	*$t_{(1/2)}$ (min)*	*Temp. (°C)*	*k (s^{-1}) x 10^5*	*$t_{(1/2)}$ (min)*
2 %	45.9 ± 0.1	7.6 ± 0.1	75.7±0.4	46.5 ± 0.3	5.32 ± 0.01	108.5±0.1	43.6 ± 0.1	10.92 ± 0.04	52.9±0.1
	43.7 ± 0.1	7.4 ± 0.1	78.3±0.6	43.8 ± 0.1	3.11 ± 0.04	185.6±1.1	39.6 ± 0.2	2.60 ± 0.04	222±2
	40.5 ± 0.2	2.7 ± 0.1	211±1	43.1 ± 0.4	2.52 ± 0.01	229±1	37.1 ± 0.4	1.31 ± 0.02	446±3
	39.5 ± 0.2	3.3 ± 0.1	178±2	41.1 ± 0.4	1.40 ± 0.02	413±3	32.1 ± 0.1	1.00 ± 0.02	580±5
	38.6 ± 0.1	3.6 ± 0.1	159±1	38.6 ± 0.3	0.72 ± 0.01	804±4	32.0 ± 0.1	0.80 ± 0.01	717±5
	35.2 ± 0.1	0.89 ± 0.01	643±2	31.8 ± 0.2	0.18 ± 0.01	3240±70			
5 %	41.8 ± 0.3	32.3 ± 0.1	17.9 ± 0.1	41.4 ± 0.1	13.1 ± 0.1	44.1±0.1	41.6 ± 0.2	42.5 ± 0.5	13.6±0.1
	40.0 ± 0.1	13.4 ± 0.1	43.0 ± 0.2	39.9 ± 0.2	11.1 ± 0.1	52.0±0.2	39.1 ± 0.2	33.0 ± 0.8	17.5±0.2
	38.2 ± 0.2	12.3 ± 0.1	47.2 ± 0.3	38.0 ± 0.1	7.92 ± 0.04	73.0±0.2	38.3 ± 0.2	23.7 ± 0.1	24.4±0.1
	36.3 ± 0.1	8.63 ± 0.03	66.9 ± 0.3	34.3 ± 0.1	3.26 ± 0.04	177±1	37.1 ± 0.1	20.0 ± 0.1	28.9±0.1
	33.6 ± 0.1	5.30 ± 0.02	109 ± 0	31.3 ± 0.2	1.62 ± 0.01	356±1	33.2 ± 0.1	5.7 ± 0.1	101±1
	29.6 ± 0.2	3.03 ± 0.02	190 ± 1				31.0 ± 0.1	3.81 ± 0.02	152±1
7 %	40.1 ± 0.2	42 ± 1	13.7±0.2	40.6 ± 0.4	33.5 ± 0.8	17.2±0.2	41.8 ± 0.4	61 ± 2	9.5±0.1
	40.1 ± 0.3	16.5 ± 0.3	35.0±0.3	39.4 ± 0.3	16.3 ± 0.3	35.4±0.3	38.9 ± 0.1	21.0 ± 0.1	27.5±0.1
	37.2 ± 0.2	11.5 ± 0.2	50.4±0.5	35.8 ± 0.1	12.2 ± 0.3	47.4±0.5	38.5 ± 0.2	12.3 ± 0.1	46.8±0.2
	37.9 ± 0.1	5.8 ± 0.2	99.5±2.0	33.9 ± 0.1	5.94 ± 0.02	97.2±0.2	37.3 ± 0.2	11.2 ± 0.5	52±2
	34.8 ± 0.1	3.23 ± 0.03	179±1	30.8 ± 0.1	2.02 ± 0.04	286±3	36.5 ± 0.1	11.5 ± 0.1	50.2±0.1
	33.8 ± 0.2	1.76 ± 0.03	328±3				35.2 ± 0.1	7.3 ± 0.3	79±1
	31.4 ± 0.2	1.34 ± 0.01	432±1				30.9 ± 0.1	3.6 ± 0.1	159±1
10 %	41.6 ± 0.1	25.7 ± 0.2	22.4 ± 0.1	38.3 ± 0.3	35.7 ± 0.8	16.2±0.2	37.8 ± 0.5	45 ± 3	12.8±0.4
	40.4 ± 0.2	18.8 ± 0.1	30.7 ± 0.2	37.0 ± 0.3	17.0 ± 0.5	33.9±0.5	36.3 ± 0.1	33.6 ± 1.5	17.2±0.4
	37.8 ± 0.1	11.9 ± 0.1	48.5 ± 0.3	34.9 ± 0.1	7.4 ± 0.1	78.5±0.6	36.2 ± 0.3	22.5 ± 0.5	25.7±0.3
	35.0 ± 0.2	8.33 ± 0.03	69.4 ± 0.3	33.0 ± 0.2	5.7 ± 0.2	102±2	33.0 ± 0.1	8.2 ± 0.1	70.2±0.5
	34.5 ± 0.1	6.67 ± 0.03	86.6 ± 0.4	31.5 ± 0.2	4.06 ± 0.02	142.3±0.4	30.4 ± 0.1	2.73 ± 0.03	212±1
	30.4 ± 0.1	2.60 ± 0.02	223 ± 1						

- Data for 5 and 10 mol % cholesterol were obtained from reference 34 and are included for comparison purposes.

At a temperature of 38 °C, the measured half-life for pure DSPC flip-flop was 614 ± 12 minutes[54] while bilayers containing 2 mol % cholesterol had a half-life of 159 ± 1 minutes at ~ 39 °C. These data indicate that even a minute addition of cholesterol in the membrane causes a substantial increase in the rate of lipid flip-flop. Compared with the kinetic rates of flip-flop for pure DSPC, addition of 5 mol % cholesterol caused the half-life of flip-flop to decrease by 567 minutes. Addition of 7 and 10 mol % cholesterol into the membrane caused the half-lives of DSPC flip-flop at 38 °C to decrease by 515 and 566 minutes, respectively, compared with the flip-flop half-life of pure DSPC. The overall change in the rate of lipid flip-flop is small between 5 and 10 mol % cholesterol with a difference in the half-lives of 1.5 minutes.

Incorporating cholestanol into a DSPC bilayer caused more drastic changes in the rate of DSPC flip-flop. The initial addition of 2 mol % cholestanol resulted in an increase in the half-life of DSPC flip-flop by 189 minutes at ~ 38 °C. Increasing the concentration to 5 mol % cholestanol resulted in a substantial decrease in the half-life by 541 minutes at ~ 38 °C. The half-life of flip-flop continued to decrease by 579 and 580 minutes for concentrations of 7 and 10 mol % cholestanol, respectively at ~ 38 °C. At the concentrations of 7 and 10 mol % cholestanol, the kinetic rates of DSPC flip-flop were statistically faster than bilayers containing comparable concentrations of cholesterol. The changes observed in the kinetics when cholestanol is present are much more pronounced compared to incorporation of cholesterol in the membrane.

Bilayers containing cholestene also exhibit a strong concentration dependence on the rate of DSPC flip-flop. The inclusion of 2 mol % cholestene into a bilayer caused the half-life of DSPC flip-flop to decrease by 392 minutes at ~ 39 °C. Sequentially

increasing the concentration to 5, 7 and 10 mol % cholestene resulted in decreases in the half-life of DSPC flip-flop of 590, 567, and 601 minutes, respectively at ~ 38 °C. The kinetic rates for DSPC flip-flop in the presence of cholestene increased as the concentration increased from 2 to 10 mol % with faster kinetic values at each percentage compared to the corresponding concentrations of cholesterol.

Several conclusions can be drawn from the measured kinetic rates of DSPC flip-flop reported in Table 2.1. Initial addition of 2 mol % cholestanol caused a decrease in the rate of DSPC flip-flop at ~ 38 °C, while both cholesterol and cholestene at 2 mol % caused a statistical increase in the rate of DSPC flip-flop over the reported temperature range. When cholesterol is present at concentrations ranging from 5 – 10 mol %, the overall change in kinetics is only 28 minutes across these concentrations. Increasing the concentration of cholestanol from 5 – 10 mol % within the membrane continued to decrease the half-life of lipid flip-flop and also caused the largest change in half-life time of 57 minutes. By comparison, concentrations of 5 – 10 mol % cholestene in the membrane resulted in the lowest observed change in half-life kinetics of only 12 minutes. The most significant modification in kinetic rates for all the sterols was between 2 and 5 mol %. To further probe the contributions to DSPC flip-flop arising from the structural differences between cholesterol, cholestanol and cholestene; an analysis of the activation thermodynamics is provided below.

2.4.4 Transition State Thermodynamics

The transition state free energy ($\Delta G^{\ddagger}$) of DSPC flip-flop for bilayers containing cholesterol, cholestanol or cholestene was calculated from the kinetic rates using Eyring

theory:[54]

$$k = \frac{k_B T}{h} \exp\left(\frac{-\Delta G^{\ddagger}}{RT}\right) \tag{2.14}$$

where $\Delta G^{\ddagger}$ is the free energy of activation, k_B is Boltzman's constant, h is Planck's constant, R is the ideal gas constant, and T is the temperature. This equation can be rearranged and solved for $\Delta G^{\ddagger}$ allowing for the determination of the free energy from the measured kinetic rate. Figure 2.5 illustrates the trends in $\Delta G^{\ddagger}$ with increasing percentages of cholesterol, cholestanol or cholestene within the bilayer. A summary of the activation free energy for lipid flip-flop of each bilayer composition is presented in Table 2.2 at a temperature of 37 °C. The errors reported in these values are propagated from the errors in the slope and intercept of the linear regression analysis shown in Figure 2.5 for each membrane composition. Values of $\Delta G^{\ddagger}$ for pure DSPC flip-flop were extrapolated from the results in reference 54 for comparison purposes and are indicated by the black dashed line in Figure 2.5.

Considering the values of $\Delta G^{\ddagger}$ presented in Table 2.2, quantitative conclusions regarding the impact of cholesterol, cholestanol and cholestene on the thermodynamic barrier to DSPC flip-flop can be made. When 2 mol % of cholestanol is present in the membrane, the free energy barrier for DSPC flip-flop is statistically identical to pure DSPC. However, values of $\Delta G^{\ddagger}$ in the presence of 2 mol % cholesterol or cholestene are statistically lower by 3 kJ/mol when compared to pure DSPC. When 5 to 10 mol% of cholesterol, cholestanol or cholestene are incorporated into the DSPC membrane, there is a significant drop in the free energy barrier of ~ 7 kJ/mol and the $\Delta G^{\ddagger}$ values for cholesterol, cholestanol and cholestene are statistically similar within this range of concentrations.

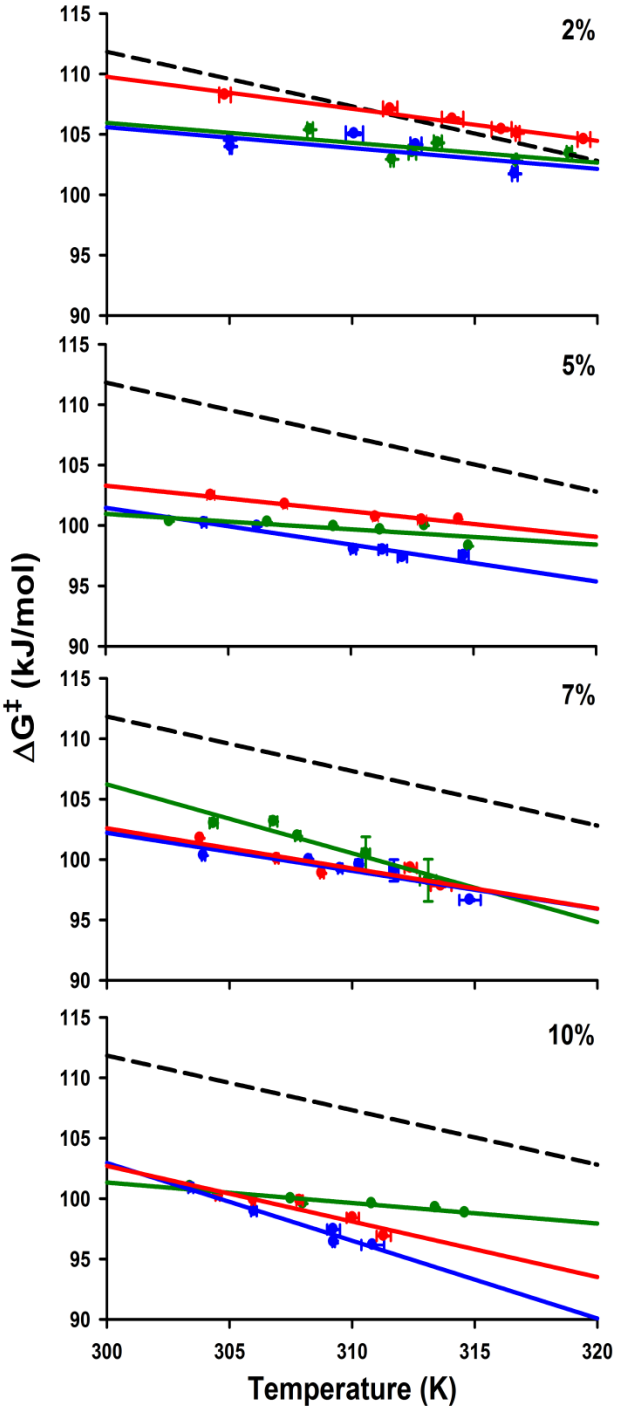

Figure 2.5: Plots of ΔG‡ for DSPC flip-flop versus temperature for membranes containing 2, 5, 7, and 10 mol % cholesterol (green), cholestanol (red), and cholestene (blue). The curve for DSPC flip-flop in a pure DSPC membrane (black dashed line)[54] was included as a reference.

Table 2.2: Transition state free energies at 37 °C, mean molecular areas and molar compression moduli at 30 mN/m for DSPC bilayers containing cholesterol, cholestanol or cholestene.

		$\Delta G^{\ddagger}$ @ 310 K (kJ/mol)	*Mean Molecular Area ($Å^2$/molecule)*	*K* (kJ/mol)*
DSPC		107 ± 3[a]	44.0 ± 0.2	77.6 ± 0.3
Cholesterol	2%	104 ± 1	40.4 ± 0.4	68 ± 2
	5%	100 ± 1[b]	40.2 ± 0.5	61 ± 2
	7%	101 ± 1	40.5 ± 0.6	62 ± 2
	10%	100 ± 1[b]	41.1 ± 0.3	57 ± 2
Cholestanol	2%	107 ± 1	40.8 ± 0.7	69 ± 2
	5%	101 ± 1	40.4 ± 0.3	60 ± 4
	7%	99 ± 1	38.7 ± 0.2	51 ± 2
	10%	98 ± 1	40.2 ± 0.2	45 ± 2
Cholestene	2%	104 ± 2	40.5 ± 0.7	68 ± 3
	5%	98 ± 1	40.7 ± 0.6	51 ± 3
	7%	99 ± 1	38.2 ± 0.5	41 ± 1
	10%	97 ± 1	39.2 ± 0.3	28 ± 6

a) $\Delta G^{\ddagger}$ data for pure DSPC bilayers was obtained from reference 54.
b) $\Delta G^{\ddagger}$ data for bilayers containing 5 and 10 mol % cholesterol were obtained from reference 34.

As stated previously, the number of gauche defects in the acyl chains decreased as cholesterol, cholestanol, or cholestene is initially introduced at 2 mol % but the CH_2 ν_s/ CH_3 ν_s does not statistically vary with increasing concentration or sterol identity. The lack of correlation between $\Delta G^{\ddagger}$ and the overall gauche defects of the lipid acyl chains indicates that an additional membrane physical property or properties must be contributing to the observed changes in the activation barrier for DSPC flip-flop.

2.4.5 Transition State Enthalpy

The transition state enthalpies for DSPC flip-flop in the presence of cholesterol, cholestanol and cholestene were calculated from the data in Table 2.1 and are listed in Table 2.3. The data illustrate the differences in enthalpy values for lipid flip-flop of pure DSPC membranes and membranes containing one of the cholesterol analogs. Compared with pure DSPC membranes, membranes containing 2 mol % cholesterol resulted in a significant decrease in the activation enthalpy for DSPC flip-flop. Previous work within our research group has demonstrated that the activation enthalpy originates from the energy required to transport the hydrophilic headgroup of the lipid through the hydrophobic acyl chain core of the membrane.[61] Incorporating cholesterol at concentrations of 2 mol % affects the membrane enough to lower the enthalpic barrier by 70 kJ/mol compared to pure DSPC membranes. However, as the concentration of cholesterol is increased, the enthalpic barrier increases but does not reach values for pure DSPC and is statistically identical to membranes containing 5 and 10 mol % cholesterol.

When cholestene is present in the membrane at a concentration of 2 mol %, there is a substantial decrease in the transition state enthalpy of DSPC flip-flop by 70 kJ/mol

Table 2.3: Transition state enthalpies of DSPC flip-flop with bilayer compositions as listed below.

	$\Delta H^{\ddagger}$ (kJ/mol)
DSPC	230 ± 40
DSPC + 2% Cholesterol	160 ± 30
DSPC + 5% Cholesterol	140 ± 20
DSPC + 7% Cholesterol	280 ± 30
DSPC + 10% Cholesterol	150 ± 10
DSPC + 2% Cholestene	160 ± 30
DSPC + 5% Cholestene	190 ± 10
DSPC + 7% Cholestene	190 ± 30
DSPC + 10% Cholestene	300 ± 20
DSPC + 2% Cholestanol	190 ± 10
DSPC + 5% Cholestanol	170 ± 10
DSPC + 7% Cholestanol	200 ± 30
DSPC + 10% Cholestanol	240 ± 40

compared with pure DSPC membranes. Increasing the concentration of cholestene in the membrane increases the activation enthalpy to a maximum value of 300 kJ/mol when 10 mol % cholestene is incorporated into the membrane. Increasing concentrations of cholestene, which lack the hydroxyl group of typical cholesterol, increases the hydrophobic content of the membrane resulting in higher values of the transition state enthalpy for DSPC flip-flop. Although the transition state enthalpy of membranes containing cholestene is higher than those of pure DSPC, the lower activation energy of flip-flop for DSPC in membranes with cholestene may be explained by a more disordered membrane. Parisio *et al.* calculated the diffusion coefficients for cholesterol flip-flop and various modified versions of cholesterol in DPPC membranes and found that cholestene exhibited a flip-flop coefficient two orders of magnitude greater than that of pure cholesterol.[50] The rapid movement of cholestene within the membrane may facilitate a more favorable flip-flop pathway for DSPC when cholestene is present.

Cholestanol in the membrane results in similar effects to cholestene when incorporated into the membrane. There is an initial decrease in the enthalpic barrier for DSPC flip-flop, but the enthalpy increases as the concentration of cholestanol increases in the membrane. However, the value for the transition state enthalpy of DSPC flip-flop when 10 mol % cholestenol was present is equal to 240 kJ/mol and is statistically smaller than when cholestene is present at the same concentration within the membrane. The lower transition state enthalpy values for DSPC flip-flop in membranes containing cholestanol could potentially be explained by the presence of the hydroxyl group and the lack of double bond in the sterol ring. The increased flexibility of the sterol ring in cholestanol could perturb the initial membrane state creating an easier pathway for lipid

translocation.

Of the three molecules investigated it can be concluded that varying the concentration of cholesterol in DSPC membranes does not significantly impact values of the transition state enthalpy. This influence is also observed for the reported values for the overall activation energy of lipid flip-flop in these systems. However, the structural alterations present in the molecules of cholestene and cholestanol alter the enthalpic values for DSPC flip-flop depending on the concentration within the membrane. The transition state enthalpy values for lipid flip-flop when either of these sterol molecules is contained within the membrane do not completely describe the observed thermodynamic results for DSPC lipid flip-flop, which led to further investigation of the physical parameters of packing and compressibility of the membrane when these steroid molecules are present.

2.4.6 Membrane Packing

The role of lipid packing on the measured activation free energy barrier to DSPC flip-flop was examined by comparing $\Delta G^{\ddagger}$ with the mean molecular area of DSPC as a function of bilayer composition. The mean molecular areas for DSPC were obtained from the pressure area isotherms shown in Figure 2.6. The mean molecular areas at a surface pressure of 30 mN/m for DSPC monolayers containing cholesterol, cholestanol or cholestene at 2, 5, 7 and 10 mol % are reported in Table 2.2. A surface pressure of 30 mN/m was chosen for these studies as it is close to values obtained for biological membranes,[70] calculated pressures from simulations[86] and values obtained from equilibrium lipid-lipid exchange between monolayers.[87] Cholesterol is known to

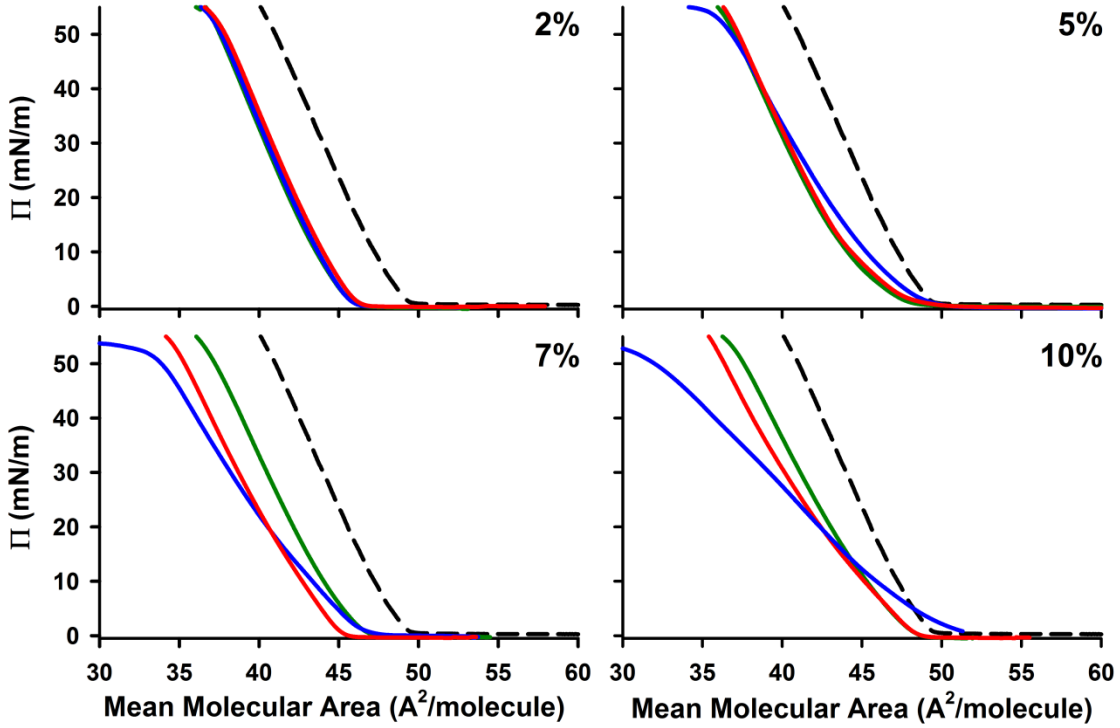

Figure 2.6: Averaged pressure area isotherms for DSPC (dashed black) and DSPCd70 (dashed gray) and DSPC monolayers containing 2, 5, 7 and 10 mol % cholesterol (green), cholestanol (red), and cholestene (blue). Isotherms were collected between 22 – 25 °C.

decrease the mean molecular area of the components in a membrane.[88-91] When 2, 5, 7, and 10 mol % cholesterol was incorporated in the membrane the mean molecular area of DSPC decreased by an average of ~ 8 % compared to a pure DSPC monolayer. A comparable effect is observed here upon the incorporation of cholestanol and cholestene. When cholestanol was incorporated, the mean molecular area of DSPC decreased on average by ~ 9 %. Cholestene incorporation resulted in the mean molecular area decreasing by an average of ~ 10 %. The measured values for the mean molecular areas reported here are within error of the values in the recent study of Miyoshi and Kato that investigated the packing area and elasticity of phosphocholine lipid/cholesterol mixtures.[89] Similar to the trend in DSPC acyl chain order, there is no apparent difference in the mean molecular area as a function of sterol structure or concentration. However, all the sterols do cause a statistical decrease in the mean molecular area of DSPC compared to a pure DSPC monolayer.

A previous study by Anglin *et al.* reported a strong correlation between $\Delta G^{\ddagger}$ for lipid flip-flop and lipid packing in membranes composed of phosphoethanolamine (PE) and PC.[61] It was found that values for $\Delta G^{\ddagger}$ increased as the mean molecular area decreased.[61] A comparison of lipid membrane packing and $\Delta G^{\ddagger}$ of DSPC flip-flop for bilayers containing cholesterol, cholestanol or cholestene is shown in Figure 2.7. Also included in Figure 2.7 are the $\Delta G^{\ddagger}$ values as a function of the mean molecular area for a pure DSPC bilayer (dashed black line). The data shown in Figure 2.7 indicate that the changes in the $\Delta G^{\ddagger}$ for DSPC flip-flop when cholesterol, cholestanol, or cholestene are present in the membrane are not correlated to the mean molecular area, as noted by the vertical distribution of the data. If $\Delta G^{\ddagger}$ were dependent on the mean molecular area of

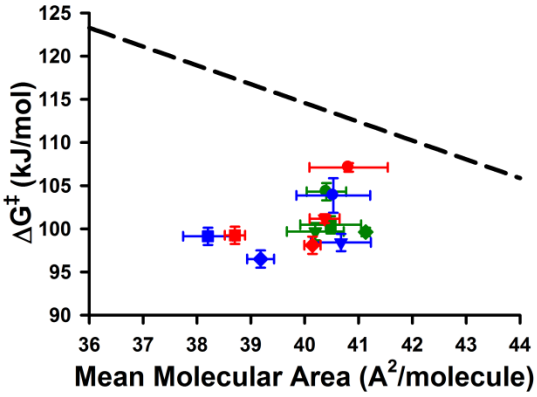

Figure 2.7: DSPC $\Delta G^{\ddagger}$ for flip-flop at 37 °C versus mean molecular area for membranes prepared at 30 mN/m for cholesterol (green), cholestanol (red) and cholestene (blue) at 22 – 25 °C. The symbols are for 2 mol % (●), 5 mol % (▼), 7 mol % (■), and 10 mol % (♦) respectively. The dashed black line represents the $\Delta G^{\ddagger}$ for pure DSPC as a function of mean molecular area obtained from reference 54.

DSPC then the maximum measured decrease in $\Delta G^{\ddagger}$ of 10 kJ/mol would necessitate an increase in the membrane mean molecular area of ~ 7 $Å^2$/molecule, which is not observed. In addition to increasing lipid packing, cholesterol is also known to affect the compression modulus of a membrane.[90-92] In order to examine the role compressibility plays in dictating the observed changes in $\Delta G^{\ddagger}$ in the presence of cholesterol, cholestanol, or cholestene the compression modulus was calculated from the pressure area isotherms shown in Figure 2.6.

2.4.7 Compression Modulus

The compression modulus (K) of a monolayer, which describes the ability of the system to respond to changes in external pressure exerted on the system, can be calculated from classical elastic theory:[27, 88, 91-93]

$$K = -A\frac{d\pi}{dA} \tag{2.15}$$

where A is the mean molecular area ($Å^2$/molecule) and π is the surface pressure (mN/m). This equation was applied to the experimentally obtained pressure-area isotherms (Figure 6) in the following form:

$$K(\pi_i) = -A_i\frac{[\pi_{i+1}-\pi_{i-1}]}{[A_{i+1}-A_{i-1}]} \tag{2.16}$$

where *i+1* and *i-1* define the interval over which the running numerical derivative was calculated. Due to noise in the experimental data, a moving average of 50 points was applied to each isotherm before calculating the compression modulus. A moving average of 200 points had to be applied to isotherms of DSPC monolayers containing 10 mol % cholestene due to the increased periodic noise resulting from increasing the compressibility of the material. The compression modulus is plotted as a function of

surface pressure and bilayer composition in Figure 2.8. The compression modulus in the surface pressure range of 15 to 45 mN/m is nearly constant, indicating a single phase.[93] A compression modulus of 293.0 ± 0.3 mN/m was obtained for a pure DSPC monolayer and a value of 278 ± 19 mN/m was obtained for a pure DSPCd70 monolayer at a surface pressure of 30 mN/m and both values are comparable to the previously reported value of 299.3 ± 10 mN/m.[92] There is a clear decrease in K as the percentage of cholesterol, cholestene, and cholestanol increases in the membrane and is consistent with values of K for saturated lipids in the gel-state containing low concentrations of cholesterol (i.e., < 20 mol %).[27]

In order to make a direct comparison between the free energy barrier of DSPC flip-flop, the compression modulus was converted to the molar compression modulus (K*) in kJ/mol using the mean molecular areas obtained from the pressure area isotherms. Values for K* are given in Table 2.2 and $\Delta G^{\ddagger}$ is plotted as a function of K* in Figure 2.9. There is a strong positive correlation between $\Delta G^{\ddagger}$ and K* seen in Figure 2.9 with a Pearson correlation coefficient of R = 0.87 ($P = 9.3 \times 10^{-5}$). A lipid undergoing flip-flop (at the transition state) occupies approximately twice the area of lipids in the ground state.[53] The transition state therefore exerts a compressive force on the surrounding lipids. Membranes with lower values of K* are more easily compressed thereby lowering the activation barrier of lipid flip-flop. It is interesting to note that all bilayers containing cholesterol have very similar values for $\Delta G^{\ddagger}$ and K*. Comparatively, incorporation of cholestanol lowers $\Delta G^{\ddagger}$ more than cholesterol and has a greater impact on the molar compression modulus. Removing the hydroxyl group (cholestene) has the greatest impact on the $\Delta G^{\ddagger}$ for DSPC flip-flop and on K*. An intriguing observation is that the

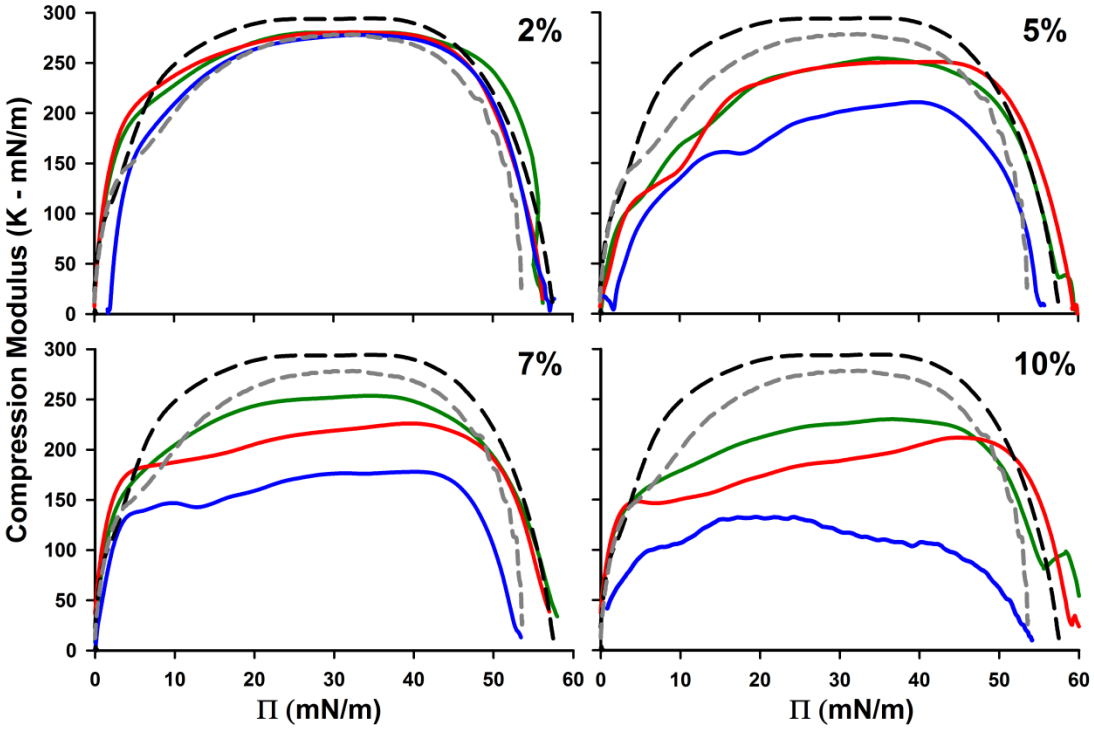

Figure 2.8: Compression modulus (K) values as a function of surface pressure at each sterol concentration for monolayers containing DSPC (black dashed) and DSPCd70 (gray dashed), cholesterol (green), cholestanol (red), and cholestene (blue).

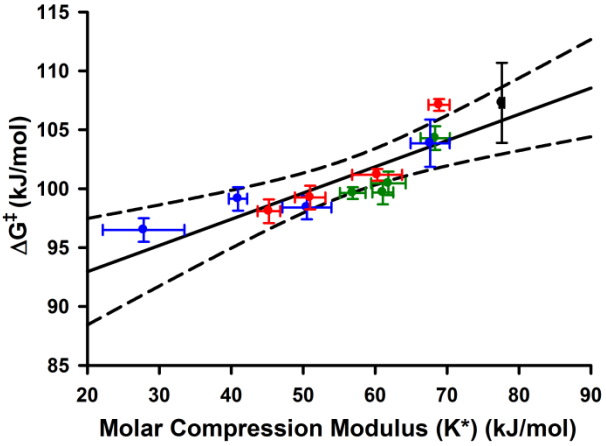

Figure 2.9: $\Delta G^{\ddagger}$ values at 37 °C for DSPC lipid flip-flop compared with molar compression moduli (K*) obtained from pressure-area isotherms for the lipid monolayers. Thermodynamic data for DSPC (black), cholesterol (green), cholestanol (red) and cholestene (blue). The solid black line (—) corresponds to the linear regression fit of the plotted data and the dashed black line (- - -) indicates the 99 % confidence intervals for the complete set of plotted data.

unique structure of cholesterol effectively prohibits large fluctuations in flip-flop over a wide concentration range due to the minimal impact on the molar compression modulus of the membrane. Removing either the double bond or hydroxyl group of cholesterol drastically impacts the energetics of DSPC flip-flop in the gel-state and is largely due to changes in the molar compression modulus of the membrane. This is the first reported correlation between the activation free energy of phospholipid flip-flop and the compression modulus of the membrane.

2.4.8 Effect of Isotopically Labeled Deuterium Lipids

In order to create asymmetric bilayers using LB/LS we employ deuterium substituted lipid components of complimentary chain length and headgroup. This results in bilayers with two vibrational modes of the terminal CH_3 ν_s and the CD_3 ν_s directly opposing each other. Each mode can be measured separately due to the difference in frequency of these vibrational transitions. There have been previous reports regarding the effect of deuterium labeled lipids shifting the phase transition temperature of unilamellar phospholipid vesicles to lower temperatures by approximately 4 °C.[94] More recently, planar supported hybrid bilayer membranes composed of deuterated outer leaflets and proteated inner leaflets with proteated thiol linkers were studied to examine the influence of the thiol linker on the phase transition temperature of the outer leaflet.[95] From these studies Anderson *et al.* concluded that the underlying thiol linker of the hybrid membrane contributed more towards the observed changes in the phase transition temperature of the outer leaflet than the deuterium labeling.[95] It was found that the phase transition of the outer lipid leaflet more closely matched the transition temperature of

vesicles if the linker was less rigid.[95] SFVS was used to examine the effect of deuterium labeled lipids on lipid flip-flop. Planar supported membranes were made consisting of DSPC and DSPCd70 supported on SiO_2 coated CaF_2 prisms. The existing SFVS spectrometer was modified to include a silver gallium selenide (AgGaSe) crystal after the optical parametric amplifier (OPA) output as depicted in Figure 2.2. The signal (ν_{signal} = 4545 – 7700 cm^{-1}) and idler (ν_{idler} = 2500 – 4800 cm^{-1}) output of the OPA combines through difference frequency mixing in the AgGaSe crystal to produce a single output radiation spanning the vibrational frequency region of 533 cm^{-1} to 2180 cm^{-1}.[96] The addition of the AgGaSe crystal makes it possible to measure flip-flop of deuterium labeled lipids with SFVS.

A spectrum of an asymmetric lipid bilayer containing DSPCd70 on the proximal leaflet and DSPC on the distal leaflet is shown in Figure 2.10A. The measured vibrational modes correspond to the CD_3 ν_s at 2070 cm^{-1}, CD_2 ν_s at 2095 cm^{-1} and the CD_3 ν_s FR at 2124 cm^{-1} as previously described.[95] By monitoring the decay in intensity of the CD_3 ν_s as a function of temperature and time, it is possible to obtain the kinetic rate of deuterated lipid flip-flop. The rate constants for a series of deuterated lipid measurements were compared to previously collected data for proteated DSPC. $\Delta G^{\ddagger}$ values were determined from DSPCd70 kinetics and plotted with previous DSPC $\Delta G^{\ddagger}$s[54] and are shown in Figure 2.10B. The values for $\Delta G^{\ddagger}$ for deuterated lipid components are statistically similar (within 99 % confidence) to values of $\Delta G^{\ddagger}$ for proteated lipid components. These measurements help to support the use of isotopically labeled lipids as a means to create asymmetric bilayers for analysis with SFVS.

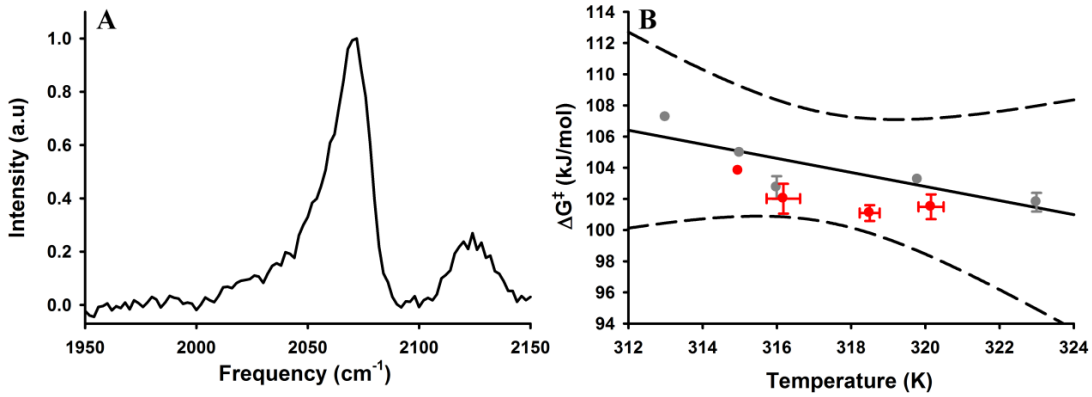

Figure 2.10: Comparison of CD vibrational modes and kinetics. A) A SFVS spectrum of DSPCd70 in an asymmetric bilayer composed of DSPCd70 and DSPC. B) $\Delta G^{\ddagger}$ vs temperature for DSPCd70 (red). Previously published data of $\Delta G^{\ddagger}$ values for DSPC are shown in gray.[54] The black solid line is the fit to these data and the dashed lines are the 99 % confidence limits.

2.5 Summary

This study utilized SFVS to investigate how the unique chemical and structural aspects of cholesterol affect its ability to facilitate lipid translocation in a lipid bilayer. Changes in the kinetic rates and the activation free energy ($\Delta G^{\ddagger}$) barrier for lipid flip-flop were analyzed and compared to corresponding changes in membrane physical properties when increasing percentages of cholesterol, cholestanol or cholestene were included into a gel-state DSPC membrane. Addition of cholesterol, cholestanol or cholestene into the membrane at 2 mol % resulted in similar values for the kinetic rates and $\Delta G^{\ddagger}$s for DSPC flip-flop compared to the $\Delta G^{\ddagger}$s and kinetic rates obtained for pure DSPC bilayers. Continued addition of cholesterol, cholestene, and cholestanol into the membrane from 5 to 10 mol % resulted in statistically faster kinetic rates and lower $\Delta G^{\ddagger}$ values for DSPC flip-flop compared to pure DSPC. Decreasing the amphiphilic nature of cholesterol by removing the hydroxyl group resulted in the lowest value for $\Delta G^{\ddagger}$, while decreasing the rigidity of cholesterol's sterol ring resulted in the largest magnitude of change in $\Delta G^{\ddagger}$.

The measured changes in the rates and energetics of DSPC flip-flop were found not to be correlated to the degree of lipid acyl chain ordering as determined from the CH_2 ν_s/CH_3 ν_s peak ratio. The addition of cholesterol, cholestene or cholestanol into a DSPC membrane caused the CH_2 ν_s/CH_3 ν_s to decrease to the same degree, compared to pure DSPC, within the concentration range of 2 to 10 mol% sterol. In addition to chain order no clear correlation was observed between the mean molecular area of DSPC in the bilayers and the measured rates of translocation.

The compression modulus of the bilayers, which was determined from the pressure-area isotherms, did show a direct positive correlation with the observed changes

in the transition state free energy of DSPC flip-flop. This strong correlation can be explained by considering the force exerted on surrounding lipids as a lipid progresses through the membrane at the transition state. If the amount of energy required to compress the surrounding lipids to accommodate the transitioning lipid is small, then there is an effective lowering of $\Delta G^{\ddagger}$. Interestingly, incorporation of cholesterol into a DSPC membrane causes much smaller changes in the $\Delta G^{\ddagger}$ and K* compared to cholestene and cholestanol. These findings present an intriguing insight into the structural aspects of cholesterol which help to moderate lipid flip-flop in membranes over a wide concentration range, and may explain why cholesterol is so prevalent within the cells of eukaryotic organisms. In order to further explore the physical properties of lipid membranes, synthesis of a conductive material to probe membrane electrochemical properties is described in the next chapter.

2.6 References

1. Berring, E. E.; Borrenpohl, K.; Fliesler, S. J.; Serfis, A. B., A Comparison of the Behavior of Cholesterol and Selected Derivatives in Mixed Sterol-Phospholipid Langmuir Monolayers: A Fluorescence Microscopy Study. *Chem. Phys. Lipids* **2005,** *136*, 1-12.

2. Krause, M. R.; Regen, S. L., The Structural Role of Cholesterol in Cell Membranes: From Condensed Bilayers to Lipid Rafts. *Acc. Chem. Res.* **2014,** *47*, 3512-3521.

3. Maxfield, F. R.; Tabas, I., Role of Cholesterol and Lipid Organization in Disease. *Nature (London, U. K.)* **2005,** *438*, 612-621.

4. McMullen, T. P. W.; Lewis, R. N. A. H.; McElhaney, R. N., Cholesterol-Phospholipid Interactions, the Liquid-Ordered Phase and Lipid Rafts in Model and Biological Membranes. *Curr. Opin. Colloid Interface Sci.* **2004,** *8*, 459-468.

5. McMullen, T. P. W.; McElhaney, R. N., Physical Studies of Cholesterol-Phospholipid Interactions. *Curr. Opin. Colloid Interface Sci.* **1996,** *1*, 83-90.

6. Ohvo-Rekila, H.; Ramstedt, B.; Leppimaki, P.; Slotte, J. P., Cholesterol Interactions with Phospholipids in Membranes. *Prog. Lipid. Res.* **2002,** *41* (Copyright © 2015 U.S. National Library of Medicine.), 66-97.

7. Xu, X.; London, E., The Effect of Sterol Structure on Membrane Lipid Domains Reveals How Cholesterol Can Induce Lipid Domain Formation. *Biochemistry* **2000,** *39* , 843-849.

8. Yamauchi, H.; Takao, Y.; Abe, M.; Ogino, K., Molecular Interactions Between Lipid and Some Steroids in a Monolayer and a Bilayer. *Langmuir* **1993,** *9* , 300-4.

9. Chaudhuri, A.; Chattopadhyay, A., Transbilayer Organization of Membrane Cholesterol at Low Concentrations: Implications in Health and Disease. *Biochim. Biophys. Acta, Biomembr.* **2011,** *1808* , 19-25.

10. Khelashvili, G.; Harries, D., How Sterol Tilt Regulates Properties and Organization of Lipid Membranes and Membrane Insertions. *Chem. Phys. Lipids* **2013,** *169* , 113-123.

11. Xu, F.; Rychnovsky, S. D.; Belani, J. D.; Hobbs, H. H.; Cohen, J. C.; Rawson, R. B., Dual Roles for Cholesterol in Mammalian Cells. *Proc. Natl. Acad. Sci. U. S. A.* **2005,** *102* , 14551-14556.

12. Gondre-Lewis, M. C.; Petrache, H. I.; Wassif, C. A.; Harries, D.; Parsegian, A.; Porter, F. D.; Loh, Y. P., Abnormal Sterols in Cholesterol-Deficiency Diseases Cause Secretory Granule Malformation and Decreased Membrane Curvature. *J. Cell Sci.* **2006,** *119* , 1876-1885.

13. Beattie, M. E.; Veatch, S. L.; Stottrup, B. L.; Keller, S. L., Sterol Structure Determines Miscibility Versus Melting Transitions in Lipid Vesicles. *Biophys. J.* **2005,** *89* , 1760-1768.

14. Khatibzadeh, N.; Gupta, S.; Farrell, B.; Brownell, W. E.; Anvari, B., Effects of Cholesterol on Nano-Mechanical Properties of the Living Cell Plasma Membrane. *Soft Matter* **2012,** *8* , 8350-8360.

15. Khattari, Z.; Maghrabi, M.; Al-Abdullah, T., Temperature Effect on Thin Lipid Film Elasticity and Phase Separation: Insights from Langmuir Monolayer and Fluorescence Microscopy Techniques. *Phase Transitions* **2015,** *88* , 668-681.

16. Milles, S.; Meyer, T.; Scheidt, H. A.; Schwarzer, R.; Thomas, L.; Marek, M.; Szente, L.; Bittman, R.; Herrmann, A.; Guenther Pomorski, T.; Huster, D.; Mueller, P., Organization of Fluorescent Cholesterol Analogs in Lipid Bilayers - Lessons from Cyclodextrin Extraction. *Biochim. Biophys. Acta, Biomembr.* **2013,** *1828* , 1822-1828.

17. Benesch, M. G. K.; Lewis, R. N. A. H.; Mannock, D. A.; McElhaney, R. N., A

DSC and FTIR Spectroscopic Study of the Effects of the Epimeric 4,6-cholestadien-3-ols and 4,6-cholestadien-3-one on the Thermotropic Phase Behaviour and Organization of Dipalmitoylphosphatidylcholine Bilayer Membranes. *Chem. Phys. Lipids* **2014,** *183* , 142-158.

18. Mannock, D. A.; Lewis, R. N. A. H.; McMullen, T. P. W.; McElhaney, R. N., The Effect of Variations in Phospholipid and Sterol Structure on the Nature of Lipid-Sterol Interactions in Lipid Bilayer Model Membranes. *Chem. Phys. Lipids* **2010,** *163* , 403-448.

19. Davis, J. H.; Schmidt, M. L., Critical Behaviour in DOPC/DPPC/Cholesterol Mixtures: Static 2H NMR Line Shapes Near the Critical Point. *Biophys. J.* **2014,** *106* , 1970-1978.

20. Ferreira, T. M.; Coreta-Gomes, F.; Ollila, O. H. S.; Moreno, M. J.; Vaz, W. L. C.; Topgaard, D., Cholesterol and POPC Segmental Order Parameters in Lipid Membranes: Solid State 1H-13C NMR and MD Simulation Studies. *Phys. Chem. Chem. Phys.* **2013,** *15*, 1976-1989.

21. Koenig, B. W.; Strey, H. H.; Gawrisch, K., Membrane Lateral Compressibility Determined by NMR and X-ray Diffraction: Effect of Acyl Chain Polyunsaturation. *Biophys. J.* **1997,** *73* , 1954-1966.

22. Lehnert, R.; Eibl, H.-J.; Mueller, K., Order and Dynamics in Lipid Bilayers from 1,2-Dipalmitoyl-sn-glycero-phospho-diglycerol as Studied by NMR Spectroscopy. *J. Phys. Chem. B* **2004,** *108* , 12141-12150.

23. Vist, M. R.; Davis, J. H., Phase Equilibria of Cholesterol/Dipalmitoylphosphatidylcholine Mixtures: Deuterium Nuclear Magnetic Resonance and Differential Scanning Calorimetry. *Biochemistry* **1990,** *29* , 451-64.

24. Evans, E.; Needham, D., Physical Properties of Surfactant Bilayer Membranes: Thermal Transitions, Elasticity, Rigidity, Cohesion and Colloidal Interactions. *J. Phys. Chem.* **1987,** *91* , 4219-28.

25. Needham, D.; Nunn, R. S., Elastic Deformation and Failure of Lipid Bilayer Membranes Containing Cholesterol. *Biophys. J.* **1990,** *58* , 997-1009.

26. Rawicz, W.; Smith, B. A.; McIntosh, T. J.; Simon, S. A.; Evans, E., Elasticity, Strength, and Water Permeability of Bilayers that Contain Raft Microdomain-Forming Lipids. *Biophys. J.* **2008,** *94* , 4725-4736.

27. Tierney, K. J.; Block, D. E.; Longo, M. L., Elasticity and Phase Behavior of DPPC Membrane Modulated by Cholesterol, Ergosterol, and Ethanol. *Biophys. J.* **2005,** *89* , 2481-2493.

28. Pan, J.; Tristram-Nagle, S.; Nagle, J. F., Effect of Cholesterol on Structural and Mechanical Properties of Membranes Depends on Lipid Chain Saturation. *Phys. Rev. E: Stat.* **2009,** *80* , 021931.

29. Wydro, P.; Knapczyk, S.; Lapczynska, M., Variations in the Condensing Effect of Cholesterol on Saturated versus Unsaturated Phosphatidylcholines at Low and High Sterol Concentration. *Langmuir* **2011,** *27* , 5433-5444.

30. Bonn, M.; Roke, S.; Berg, O.; Juurlink, L. B. F.; Stamouli, A.; Mueller, M., A Molecular View of Cholesterol-Induced Condensation in a Lipid Monolayer. *J. Phys. Chem. B* **2004,** *108* , 19083-19085.

31. Kett, P. J. N.; Casford, M. T. L.; Davies, P. B., Structure of Mixed Phosphatidylethanolamine and Cholesterol Monolayers in a Supported Hybrid Bilayer Membrane Studied by Sum Frequency Generation Vibrational Spectroscopy. *J. Phys. Chem. B* **2011,** *115* , 6465-6473.

32. Kett, P. J. N.; Casford, M. T. L.; Davies, P. B., Sum Frequency Generation Vibrational Spectroscopy of Cholesterol in Hybrid Bilayer Membranes. *J. Phys. Chem. B* **2013,** *117* , 6455-6465.

33. Kett, P. J. N.; Casford, M. T. L.; Davies, P. B., Orientation of Cholesterol in Hybrid Bilayer Membranes Calculated from the Phases of Methyl Resonances in Sum Frequency Generation Spectra. *J. Chem. Phys.* **2013,** *138* , 225101.

34. Liu, J.; Brown, K. L.; Conboy, J. C., The Effect of Cholesterol on the Intrinsic Rate of Lipid Flip-Flop as Measured by Sum-Frequency Vibrational Spectroscopy. *Faraday Discuss.* **2013,** *161* , 45-61.

35. Liu, J.; Conboy, J. C., Phase Behavior of Planar Supported Lipid Membranes Composed of Cholesterol and 1,2-distearoyl-sn-glycerol-3-phosphocholine Examined by Sum-Frequency Vibrational Spectroscopy. *Vib. Spectrosc.* **2009,** *50* , 106-115.

36. Ma, S.; Li, H.; Tian, K.; Ye, S.; Luo, Y., In Situ and Real-Time SFG Measurements Revealing Organization and Transport of Cholesterol Analogue 6-Ketocholestanol in a Cell Membrane. *J. Phys. Chem. Lett.* **2014,** *5* , 419-424.

37. Ohe, C.; Sasaki, T.; Noi, M.; Goto, Y.; Itoh, K., Sum Frequency Generation Spectroscopic Study of the Condensation Effect of Cholesterol on a Lipid Monolayer. *Anal. Bioanal. Chem.* **2007,** *388* , 73-79.

38. Devaux, P. F.; Fellmann, P.; Herve, P., Investigation on Lipid Asymmetry Using Lipid Probes. Comparison Between Spin-Labeled Lipids and Fluorescent Lipids. *Chem. Phys. Lipids* **2002,** *116* , 115-134.

39. McConnell, H. M.; Kornberg, R. D., Inside-Outside Transitions of Phospholipids

in Vesicle Membranes. *Biochemistry* **1971,** *10* , 1111-20.

40. Devaux, P. F.; Herrmann, A., Methods for the Determination of Lipid Transmembrane Distribution and Movement in Biological Membranes. In *Transmembrane Dynamics of Lipids*, John Wiley & Sons, Inc.: 2011; pp 1-24.

41. López-Montero, I.; Vélez, M.; Devaux, P. F., Detection and Measurement of Unlabeled Lipid Transmembrane Movement. In *Transmembrane Dynamics of Lipids*, John Wiley & Sons, Inc.: 2011; pp 25-43.

42. Nakano, M.; Fukuda, M.; Kudo, T.; Endo, H.; Handa, T., Determination of Interbilayer and Transbilayer Lipid Transfers by Time-Resolved Small-Angle Neutron Scattering. *Phys. Rev. Lett.* **2007,** *98* , 238101.

43. Nakano, M.; Fukuda, M.; Kudo, T.; Matsuzaki, N.; Azuma, T.; Sekine, K.; Endo, H.; Handa, T., Flip-Flop of Phospholipids in Vesicles: Kinetic Analysis with Time-Resolved Small-Angle Neutron Scattering. *J. Phys. Chem. B* **2009,** *113* , 6745-6748.

44. John, K.; Schreiber, S.; Kubelt, J.; Herrmann, A.; Muller, P., Transbilayer Movement of Phospholipids at the Main Phase Transition of Lipid Membranes: Implications for Rapid Flip-Flop in Biological Membranes. *Biophys. J.* **2002,** *83* , 3315-3323.

45. Leventis, R.; Silvius, J. R., Use of Cyclodextrins to Monitor Transbilayer Movement and Differential Lipid Affinities of Cholesterol. *Biophys. J.* **2001,** *81* , 2257-2267.

46. McLean, L. R.; Phillips, M. C., Mechanism of Cholesterol and Phosphatidylcholine Exchange or Transfer Between Unilamellar Vesicles. *Biochemistry* **1981,** *20* , 2893-900.

47. Shieh, H.-S.; Hoard, L. G.; Nordman, C. E., The Structure of Cholesterol. *Acta Crystallogr., Sect. B* **1981,** *B37* , 1538-43.

48. Seyama, Y., Cholestanol Metabolism, Molecular Pathology, and Nutritional Implications. *J. Med. Food* **2003,** *6* , 217-224.

49. Salen, G.; Grundy, S. M., The Metabolism of Cholestanol, Cholesterol, and Bile Acids in Cerebrotendinous Xanthomatosis. *J. Clin. Invest.* **1973,** *52* (Copyright (C) 2016 U.S. National Library of Medicine.), 2822-35.

50. Parisio, G.; Sperotto, M. M.; Ferrarini, A., Flip-Flop of Steroids in Phospholipid Bilayers: Effects of the Chemical Structure on Transbilayer Diffusion. *J. Am. Chem. Soc.* **2012,** *134* , 12198-12208.

51. Mast, N.; Murtazina, D.; Liu, H.; Graham, S. E.; Bjorkhem, I.; Halpert, J. R.;

Peterson, J.; Pikuleva, I. A., Distinct Binding of Cholesterol and 5β-Cholestane-3α,7α,12α-triol to Cytochrome P450 27A1: Evidence from Modeling and Site-Directed Mutagenesis Studies. *Biochemistry* **2006,** *45* , 4396-4404.

52. Klein, U.; Gimpl, G.; Fahrenholz, F., Alteration of the Myometrial Plasma Membrane Cholesterol Content with β-Cyclodextrin Modulates the Binding Affinity of the Oxytocin Receptor. *Biochemistry* **1995,** *34* , 13784-93.

53. Anglin, T. C.; Conboy, J. C., Lateral Pressure Dependence of the Phospholipid Transmembrane Diffusion Rate in Planar-Supported Lipid Bilayers. *Biophys. J.* **2008,** *95*, 186-193.

54. Anglin, T. C.; Cooper, M. P.; Li, H.; Chandler, K.; Conboy, J. C., Free Energy and Entropy of Activation for Phospholipid Flip-Flop in Planar Supported Lipid Bilayers. *J. Phys. Chem. B* **2010,** *114* , 1903-1914.

55. Liu, J.; Conboy, J. C., Direct Measurement of the Transbilayer Movement of Phospholipids by Sum-Frequency Vibrational Spectroscopy. *J. Am. Chem. Soc.* **2004,** *126* , 8376-8377.

56. Liu, J.; Conboy, J. C., 1,2-Diacyl-Phosphatidylcholine Flip-Flop Measured Directly by Sum-Frequency Vibrational Spectroscopy. *Biophys. J.* **2005,** *89* , 2522-2532.

57. Brown, K. L.; Conboy, J. C., Lipid Flip-Flop in Binary Membranes Composed of Phosphatidylserine and Phosphatidylcholine. *J. Phys. Chem. B* **2013,** *117* , 15041-15050.

58. Brown, K. L.; Conboy, J. C., Phosphatidylglycerol Flip-Flop Suppression due to Headgroup Charge Repulsion. *J. Phys. Chem. B* **2015,** *119*(32), 10252-10260.

59. Anglin, T. C.; Brown, K. L.; Conboy, J. C., Phospholipid Flip-Flop Modulated by Transmembrane Peptides WALP and Melittin. *J. Struct. Biol.* **2009,** *168* , 37-52.

60. Anglin, T. C.; Liu, J.; Conboy, J. C., Facile Lipid Flip-Flop in a Phospholipid Bilayer Induced by Gramicidin A Measured by Sum-Frequency Vibrational Spectroscopy. *Biophys. J.* **2007,** *92* , L01-L03.

61. Anglin, T. C.; Conboy, J. C., Kinetics and Thermodynamics of Flip-Flop in Binary Phospholipid Membranes Measured by Sum-Frequency Vibrational Spectroscopy. *Biochemistry* **2009,** *48* , 10220-10234.

62. Lambert, A. G.; Davies, P. B.; Neivandt, D. J., Implementing the Theory of Sum Frequency Generation Vibrational Spectroscopy: A Tutorial Review. *Appl. Spectrosc. Rev.* **2005,** *40* , 103-145.

63. Roy, S.; Covert, P. A.; FitzGerald, W. R.; Hore, D. K., Biomolecular Structure at Solid-Liquid Interfaces As Revealed by Nonlinear Optical Spectroscopy. *Chem. Rev.*

(Washington, DC, U. S.) **2014,** *114* , 8388-8415.

64. Shen, Y. R., Surface Properties Probed by Second-Harmonic and Sum-Frequency Generation. *Nature (London)* **1989,** *337* , 519-25.

65. Liu, J.; Conboy, J. C., Phase Transition of a Single Lipid Bilayer Measured by Sum-Frequency Vibrational Spectroscopy. *J. Am. Chem. Soc.* **2004,** *126* , 8894-8895.

66. Li, B.; Wang, H.-Y.; Feng, P.; Han, X.; Chen, Z.; Lu, X.; Wu, F.-G., Qualitative and Quantitative Analyses of the Molecular-Level Interaction between Memantine and Model Cell Membranes. *J. Phys. Chem. C* **2015,** *119* (30), 17074-17083.

67. Wu, F.-G.; Yang, P.; Zhang, C.; Han, X.; Song, M.; Chen, Z., Investigation of Drug-Model Cell Membrane Interactions Using Sum Frequency Generation Vibrational Spectroscopy: A Case Study of Chlorpromazine. *J. Phys. Chem. C* **2014,** *118* (31), 17538-17548.

68. Wu, F.-G.; Yang, P.; Zhang, C.; Li, B.; Han, X.; Song, M.; Chen, Z., Molecular Interactions Between Amantadine and Model Cell Membranes. *Langmuir* **2014,** *30* (28), 8491-8499.

69. Zhang, C.; Wu, F.-G.; Hu, P.; Chen, Z., Interaction of Polyethylenimine with Model Cell Membranes Studied by Linear and Nonlinear Spectroscopic Techniques. *J. Phys. Chem. C* **2014,** *118* (23), 12195-12205.

70. Marsh, D., Lateral Pressure in Membranes. *Biochim. Biophys. Acta, Rev. Biomembr.* **1996,** *1286* , 183-223.

71. Liu, J.; Conboy, J. C., Structure of a Gel Phase Lipid Bilayer Prepared by the Langmuir-Blodgett/Langmuir-Schaefer Method Characterized by Sum-Frequency Vibrational Spectroscopy. *Langmuir* **2005,** *21* , 9091-9097.

72. Marquardt, D., An Algorithm for Least-Squares Estimation of Nonlinear Parameters. *Journal of the Society for Industrial and Applied Mathematics* **1963,** *11* (2), 431-441.

73. Hamilton, J. A., Fast Flip-Flop of Cholesterol and Fatty Acids in Membranes: Implications for Membrane Transport Proteins. *Curr. Opin. Lipidol.* **2003,** *14* , 263-271.

74. Steck, T. L.; Ye, J.; Lange, Y., Probing Red Cell Membrane Cholesterol Movement with Cyclodextrin. *Biophys. J.* **2002,** *83* , 2118-2125.

75. Conboy, J. C.; Messmer, M. C.; Richmond, G. L., Investigation of Surfactant Conformation and Order at the Liquid-Liquid Interface by Total Internal Reflection Sum-Frequency Vibrational Spectroscopy. *J. Phys. Chem.* **1996,** *100* , 7617-22.

76. Mendelsohn, R.; Davies, M. A.; Brauner, J. W.; Schuster, H. F.; Dluhy, R. A., Quantitative Determination of Conformational Disorder in the Acyl Chains of Phospholipid Bilayers by Infrared Spectroscopy. *Biochemistry* **1989,** *28* , 8934-9.

77. Miranda, P. B.; Pflumio, V.; Saijo, H.; Shen, Y. R., Chain-Chain Interaction between Surfactant Monolayers and Alkanes or Alcohols at Solid/Liquid Interfaces. *J. Am. Chem. Soc.* **1998,** *120* , 12092-12099.

78. Tuchtenhagen, J.; Ziegler, W.; Blume, A., Acyl Chain Conformational Ordering in Liquid-Crystalline Bilayers: Comparative FT-IR and 2H-NMR Studies of Phospholipids Differing in Headgroup Structure and Chain length. *Eur. Biophys. J.* **1994,** *23* , 323-35.

79. Ward, R. N.; Duffy, D. C.; Davies, P. B.; Bain, C. D., Sum-Frequency Spectroscopy of Surfactants Adsorbed at a Flat Hydrophobic Surface. *J. Phys. Chem.* **1994,** *98* , 8536-42.

80. Rog, T.; Pasenkiewicz-Gierula, M.; Vattulainen, I.; Karttunen, M., Ordering Effects of Cholesterol and Its Analogues. *Biochim. Biophys. Acta, Biomembr.* **2009,** *1788* , 97-121.

81. Guyot-Sionnest, P.; Hunt, J. H.; Shen, Y. R., Sum-Frequency Vibrational Spectroscopy of a Langmuir Film: Study of Molecular Orientation of a Two-Dimensional System. *Phys. Rev. Lett.* **1987,** *59* , 1597-600.

82. Davies, M. A.; Schuster, H. F.; Brauner, J. W.; Mendelsohn, R., Effects of Cholesterol on Conformational Disorder in Dipalmitoylphosphatidylcholine Bilayers. A Quantitative IR Study of the Depth Dependence. *Biochemistry* **1990,** *29* , 4368-73.

83. Hofsass, C.; Lindahl, E.; Edholm, O., Molecular Dynamics Simulations of Phospholipid Bilayers with Cholesterol. *Biophys. J.* **2003,** *84* , 2192-2206.

84. Tamm, L. K.; Tatulian, S. A., Infrared Spectroscopy of Proteins and Peptides in Lipid Bilayers. *Q. Rev. Biophys.* **1997,** *30* , 365-429.

85. Yan, W.-H.; Strauss, H. L.; Snyder, R. G., Conformation of the Acyl Chains in Diacylphospholipid Gels by IR Spectroscopy. *J. Phys. Chem. B* **2000,** *104* (17), 4229-4238.

86. Baoukina, S.; Mendez-Villuendas, E.; Bennett, W. F. D.; Tieleman, D. P., Computer Simulations of the Phase Separation in Model Membranes. *Faraday Discuss.* **2013,** *161* , 63-75.

87. Jahnig, F., Lipid Exchange Between Membranes. *Biophys J* **1984,** *46* (Copyright © 2016 U.S. National Library of Medicine.), 687-94.

88. Kodama, M.; Shibata, O.; Nakamura, S.; Lee, S.; Sugihara, G., A Monolayer Study on Three Binary Mixed Systems of Dipalmitoyl Phosphatidyl Choline with Cholesterol, Cholestanol and Stigmasterol. *Colloids Surf., B* **2004,** *33* , 211-226.

89. Miyoshi, T.; Kato, S., Detailed Analysis of the Surface Area and Elasticity in the Saturated 1,2-diacylphosphatidylcholine/Cholesterol Binary Monolayer System. *Langmuir* **2015,** *31* , 9086-9096.

90. Smaby, J. M.; Brockman, H. L.; Brown, R. E., Cholesterol's Interfacial Interactions with Sphingomyelins and-Phosphatidylcholines: Hydrocarbon Chain Structure Determines the Magnitude of Condensation. *Biochemistry* **1994,** *33* , 9135-42.

91. Smaby, J. S.; Momsen, M. M.; Brockman, H. L.; Brown, R. E., Phosphatidylcholine Acyl Unsaturation Modulates the Decrease in Interfacial Elasticity Induced by Cholesterol. *Biophys. J.* **1997,** *73* , 1492-1505.

92. Smaby, J. M.; Kulkarni, V. S.; Momsen, M.; Brown, R. E., The Interfacial Elastic Packing Interactions of Galactosylceramides, Sphingomyelins, and Phosphatidylcholines. *Biophys. J.* **1996,** *70* , 868-77.

93. Lozano, M. M.; Longo, M. L., Complex Formation and Other Phase Transformations Mapped in Saturated Phosphatidylcholine/DSPE-PEG2000 Monolayers. *Soft Matter* **2009,** *5* , 1822-1834.

94. Guard-Friar, D.; Chen, C. H.; Engle, A. S., Deuterium Isotope Effect on the Stability of Molecules: Phospholipids. *J. Phys. Chem.* **1985,** *89* , 1810-13.

95. Anderson, N. A.; Richter, L. J.; Stephenson, J. C.; Briggman, K. A., Characterization and Control of Lipid Layer Fluidity in Hybrid Bilayer Membranes. *J. Am. Chem. Soc.* **2007,** *129* , 2094-2100.

96. Bosenberg, W. R.; Guyer, D. R., Broadly Tunable, Single-Frequency Optical Parametric Frequency-Conversion System. *J. Opt. Soc. Am. B: Opt. Phys.* **1993,** *10* , 1716-22.

CHAPTER 3

PREPARATION AND CHARACTERIZATION OF CONDUCTIVE AND TRANSPARENT RUTHENIUM DIOXIDE SOL-GEL FILMS

3.1 Introduction

In the previous chapter, it was shown that the physical characteristics of lipid membranes can directly impact the rate of translocation of lipid components. This chapter details the synthesis of a new material that could aid in examining the electrochemical properties of supported lipid membranes in conjunction with SFVS studies. Optically transparent conductive materials have played a critical role in the energy and electronic industries over the past decade. One of the most common and well characterized materials in these industries is indium tin oxide (ITO). ITO is a particularly valuable material for thin conductive films due to its high conductivity and transparency.[1-5] It is used in liquid crystal displays, photovoltaic cells and a variety of other electronic devices. Although there are multiple applications for ITO, there are a

number of drawbacks, such as the cost and inefficiency of the manufacturing process and the ease with which the film may be etched in oxidative environments.[1-2, 5-6] Alternatives to ITO include carbon nanotubes, graphene films, metal meshes and other metal oxide combinations.[1, 6-13] Carbon nanotubes and graphene films have been successfully applied to flexible substrates, but they are also unstable in highly oxidizing environments as well as difficult to apply to a flat, insulating, glass substrate.[1, 6] Ruthenium dioxide (RuO_2) is another appealing compound for creating optically transparent conductive materials due to its high electronic conductivity at room temperature and resistance to chemical oxidation.[14]

RuO_2 is an incredibly versatile compound which is found in supercapacitors, catalysts and thin film resistors.[15] Recent studies have examined characteristics of nanoscopic RuO_2 films formed via a modified chemical bath deposition.[16] Here the authors characterized the surface morphology, optical and electrical properties as well as the supercapacitive characteristics of the formed RuO_2 films. Patake and Lokhande reported an optical band gap for their amorphous RuO_2 films at 2.2 Ev which was lower than the optical band gap of 2.4 Ev for spray deposited RuO_2 films.[16] Their conductivity measurements indicated that their films exhibit p-type electrical conductivity and described that the supercapacitive properties may increase as the film thickness increases.[16] These thorough studies have provided some foundation for other researchers to expand applications and interests in ruthenium dioxide thin films.

In 2009, Chervin *et al.* demonstrated the ability to deposit RuO_2 particles onto a flexible, insulating substrate of silica paper resulting in a crust of RuO_2 conductive particles on the surface of the substrate.[17-18] A sub-ambient precursor solution of RuO_4

was allowed to thermally decompose to RuO_2 nanoparticles in solution at room temperature. These nanoparticles were then allowed to physisorb onto a substrate.[17-18] The resulting RuO_2 nanoskins exhibited conductivity values ranging from 14 to 830 Ms cm^{-1}. The conductivity was also found to be dependent on the temperature at which the films were annealed.[18] This RuO_2 direct deposition method has also been employed by Long *et al.* to create conductive films on titanium foil and a variety of transparent substrates resulting in films with conductivities on the order of 10^3 S cm^{-1} and visible transmission values as high as 85 %.[19-20] However, the method of depositing ruthenium dioxide onto insulating substrates developed by Chervin *et al.* results in a high level of film variability from deposition to deposition, and produces films with a wide range of measured sheet resistance values (1000 to 5000 Ω).[19] In addition, the deposited films lack mechanical strength and can easily be removed with gentle abrasion. Development of a method for creating conductive and transparent RuO_2 films in a convenient, low cost and highly reproducible manner with increased stability (chemical and mechanical) would be very beneficial.

Jeng *et al.* have described a more reproducible method to create conductive RuO_2 films, involving the incorporation of RuO_2 particles into a silica dioxide (SiO_2) sol-gel matrix.[21] The resistivity of the coatings reported by Jeng *et al.* varies from ~10^{-1} to 10^{-3} Ω·cm with optical transmission values reported from 55% to 90%.[21] An increase in the ratio of Ru/Si in the sol-gel was accompanied by a decrease in resistivity and transmission. The sol-gel procedure for creating RuO_2 films is easily customizable, allowing for control of the transparency and conductivity of the deposited film.[22] In addition, there are many different SiO_2 precursor compounds to choose from when

attempting to synthesize sol-gel materials.[23] If high optical quality sol-gel films are desired, a previous study published by Yang *et al.* reported that the use of a methyl alkoxide precursor and silica tetrachloride ($SiCl_4$) as a catalyst resulted in films with low optical loss (<0.2 Db/cm) and highly homogeneous films compared to sol-gels catalyzed with HCl, which was used by Jeng *et al*.[24-25]

The work described in this article utilizes a method of producing optically transparent conductive RuO_2 films on glass substrates using the methyl alkoxide precursor methyltriethoxysilane (MTES) and $SiCl_4$ as a catalyst to create a sol-gel material with high conductance and excellent optical properties. The films were deposited through a dip-coating procedure, which also has the ability to coat substrates with curved surfaces. The resulting films were characterized using a variety of surface techniques to examine thickness, roughness, and surface composition. The optical properties were explored in both the infrared and visible regions. These novel films were then tested as electrodes for spectroelectrochemistry and their electrochemical performance was compared with a standard platinum disk electrode. Robustness of the sol-gel films was tested by exposing the electrodes to a highly oxidizing environment of 70% H_2SO_4 – 30% H_2O_2 v/v (Piranha) solution. The thorough characterization conducted in this study demonstrates that an optically transparent conductive material can be reliably and efficiently created using simple sol-gel dip-coating methods. The resulting films are extremely stable and resistant to oxidation and acidic conditions.

3.2 Experimental

3.2.1 Sol-Gel Preparation

Absolute ethanol (200 proof) was obtained from Decon Laboratories. Methyltriethoxysilane (MTES) and silicon tetrachloride ($SiCl_4$) were obtained from Sigma Aldrich. *MTES is a flammable liquid and should be kept away from ignition sources.* *$SiCl_4$ is extremely toxic when inhaled; handle this material under proper ventilation conditions.* Ruthenium trichloride x-hydrate ($RuCl_3 \cdot xH_2O$) was obtained from Alfa Aesar. *$RuCl_3 \cdot xH_2O$ causes severe skin burns and eye damage upon contact; proper protection should be used when handling this product*. All chemicals were used as received and without further purification. Premiere brand silica microscope slides were used as the substrate for deposition of the films. The slides were first cleaned with Alconox cleaning detergent, and then rinsed sequentially with 18 MΩ·cm Nanopure water, isopropanol, ethanol, and Nanopure water again. The substrates were then submerged in a solution of Piranha for a minimum of 8 hours. *Warning, Piranha is a highly reactive solution which will react violently with organic materials and metals; care should be taken when handling this material.* After treatment in Piranha, the slides were thoroughly rinsed with Nanopure water and submerged in a 100 mM HCl solution for a minimum of 3 hours. Once removed, the slides were rinsed thoroughly with Nanopure water and then ozone cleaned (Jelight UVO Cleaner) for 5 minutes.

The RuO_2:SiO_2 sol-gels were synthesized from two precursor solutions. Initially MTES and $SiCl_4$ were added, in a 6:1 molar ratio to 10 mL of absolute ethanol. This solution was stirred constantly for 2 hours. A separate precursor solution containing 0.5, 1, 2 or 4 mmol of $RuCl_3 \cdot xH_2O$ dissolved in 10 mL of absolute ethanol was stirred for 1

hour. The two precursor solutions were combined together and then stirred constantly for 1 hour. The final solutions contained a molar ratio of 24:6:1 $RuCl_3 \cdot xH_2O$:MTES:$SiCl_4$ (3.43:1 Ru:Si), 12:6:1 $RuCl_3 \cdot xH_2O$:MTES:$SiCl_4$ (1.71:1 Ru:Si), 6:6:1 $RuCl_3 \cdot xH_2O$:MTES:$SiCl_4$ (0.83:1 Ru:Si) or 3:6:1 $RuCl_3 \cdot xH_2O$:MTES:$SiCl_4$ (0.43:1 Ru:Si). The sol-gel was allowed to age for a minimum of 48 hours in a sealed container prior to dip coating.

A KSV Minitrough substrate dipper was used for dip coating the silica slides with the sol-gel. The substrates were withdrawn at speeds of 8.5 cm/min and 4.2 cm/min. The coated substrates were allowed to dry under ambient conditions before the annealing process. Each sample was then annealed at a temperature of 450 °C for 15 minutes. The samples were then slowly cooled to room temperature in the furnace before use.

3.2.2 Characterization

Thickness: The thickness of the sol-gel films was determined using ellipsometry. For the ellipsometric measurements, sol-gel films were deposited on p-type silicon wafers (Silicon Quest International) and the thickness was determined using a J.A. Woollam variable angle spectroscopic ellipsometer. The p-type silicon wafers used as a substrate were cleaned using the method described above for the glass slides.

Optical Transmission: A Perkin Elmer Spectrum One FT-IR spectrometer and Lambda 25 UV-Vis spectrophotometer were used to examine the transparency of the deposited coatings in the infrared and ultraviolet-visible regions, respectively. The transmission in the infrared was recorded from 2000 to 4000 cm^{-1} and transmission in the visible was recorded from 350 to 850 nm. For each spectrum collected a clean silica

slide served as the background.

IR spectra were recorded for bulk sol-gel materials. The precursor solutions were gently heated to ~120 °C until all of the solvent was removed. A small amount (0.020 g) of the resulting solid was combined with 1.98 g KBr using a mortar and pestle. The amount of powder used to make a pellet was 0.100 g, yielding a pellet with a thickness < 1 mm. A small amount of the 3.43:1 Ru:Si solid powder was annealed at 450 °C for 15 minutes. A blank spectrum was recorded using KBr without any sol-gel material. Spectra were baseline corrected and fit using Grams AI software.

Surface Characterization: A Bruker Dimension Icon atomic force microscope (AFM) was used to characterize the surface roughness of the as-prepared sol-gel film. Images were collected using PeakForce Quantitative Nanomechanical Property Mapping mode (PeakForce QNM). A silicon tip on a nitride cantilever with a force constant of k = 0.4 N/m was used for imaging. Images were collected for each sample as well as an uncoated clean silica slide and the root-mean-square (RMS) roughness was determined. Several topographical images were collected at various positions on the sample in order to obtain a statistical average of the RMS roughness.

X-ray photoelectron spectroscopy (XPS) was used to determine the surface composition of the sol-gel films. Sol-gel films were prepared on p-type silicon wafers for analysis. A Kratos AXIS Ultra DLD x-ray photoelectron spectrometer was used to collect the XPS data. A monochromatic aluminum kα source at 1486.6 eV was used to excite electrons within the sample. Initial survey scans were collected at a pass energy of 160 eV and high resolution scans were collected at 40 eV. The measured peak resolution for this instrument is 0.7 eV for a smooth, conductive silver surface. XPS data were

collected for as-prepared sol-gel films before and after sputtering with an argon source for 30 seconds. The sample area examined was 700 x 300 μm. Several spectra were taken at various positions in the sample in order to obtain a statistical average of the surface composition of the sample.

Conductivity: The resistivity of the sol-gel films was measured using a four-wire resistance measurement (Keithley 2000 multimeter). Copper wire leads were attached to the surface of the sol-gel films with silver epoxy (Alfa Aesar). A line of silver epoxy was applied at each end of the coating spanning the width of the coating allowing for the resistance to be measured across the entirety of the coated film. The four-wire configuration forces a test current through the sample and measures the resistance with a set of test leads, while the voltage across the sample is measured through a second set of leads (sense leads). This setup allows for a more accurate determination of resistance by excluding the voltage drop that may be present in the test leads.

Electrochemistry: A Princeton Applied Research (PAR) 273 potentiostat was used for all electrochemical experiments. A standard solution of 0.9 mM ferrocenemethanol (FcMeOH, Sigma Aldrich) in 100 mM NaCl was prepared and degassed for 30 minutes with argon before electrochemical measurements were taken. Cyclic voltamograms (CVs) were collected from -200 to +650 mV, using a Ag|AgCl reference electrode and a platinum wire counter electrode. A reference CV was collected using a platinum disk working electrode (area = 2.011 mm^2, BASi), platinum wire counter electrode, and a Ag|AgCl reference electrode (BASi). The stability of the sol-gel coatings was tested by exposing the previously described sol-gel coated working electrode to Piranha solution five consecutive times for a minimum of 8 hours per

exposure. Cyclic voltammograms were collected after each Piranha exposure until the current reached a stable value.

The electroactive area of the platinum electrode was determined using the current obtained from the reduction of ferrocenemethanol. The platinum electrode was mechanically polished (Buehler Master Polish 2) and then thoroughly rinsed with methanol and Nanopure water. The Pt working electrode was then sonicated in Nanopure water for 5 minutes before use. The electroactive area of the RuO_2 sol-gel electrode was calculated by comparing the ratio of the integrated FcMeOH reduction current to the integrated FcMeOH reduction current measured using a platinum electrode.

Spectroelectrochemistry: The spectroelectrochemistry of ferrocenemethanol oxidation and reduction was measured using the three-electrode setup described above and a Perkin Elmer Lambda 25 spectrophotometer. Absorbance spectra were recorded while the applied potential was cycled between -200 to +650 mV at a scan rate of 1 mV/s. The sol-gel films containing 1.71:1 Ru:Si withdrawn at a speed of 8.5 cm/min were used for all the spectroelectrochemical experiments. The wavelength region probed by the UV-Vis spectrophotometer was 500 to 800 nm with a scan rate of 2880 nm/min, which corresponds to a spectrum collected every ~25 mV. The instrument collected data in a double beam mode and the blank contained 100 mM NaCl and a 1.71:1 Ru:Si sol-gel coated silica slide.

3.3 Results and Discussion

In order to fully characterize the performance of the novel RuO_2 sol-gel derived material, several key physical properties were investigated; thickness, optical

transmission, surface roughness, composition and conductivity. The thickness of dip-coated sol-gel films is governed by the following equation for the dip coating processes:[22]

$$h = c\sqrt{\frac{\eta U_o}{\rho g}}, \tag{3.1}$$

where h is the film thickness, c is a constant, η is the viscosity of the solution, U_o is the withdrawal rate, ρ is the density of the solution and g is the gravitational force constant.[22] The thickness of the films is most easily adjusted by varying the withdrawal rate used for film deposition. Film thickness was determined by ellipsometry for the sol-gel films deposited on p-type silicon. Thickness values varied with solution composition and withdrawal speed and are reported in Table 3.1. The thickness values we measured range from 7.5 to 11.4 nm. These values are more than an order of magnitude lower than the values reported for sol-gel coatings prepared by Jeng *et al.* (~140 nm).[21] However, these values are only two to three times higher than values obtained by Chervin *et al.* for direct deposition of RuO_2 nanoparticles (~3 nm).[17]

Optical transmission characteristics of the sol-gel films are also highly dependent upon the withdrawal rate and fraction of ruthenium in the sol-gel. Figure 3.1A demonstrates that our technique results in a highly transparent coating applied to a glass substrate. The UV-Vis and IR transmission spectra in Figure 3.1B were used to quantify the impact of ruthenium concentration and withdrawal rate on the optical transmission of the films. UV-Vis spectra were recorded for both pre-annealed and annealed sol-gel films. A small peak is observed in the UV-Vis spectra at ~430 nm for the unannealed films and is likely due to the O → Ru charge transfer of the highly oxidized RuO_4 species formed in solution.[26] When the films are annealed, this absorbance decreases as RuO_4 is converted to RuO_2. A noticeable increase in absorption around 350 nm is

Table 3.1: Thickness, RMS surface roughness, resistivity, optical transmission and surface composition of the annealed RuO2 sol-gel films.

Withdrawal Speed (cm/min)	Ru:Si (solution)	Thickness (nm)	RMS Surface roughness (nm)	Resistivity (Ω·cm)	% T at 600 nm	Ru:Si (surface)
8.5	*0.43:1	-	-	-	97.4	-
8.5	0.86:1	(9.63)	-	1.134	93.4	0.1 ± 0.1:1
8.5	1.71:1	9.6 ± 0.2	0.7	1.02×10^{-3}	83.5	0.4 ± 0.1:1
8.5	3.43:1	16.0 ± 0.8	0.7	1.03×10^{-3}	71.0	1.0 ± 0.2:1
4.2	1.71:1	7.5 ± 0.7	0.7	1.72×10^{-3}	88.5	
4.2	3.43:1	11.4 ± 0.1	1.2	1.24×10^{-3}	78.9	

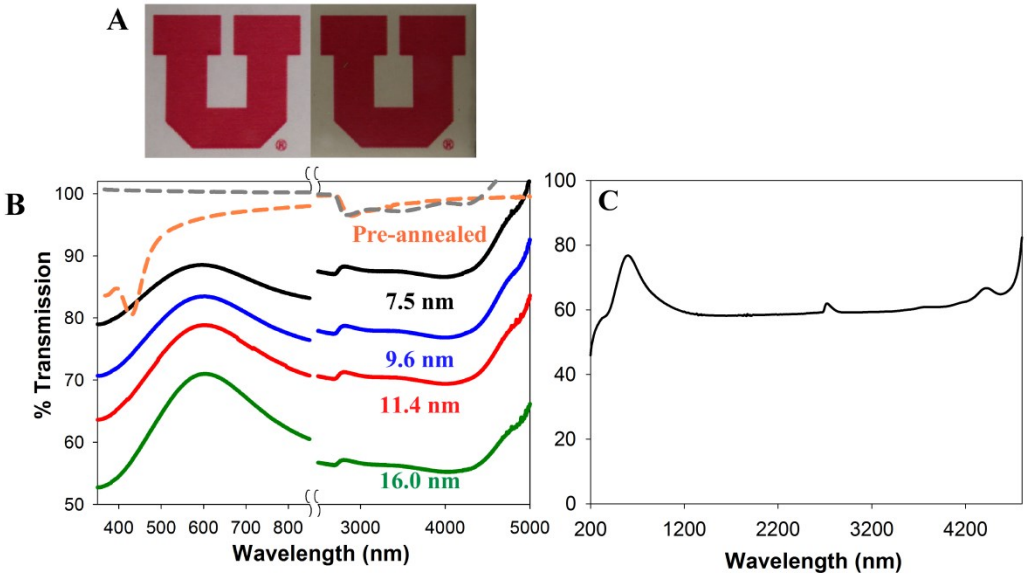

Figure 3.1: Optical properties of the synthesized RuO_2 films. A) Photograph of a silica slide coated with 1.71:1 Ru:Si sol-gel film withdrawn at 8.5 cm/min with a thickness of 9.6 nm. B) Transmission spectra for pre-annealed and annealed RuO_2 sol-gel films of four different thicknesses. The spectrum for an annealed sol-gel without ruthenium is shown in gray for comparison. C) Optical transmission spectrum from 200 – 4800 nm for a 3.43:1 Ru:Si sol-gel film withdrawn at 8.5 cm/min on a quartz substrate.

observed with increasing film thickness. This increase stems from the increase in the RuOH content within the film,[27] which was verified by collecting a UV-Vis spectrum for a sol-gel film prepared without any ruthenium. The appearance of the peak around 350 nm is not due to thin-film interference effect, which was verified by collecting a spectrum from 200 to 4800 nm on a fused silica substrate for a 3.43:1 Ru:Si film as shown in Figure 3.1C. The IR spectra of the unannealed sol-gel films displayed a broad absorbance at 2870 nm (3484 cm^{-1}) which is associated with the water in the sample. This peak disappears upon annealing resulting in a flat featureless spectrum from 2500 nm (4000 cm^{-1}) to 5000 nm (2000 cm^{-1}).

FT-IR spectra of bulk sol-gels were used to characterize the composition of the materials before and after annealing (Figure 3.2). The spectra have been normalized to the peak at 1100 cm^{-1}. The annealed and unannealed materials show the same vibrational resonances. Vibrational modes were observed at 600, 800, 1100, 1600 and 3100 cm^{-1} for each sol-gel composition. The vibrational mode at 600 cm^{-1} is attributed to that of rutile RuO_2.[28-29] The peak around 800 cm^{-1} can be assigned to the Ru–O–Ru asymmetric stretch[28] or the Ru=O vibrational mode.[28, 30] The broad peak at 1100 cm^{-1} is a combination of both Si–O–Si bonds[25, 30] and RuOH vibrational stretches.[28] The vibrational band at 1600 cm^{-1} is a result of H-O-H stretching from water.[28-29] The peak at ~ 3100 cm^{-1} is attributed to hydroxide species, either Si-OH or Ru-OH.[29, 31] Upon annealing at 450 °C a peak begins to emerge around 1200 cm^{-1} that can be attributed to a secondary phase of silica as the films becomes denser.[25, 30, 32] The intensity or positions of the other vibrational modes do not change upon annealing.

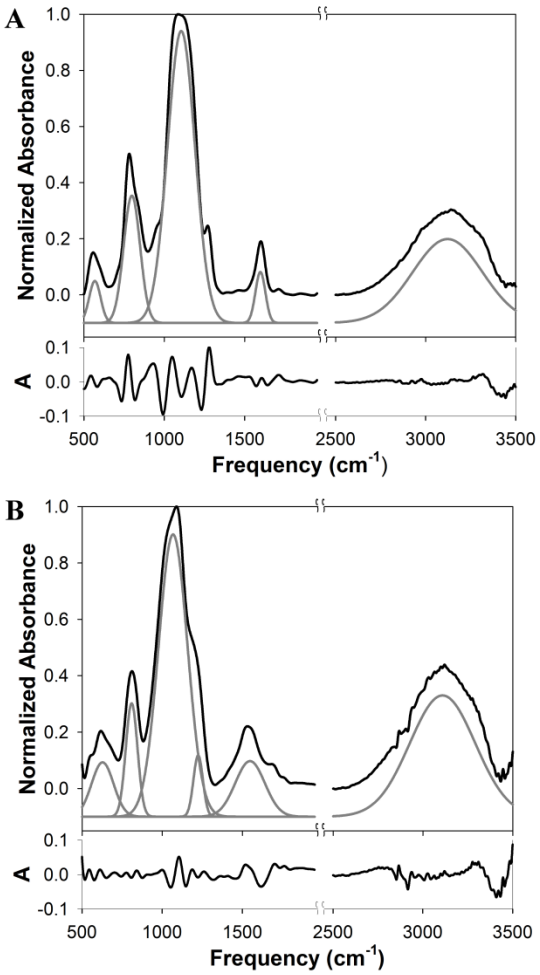

Figure 3.2: FTIR spectra of bulk A) unannealed and B) sol-gel material annealed at 450 °C for 15 minutes. The peak fits are offset by 0.1 absorbance units for clarity. The residuals for the peak fits are shown below each spectrum.

We have compared the optical properties of the RuO_2 sol-gel films prepared here with other conductive and transparent materials. Hu *et al.* have reported the optical transmission characteristics for a variety of optically transparent conductive materials as a function of thickness.[33] The values presented by Hu *et al.* were used to calculate the transmission for films with thicknesses of 10 nm as a comparison to the RuO_2 sol-gel films in this study. For a carbon nanotube film with a thickness of 10 nm the transmission at 550 nm was 92 %, while a graphene film had a transmission of 70 % at the same wavelength and ITO films had a transmission of 99% at 550 nm.[33] The films reported in this study have transmissions of 71, 79, 84 and 89% at 600 nm depending on the Ru content and thickness. Similar RuO_2 sol-gel films created by Jeng *et al.* have calculated transmission values for 10 nm thick films ranging from 96-99 % at 600 nm.[21]

The transmission characteristics in the infrared are of particular interest because highly conductive ITO films begin to absorb around 1000 nm.[9, 33] The infrared transmission values described by Hu *et al.* at 3 μm calculated for a 10 nm thick film of carbon nanotubes, graphene or ITO were 96, 75 and 73 %, respectively.[33] The RuO_2 sol-gel films described here maintain an average percent transmission from 56 % to 88 % at 3 μm and the transmission spectrum in the IR is nearly flat and featureless as seen in Figure 3.1. Infrared transmission values of the RuO_2 sol-gel films synthesized by Jeng *et al.* were not reported; however they did report the decrease in OH stretching modes in annealed films as compared to pre-annealed films, as we have observed here.[21]

The surface morphology of the sol-gel samples was investigated to characterize the uniformity of the as-prepared sol-gel films. Surface morphology can significantly impact the optical and electrochemical behavior of the deposited film. For example,

surface defects would create a discontinuity in the coating thereby increasing the resistance of the deposited films. AFM images are shown for a bare glass slide and a sol-gel film with the composition of 1.71:1 Ru:Si, Figure 3.3. The bare glass slide used as the substrate for the RuO_2 sol-gel films had an RMS surface roughness of 1.0 nm while the deposited and annealed RuO_2 sol-gel film had a measured RMS surface roughness of 0.7 nm. Height histograms are shown for the entire surface area of both samples. The bare glass slide had a broader topographical distribution compared to the sol-gel coated sample, which results in a larger RMS surface roughness value. The fact that these films are uniform and smooth across the measured area makes this material a promising transparent conductive film. Mapping the morphology of the films allows for the visualization of any defects present within the film, but does not provide any information on the composition at the surface of the film; for this we turned to XPS analysis.

The surface composition of the RuO_2 sol-gel films was quantified using XPS. XPS spectra were collected for films created with sol-gel solutions containing 0.83:1 Ru:Si, 1.71:1 Ru:Si and 3.43:1 Ru:Si withdrawn at rates of 8.5 cm/min and 4.2 cm/min. Initial survey scans were measured from 1200 to 0 eV at a pass energy of 160 eV to provide a broad compositional overview of the surface. In these survey scans, chlorine (binding energy between 199 – 269 eV)[34-35] is not detected as shown in Figure 3.4.

Individual binding energy regions were selected based on the survey scans in order to quantify the surface content of the formed films as shown in Figure 3.5. The Ru 3d doublet is depicted in Figure 3.5 for the 3.43:1 Ru:Si, 1.71:1 Ru:Si, and 0.83:1 Ru:Si sol-gel films. The Ru $3d_{5/2}$ peak at 280.5 eV has been previously assigned to RuO_2 and is the main ruthenium component within the synthesized films.[18, 36-38] The shoulder at

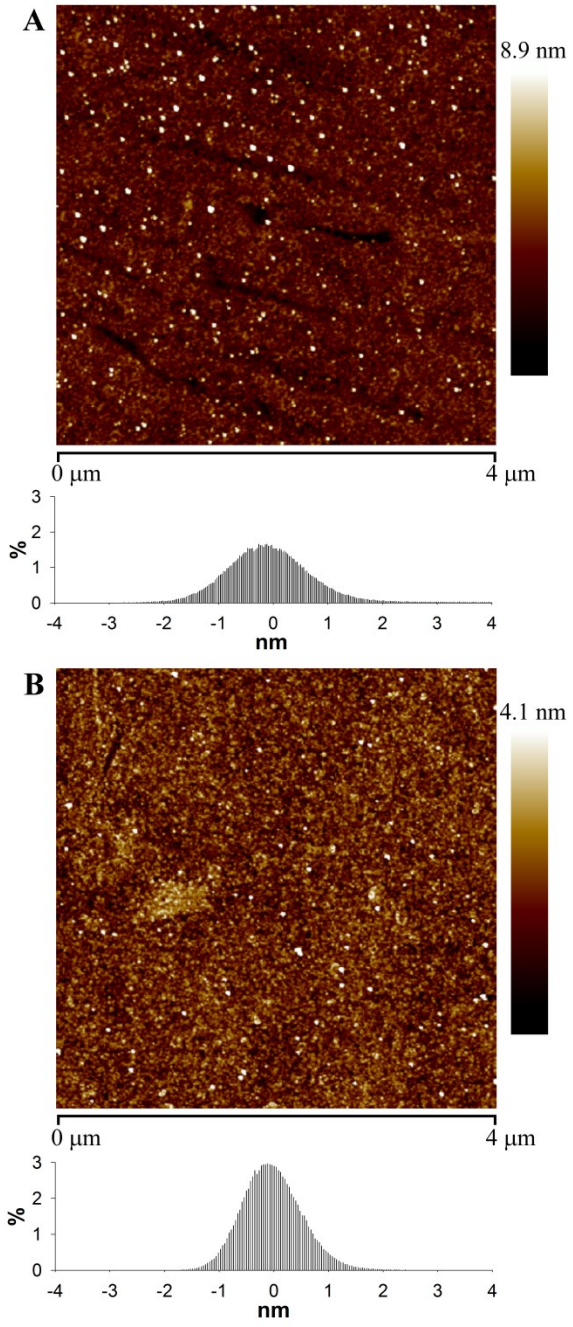

Figure 3.3: AFM images of A) a bare glass slide and B) a 1.71:1 Ru:Si sol-gel coated glass slide. Height histograms are shown for each of the collected images.

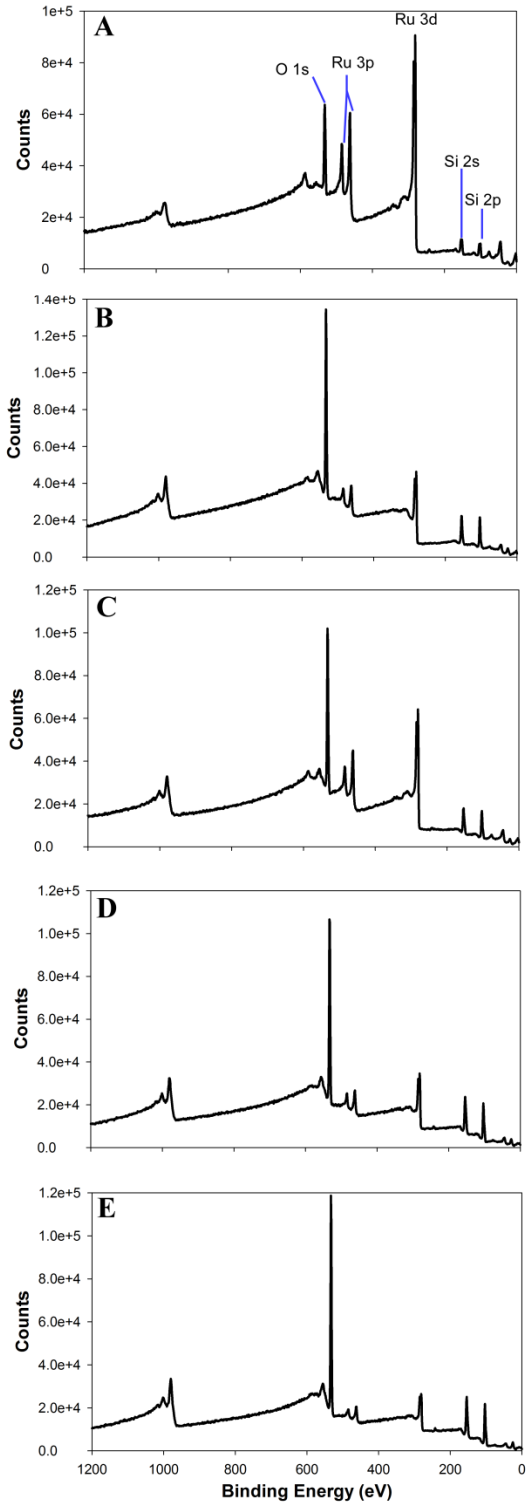

Figure 3.4: XPS survey scans for sol-gel films. A) 3.43:1 Ru:Si withdrawn at 8.5 cm/min, B) 1.71:1 Ru:Si withdrawn at 8.5 cm/min, C) 3.43:1 Ru:Si withdrawn at 4.2 cm/min, D) 1.71:1 Ru:Si withdrawn at 4.2 cm/min and E) 0.83:1 Ru:Si withdrawn at 8.5 cm/min. The present peaks are identified and chlorine was found to be nonexistent.

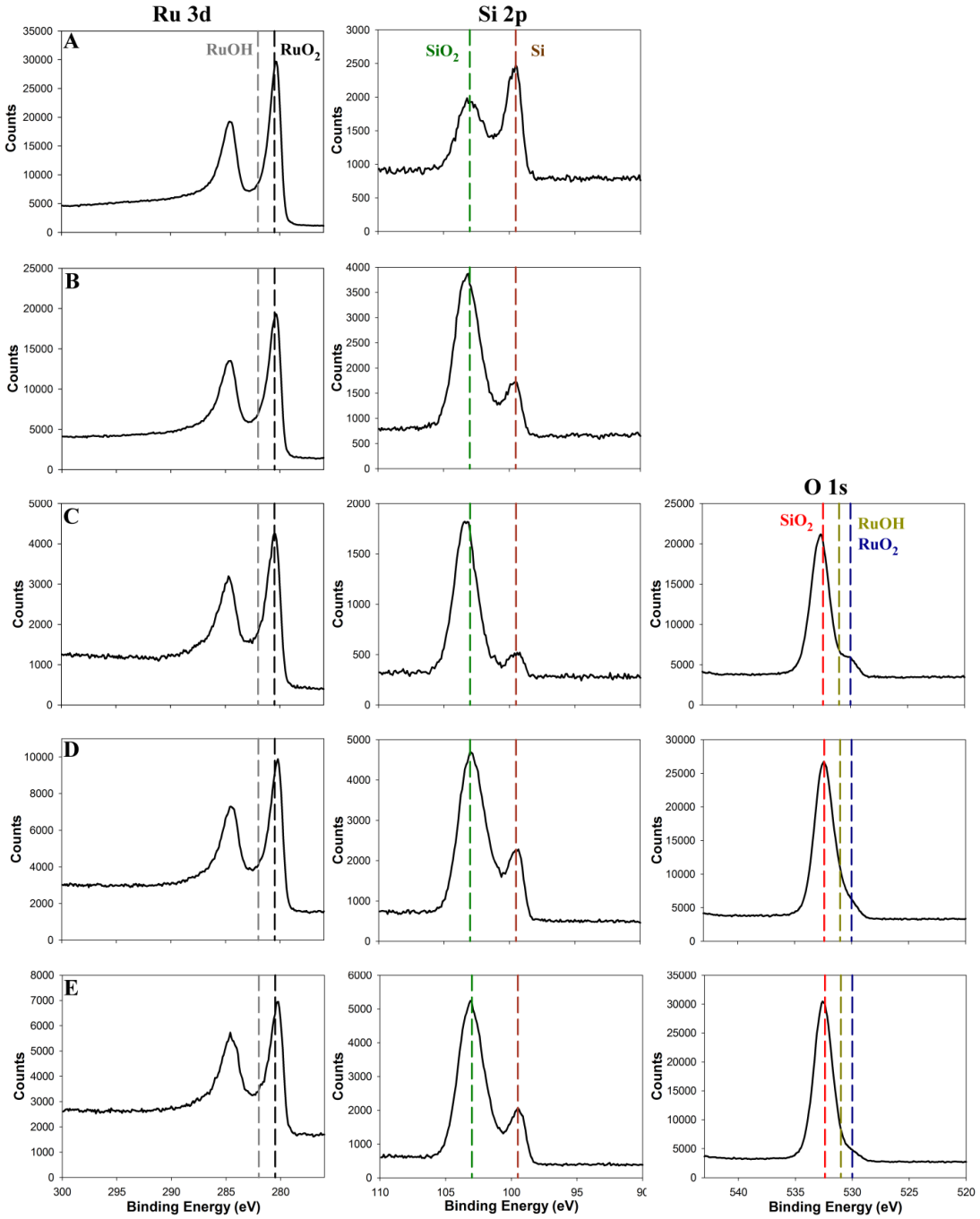

Figure 3.5: XPS spectra for the Ru 3d orbital , the Si 2p orbital , and the O 1s orbital for Ru:Si samples. A) 3.43:1 Ru:Si withdrawn at 8.5 cm/min, B) 1.71:1 Ru:Si withdrawn at 8.5 cm/min, C) 3.43:1 Ru:Si withdrawn at 4.2 cm/min, D) 1.71:1 Ru:Si withdrawn at 4.2 cm/min and E) 0.83:1 Ru:Si withdrawn at 8.5 cm/min.

282 eV is attributed to RuOH as previously reported by Chervin *et al.* for ruthenium nanoskins.[18] The peak at 285 eV is a composite of both Ru $3d_{3/2}$ and adventitious carbon on the surface.[18] The two peaks present within the Si 2p region are indicative of SiO_2 and Si metal located at 103 eV and 99 eV, respectively.[39-40] The Si metal peak is most likely due to exposure of the silicon wafer substrate after sputtering. The noticeable difference for the 3.43:1 Ru:Si sol-gel film withdrawn at 8.5 cm/min could be a result of measuring the bare substrate as this film had noticeable pore formations as imaged by AFM (data not shown). The O 1s binding energy at 532 eV is largely indicative of SiO_2 within the film with possible contributions from Si-OH.[18, 39, 41] The shoulder located at ~531 eV[18, 28, 38] is attributed to Ru-OH and RuO_2 which is consistent with the FTIR spectra discussed previously. As the ruthenium concentration increases within the film, the intensity of the shoulder at ~530 eV suggesting an increase in Ru-OH and RuO_2 species in the film. To determine the ratio of ruthenium and silica present at the surface, the excitation regions of the Ru 3d and Si 2p orbitals were measured. The Ru $3d_{5/2}$ and Si 2p peaks were fit with a Gaussian/Lorentzian function after the spectra were baseline corrected using Grams AI software.[42] Relative sensitivity factor (RSF) values were obtained from Briggs and Seah for Ru $3d_{5/2}$ and Si 2p.[42] The samples were cleaned by argon sputtering for 30 seconds to remove any adventitious carbon adsorption. After removal of any surface contaminants, the relative surface densities of Ru and Si were determined to be 0.4 ± 0.1:1 Ru:Si for films cast from the 1.71:1 Ru:Si solution and 1.0 ± 0.2:1 Ru:Si for films created from the 3.43:1 Ru:Si sol-gel solutions, respectively. These surface concentrations indicate that the surface is Si rich with the possibility of the majority of ruthenium being located below the analyzed depth.

In addition to the surface properties, the resistivity of the Ru sol-gel films was calculated from the resistance measured using a four wire technique at a temperature of 25 °C, with the calculated values listed in Table 3.1. The films withdrawn at 8.5 cm/min with molar solution ratios of 3.43:1 Ru:Si, 1.71:1 Ru:Si, 0.83:1 Ru:Si, 0.43:1 Ru:Si had resistivity values of 1.03×10^{-3}, 1.02×10^{-3}, 1.13 Ω·cm and >1 GΩ, respectively. These values indicate that the resistivity of the sol-gel films is relatively constant for films deposited from solutions with a composition ≥1.71:1 Ru:Si. The reported resistivity values are within the range reported by Jeng *et al.* for their 30:1 Ru:Si sol-gel films.[21] Jeng *et al.* annealed their films in a nitrogen atmosphere,[21] which is known to inhibit the growth of RuO_2 particles as confirmed by Shimamura *et al*.[43] The sol-gel films prepared here were annealed under ambient atmospheric conditions allowing the RuO_2 particles to expand in size and become fully oxidized. This increase in particle size creates more contacts throughout the films causing the resistivity to decrease. It is important to note that the film with the lowest resistivity has a transmission value of ~84 % at 600 nm, whereas the transmission achieved be Jeng *et al*.'s film of lowest resistivity of $\sim 9 \times 10^{-4}$ Ω·cm was ~55 % at 600 nm.[21] The RuO_2 sol-gel film with a solution composition of 1.71:1 Ru:Si, which was withdrawn at a rate of 8.5 cm/min is a prime candidate for spectroelectrochemical experiments due to the high optical transmission (>70%) throughout the visible region, and a modest resistivity of 1.02×10^{-3} Ω·cm. In addition, sol-gel films prepared with this composition and withdrawal speed also possess the greatest surface uniformity as confirmed by AFM measurements.

The electrochemical potential window of the synthesized sol-gel films was measured in a 0.1 M potassium chloride solution. The potential was scanned from -0.45

to + 0.65 V versus a Ag|AgCl reference electrode. CVs were recorded at scan rates of 50, 20, and 0.5 mV/s and are reported in Figure 3.6.

The results in Figure 3.6 indicate that the synthesized films are capable of interrogating a wide range of electrochemical reactions as there is an approximate potential window of 1.2 V. The films behaved similarly to previously reported RuO_2 materials.[17-18] There is a linear correlation between the scan rate and the measured capacitive response. This is congruent with previously reported measurements by Rolison *et al.*[18] These results allowed for further characterizing the electrochemical performance of the synthesized ruthenium sol-gel films.

The electrochemical performance of the sol-gel films was tested by measuring the reversible electrochemistry of a solution containing 0.9 mM ferrocenemethanol in 100 mM NaCl supporting electrolyte by cyclic voltammetry. The results were compared against cyclic voltammograms of ferrocenemethanol recorded with a platinum electrode (area = 2.011 mm^2) and have been normalized to the electroactive area of either the Pt WE or the RuO_2 sol-gel electrodes (area = 4.8 cm^2) depending on which electrode was the active working electrode. The recorded CVs (Figure 3.7) measured with the RuO_2 working electrodes were mathematically corrected to compensate for the resistance of the electrode using the values reported previously. The measured half-wave potential ($E_{1/2}$) for ferrocenemethanol at a Pt electrode was $E_{1/2}$ = 211 ± 2 mV versus Ag|AgCl and the peak separation measured for the Pt electrode was ΔE = 69 ± 2 mV. This value is above the value of ΔE = 59 mV for a one electron process due to the inherent solution resistance and possible surface contaminants that remained after the reported cleaning processes. The RuO_2 sol-gel electrode was cleaned in Piranha solution to remove any surface

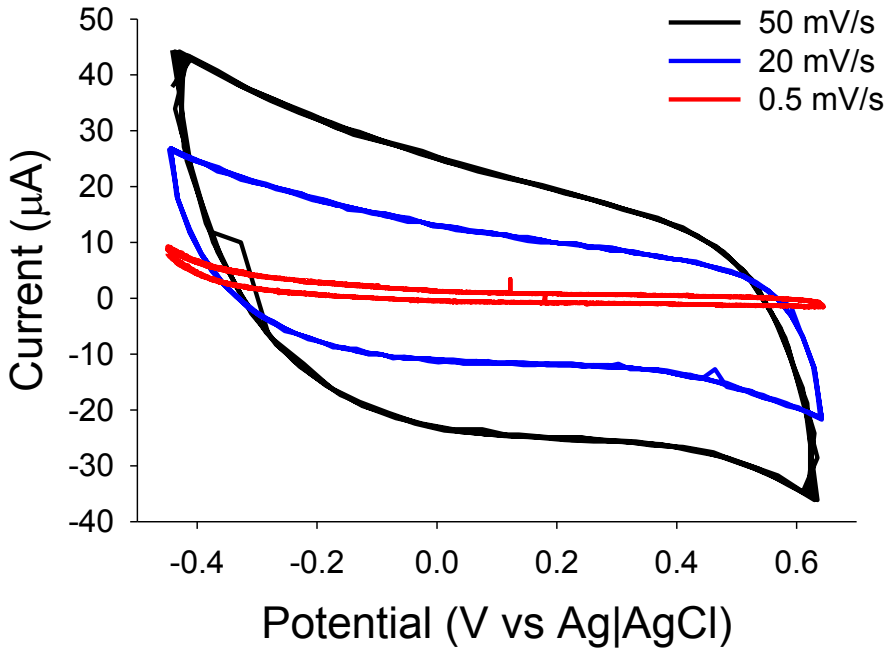

Figure 3.6: Electrochemical potential window of the synthesized RuO_2 sol-gel films in 0.1 M KCl. Scan rates were 50, 20, and 0.5 mV/s second as indicated by the black, blue and red lines, respectively.

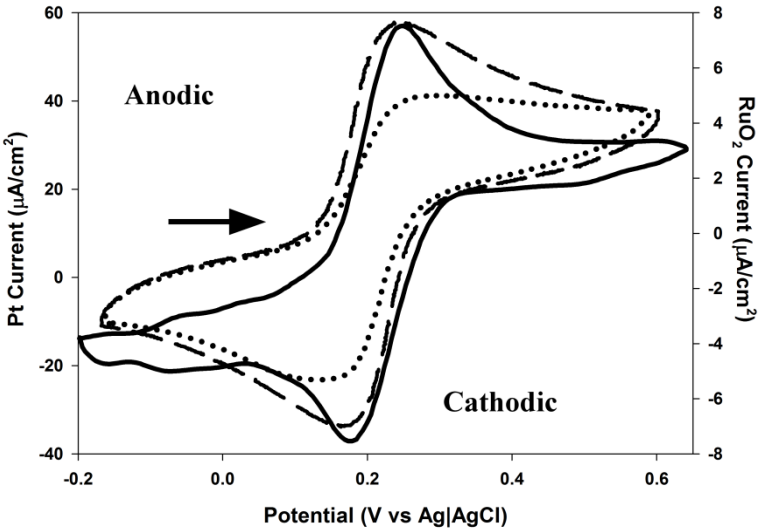

Figure 3.7: Cyclic voltammograms of FcMeOH using platinum, RuO_2 sol-gel films, and piranha treated RuO_2 sol-gel films as working electrodes. The solid line (—) is the CV collected with a Pt WE at a scan rate of 5 mV/s in 0.9 mM FcMeOH. The dotted line (·····) is a CV collected using a RuO_2 sol-gel film as the WE. The dashed line (- - -) is a CV of the same RuO_2 sol-gel film after repeated cleanings in a Piranha solution. Scan direction is indicated by the arrow.

contaminants and CVs were recorded after each cleaning until the measured current stabilized. The final CV is shown in Figure 3.7 after the fifth consecutive cleaning in Piranha solution where the measured half-wave potential was $E_{1/2}$ = 206 ± 1 mV with a peak separation of ΔE = 83 ± 1 mV. Similar electrochemical behavior for RuO_2 films has been demonstrated by Chervin *et al.* for RuO_2 particles deposited onto silica paper where they reported a peak separation of 76 mV for the reduction and oxidation peaks of ferricyanide.[17] The difference in the peak separation values between the Pt and RuO_2 sol-gel working electrodes can be attributed to the inherent capacitance of RuO_2. The electroactive area for the clean RuO_2 sol-gel electrodes was calculated to be 32.0 ± 0.6%. This value was determined by integrating the normalized cathodic peak current for ferrocenemethanol recorded using the RuO_2 sol-gel electrode and then dividing this value by the integrated normalized cathodic current measured with a Pt working electrode. This value is consistent with the surface concentration of ruthenium determined by the previously described XPS measurements. These measurements yielded a value for the surface concentration of ruthenium to be 30 ± 4 %.

The mechanical and chemical stability of the synthesized RuO_2 sol-gel electrodes was tested by physical abrasion and multiple cleanings in highly oxidative Piranha solution, respectively. Physical abrasive tests including vigorously rubbing the substrate with a methanol soaked cloth and mechanical polishing using Buehler's Master Polish 2. The RuO_2 sol-gel films withstood rubbing with a methanol soaked cloth without any change in visible appearance or conductivity as measured by a 2-point probe. When mechanically polished by hand, the RuO_2 coatings required a period of time on the order of hours before complete removal of the sol-gel film from the substrate. The mechanical

stability of the RuO_2 sol-gel films prepared here is similar to that observed for other thin conducting oxides such as ITO. However the RuO_2 sol-gel films exhibit superior mechanical stability compared to carbon nanotubes[44] or graphene[45] films, which can peel away from the substrate under fluid flow. Exposing the RuO_2 sol-gel films to highly acidic Piranha solution did not damage the integrity of the films, but instead, increased the electrochemical efficiency of the sol-gel films, as noted in the electrochemical experiments discussed above. The chemical stability of the synthesized RuO_2 films is exceptional compared to ITO which is known to easily etch in 0.2 M HCl.[46] When exposed to highly oxidizing Piranha solution, it was found that multiwalled carbon nanotubes become more oxidized and fragmented.[47] The oxidation of graphene films is known to proceed rapidly for single layer films when exposed to O_2 at temperatures < 300 °C.[48] This oxidation causes holes in the film and can lead to irreversible damage.[48] The RuO_2 sol-gel films presented in this study exhibit outstanding mechanical and chemical stability, making them an appealing alternative to current thin film transparent conductive electrodes when a high level of robustness is required.

The ability of these electrodes to be used as substrates for spectroelectrochemistry experiments was also demonstrated. The RuO_2 sol-gel electrode was positioned at normal incidence to the light source in the UV-Vis spectrometer. The spectrophotometer was configured in a double beam arrangement with an identical RuO_2 sol-gel electrode in 100 mM NaCl supporting electrolyte solution placed in the reference path to ensure that the measured response was due to redox changes to ferrocenemethanol and not the electrode itself. By monitoring the absorbance from 500 to 800 nm it was possible to observe the absorbance of the oxidized ferrocenemethanol species (FcMeOH+) at around

~625 nm.[49] The reduced form of ferrocenemethanol (FcMeOH) does not absorb within this region. Prior to recording spectra, the potential was cycled three times to establish a chemical equilibrium between FcMeOH and FcMeOH+. Figure 3.8 depicts the results of the spectroelectrochemistry experiments. These data are plotted as a function of the change in absorbance (z-axis) versus wavelength (x-axis) as the applied potential is scanned (y-axis). At negative applied potential there is depletion in concentration of FcMeOH+ relative to the equilibrium concentration resulting in a negative value for the change in absorbance. As the scanned applied potential approaches the oxidation potential of E_{ox} = 247 ± 7 mV, evolution of FcMeOH+ starts to occur. This evolution increases drastically past E_{ox} continuing to increase the concentration of FcMeOH+ yielding an increase in the measured change in absorbance. The absorbance continues to increase as the potential is reversed until the reduction potential E_{red} = 164 ± 6 mV is approached. At this point, FcMeOH+ will become depleted as FcMeOH predominates in solution. The evolution of FcMeOH causes a decrease in the change in absorbance at ~625 nm as FcMeOH+ is depleted from the system. The absorbance continues to decrease as the potential remains negative of E_{ox} due to the decrease in concentration of FcMeOH. This spectroelectrochemical behavior continues as the potential is cycled. The application of the RuO_2 sol-gel films as electrodes in spectroelectrochemistry demonstrates the utility of these novel robust optically transparent conductive materials.

3.4 Summary

The RuO_2 sol-gel films synthesized in this chapter indicate promising potential for future implementation into a variety of optically transparent conductive devices. The

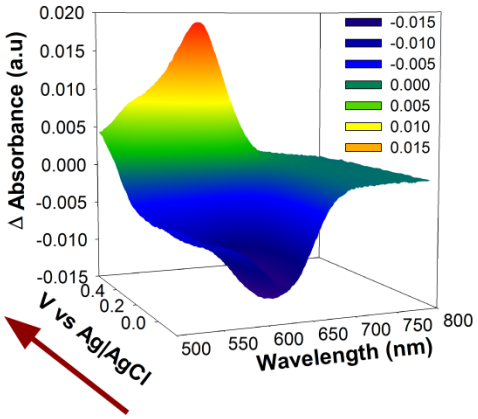

Figure 3.8: 3D spectra of absorbance versus wavelength and applied potential for a RuO_2 sol-gel electrode in 0.9 mM FcMeOH with 100 mM NaCl supporting electrolyte. The scan direction is indicated by the arrow. The evolution and depletion of oxidized FcMeOH+ are observable by the increase and decrease in absorbance as the applied potential is scanned.

optical transmission characteristics of these films are comparable to current alternative technologies and range from 70 to >90% in the visible region and from 50 to 90% in the infrared region. The infrared transmission profile is particularly impressive as no noticeable absorption occurs from 2000 to 4000 cm^{-1} making these films suitable for studying the effect of an applied potential on molecular chemistry in this region. The resistivity of these RuO_2 sol-gel films is easily tailored and is mostly dependent on the Ru precursor concentration and withdraw rate used for dip coating. The reported resistivity ranged from 1.134 to 1.02 x 10^{-3} Ω·cm allowing for efficient use of these films as electrodes. The films are very robust and maintain their electrochemical integrity after multiple consecutive exposures to extreme acidic, oxidative environments. These films are viable alternatives for use in spectroelectrochemistry and optoelectronics because of their low cost, long-term stability and high performance as transparent electrodes. Finally, these films are appealing for use with biological materials due to the described chemical structure.

3.5 References

1. Granqvist, C. G., Transparent Conductors as Solar Energy Materials: A Panoramic Review. *Sol. Energy Mater. Sol. Cells* **2007,** *91* , 1529-1598.

2. Fahland, M.; Karlsson, P.; Charton, C., Low Resistivity Transparent Electrodes for Displays on Polymer Substrates. *Thin Solid Films* **2001,** *392* , 334-337.

3. Kim, H.; Gilmore, C. M.; Pique, A.; Horwitz, J. S.; Mattoussi, H.; Murata, H.; Kafafi, Z. H.; Chrisey, D. B., Electrical, Optical, and Structural Properties of Indium-Tin-Oxide Thin Films for Organic Light-Emitting Devices. *J. Appl. Phys.* **1999,** *86* , 6451-6461.

4. Kim, H.; Horwitz, J. S.; Kushto, G.; Pique, A.; Kafafi, Z. H.; Gilmore, C. M.; Chrisey, D. B., Effect of Film Thickness on the Properties of Indium Tin Oxide Thin Films. *J. Appl. Phys.* **2000,** *88* , 6021-6025.

5. Tak, Y.-H.; Kim, K.-B.; Park, H.-G.; Lee, K.-H.; Lee, J.-R., Criteria for ITO Thin Films as the Bottom Electrode of an Organic Light Emitting Diode. *Thin Solid Films* **2002,** *411* , 12-16.

6. Minami, T., Present Status of Transparent Conducting Oxide Thin-Film Development for Indium-Tin-Oxide (ITO) Substitutes. *Thin Solid Films* **2008,** *516* , 5822-5828.

7. de, H. W. A.; Bacsa, W. S.; Chatelain, A.; Gerfin, T.; Humphrey-Baker, R.; Forro, L.; Ugarte, D., Aligned Carbon Nanotube Films: Production and Optical and Electronic Properties. *Science (Washington, D. C.)* **1995,** *268* , 845-7.

8. Donner, S.; Li, H.-W.; Yeung, E. S.; Porter, M. D., Fabrication of Optically Transparent Carbon Electrodes by the Pyrolysis of Photoresist Films: Approach to Single-Molecule Spectroelectrochemistry. *Analytical Chemistry* **2006,** *78* (8), 2816-2822.

9. Hecht, D. S.; Hu, L.-B.; Irvin, G., Emerging Transparent Electrodes Based on Thin Films of Carbon Nanotubes, Graphene, and Metallic Nanostructures. *Adv. Mater. (Weinheim, Ger.)* **2011,** *23* , 1482-1513.

10. Mattevi, C.; Eda, G.; Agnoli, S.; Miller, S.; Mkhoyan, K. A.; Celik, O.; Mastrogiovanni, D.; Granozzi, G.; Garfunkel, E.; Chhowalla, M., Evolution of Electrical, Chemical, and Structural Properties of Transparent and Conducting Chemically Derived Graphene Thin Films. *Adv. Funct. Mater.* **2009,** *19* , 2577-2583.

11. Watcharotone, S.; Dikin, D. A.; Stankovich, S.; Piner, R.; Jung, I.; Dommett, G. H. B.; Evmenenko, G.; Wu, S.-E.; Chen, S.-F.; Liu, C.-P.; Nguyen, S. T.; Ruoff, R. S., Graphene-Silica Composite Thin Films as Transparent Conductors. *Nano Lett.* **2007,** *7* , 1888-1892.

12. Wu, J.; Agrawal, M.; Becerril, H. A.; Bao, Z.; Liu, Z.; Chen, Y.; Peumans, P., Organic Light-Emitting Diodes on Solution-Processed Graphene Transparent Electrodes. *ACS Nano* **2010,** *4* , 43-48.

13. Zheng, Q. B.; Gudarzi, M. M.; Wang, S. J.; Geng, Y.; Li, Z.; Kim, J.-K., Improved Electrical and Optical Characteristics of Transparent Graphene Thin Films Produced by Acid and Doping Treatments. *Carbon* **2011,** *49* , 2905-2916.

14. Over, H., Surface Chemistry of Ruthenium Dioxide in Heterogeneous Catalysis and Electrocatalysis: From Fundamental to Applied Research. *Chem. Rev. (Washington, DC, U. S.)* **2012,** *112* , 3356-3426.

15. Gujar, T. P.; Shinde, V. R.; Lokhande, C. D.; Kim, W.-Y.; Jung, K.-D.; Joo, O.-S., Spray Deposited Amorphous RuO2 for an Effective Use in Electrochemical Supercapacitor. *Electrochem. Commun.* **2007,** *9* , 504-510.

16. Patake, V. D.; Lokhande, C. D., Chemical Synthesis of Nano-Porous Ruthenium Oxide (RuO2) Thin Films for Supercapacitor Application. *Appl. Surf. Sci.* **2008,** *254* , 2820-2824.

17. Chervin, C. N.; Lubers, A. M.; Pettigrew, K. A.; Long, J. W.; Westgate, M. A.; Fontanella, J. J.; Rolison, D. R., Making the Most of a Scarce Platinum-Group Metal: Conductive Ruthenia Nanoskins on Insulating Silica Paper. *Nano Lett.* **2009,** *9* , 2316-2321.

18. Chervin, C. N.; Lubers, A. M.; Long, J. W.; Rolison, D. R., Effect of Temperature and Atmosphere on the Conductivity and Electrochemical Capacitance of Single-Unit-Thick Ruthenium Dioxide. *J. Electroanal. Chem.* **2010,** *644* (2), 155-163.

19. Long, J. W.; Owrutsky, J. C.; Chervin, C. N.; Rolison, D. R.; Melinger, J. S. Coating an Insulating Substrate With a Transparent Conducting RuO2 Coating. WO2011066488A1, 2011.

20. Rolison, D. R.,U.S. Naval Research Laboratories, Washington, DC. Personal Communication. May 2011.

21. Jeng, J.-S.; Lin, Y.-T.; Chen, J. S., Preparation and Characterization of Transparent Semiconductor RuO2–SiO2 Films Synthesized by Sol–Gel Route. *Thin Solid Films* **2010,** *518* (19), 5416-5420.

22. Brinker, C. J.; Hurd, A. J.; Frye, G. C.; Shunk, P. R.; Ashley, C. S., Sol-Gel Thin Film Formation. *Nippon Seramikkusu Kyokai Gakujutsu Ronbunshi* **1991,** *99* , 862-77.

23. Brinker, C. J., Scherer, George W., *Sol-Gel Science*. Academic Press, Inc.: San Diego, CA, 1990.

24. Yang, L.; Saavedra, S. S., Chemical Sensing Using Sol-Gel Derived Planar Waveguides and Indicator Phases. *Anal. Chem.* **1995,** *67* , 1307-14.

25. Yang, L.; Saavedra, S. S.; Armstrong, N. R.; Hayes, J., Fabrication and Characterization of Low-Loss, Sol-Gel Planar Waveguides. *Anal. Chem.* **1994,** *66* , 1254-63.

26. Neumann, R.; Khenkin, A. M., Noble Metal (RuIII, PdII, PtII) Substituted "Sandwich" Type Polyoxometalates: Preparation, Characterization, and Catalytic Activity in Oxidations of Alkanes and Alkenes by Peroxides. *Inorg. Chem.* **1995,** *34* (23), 5753-5760.

27. Kitamura, R.; Pilon, L.; Jonasz, M., Optical Constants of Silica Glass from Extreme Ultraviolet to Far Infrared at Near Room Temperature. *Appl. Opt.* **2007,** *46*, 8118-8133.

28. Ferrere, S.; A. Gregg, B., Chloride Oxidation Catalysis by a Polymeric Oxide Derived from [Ru(4,4[prime or minute]-dimethyl-2,2[prime or minute]-bipyridine)(Cl)3(H2O)]. *J. Chem. Society, Farad. Trans.* **1998,** *94* (18), 2827-2833.

29. Patil, U. M.; Kulkarni, S. B.; Jamadade, V. S.; Lokhande, C. D., Chemically Synthesized Hydrous RuO2 Thin Films for Supercapacitor Application. *J. Alloys Compd.* **2011,** *509* (5), 1677-1682.

30. Park, S. K.; Kanjolia, R.; Anthis, J.; Odedra, R.; Boag, N.; Wielunski, L.; Chabal, Y. J., Atomic Layer Deposition of Ru/RuO2 Thin Films Studied by In Situ Infrared Spectroscopy. *Chem. Mater.* **2010,** *22* (17), 4867-4878.

31. Zhu, H.; Ma, Y.; Fan, Y.; Shen, J., Fourier Transform Infrared Spectroscopy and Oxygen Luminescence Probing Combined Study of Modified Sol-Gel Derived Film. *Thin Solid Films* **2001,** *397* , 95-101.

32. Tian, R.; Seitz, O.; Li, M.; Hu, W.; Chabal, Y. J.; Gao, J., Infrared Characterization of Interfacial Si-O Bond Formation on Silanized Flat SiO2/Si Surfaces. *Langmuir* **2010,** *26* , 4563-4566.

33. Hu, L.; Hecht, D. S.; Gruener, G., Infrared Transparent Carbon Nanotube Thin Films. *Appl. Phys. Lett.* **2009,** *94* , 081103/1-081103/3.

34. Kim, Y. I.; Hatfield, W. E., Electrical, Magnetic and Spectroscopic Properties of Tetrathiafulvalene Charge Transfer Compounds with Iron, Ruthenium, Rhodium and Iridium Halides. *Inorg. Chim. Acta* **1991,** *188* , 15-24.

35. Pollini, I., Photoemission Study of the Electronic Structure of CrCl3 and RuCl3 Compounds. *Phys. Rev. B: Condens. Matter* **1994,** *50* , 2095-103.

36. Chan, H. Y. H.; Takoudis, C. G.; Weaver, M. J., High-Pressure Oxidation of Ruthenium as Probed by Surface-Enhanced Raman and X-ray Photoelectron Spectroscopies. *J. Catal.* **1997,** *172* , 336-345.

37. Iwasaki, Y.; Izumi, A.; Tsurumaki, H.; Namiki, A.; Oizumi, H.; Nishiyama, I., Oxidation and Reduction of Thin Ru Films by Gas Plasma. *Appl. Surf. Sci.* **2007,** *253* , 8699-8704.

38. Kim, K. S.; Winograd, N., X-ray Photoelectron Spectroscopic Studies of Ruthenium-Oxygen Surfaces. *J. Catal.* **1974,** *35* , 66-72.

39. Miller, M. L.; Linton, R. W., X-ray Photoelectron Spectroscopy of Thermally Treated SiO_2. *Anal. Chem.* **1985,** (57), 2314-2319.

40. Sirotti, F.; DeSantis, M.; Rossi, G., Synchrotron-Radiation Photoemission and X-ray Absorption of Iron Silicides. *Phys. Rev. B: Condens. Matter* **1993,** *48* , 8299-306.

41. Barr, T. L., An ESCA Study of the Termination of the Passivation of Elemental Metals. *J. Phys. Chem.* **1978,** *82* , 1801-10.

42. Briggs, D., Seah, M. P., *Practical Surface Analysis*. Second ed.; John Wiley and Sons: Chichester, England, 1996; Vol. 1: Auger and X-ray Photoelectron Spectroscopy.

43. Shimamura, A.; Huebert, T.; Thust, H., Characterization of Sol-Gel Derived Glass Composite Thin Films. *Surf. Interface Anal.* **2004,** *36* , 1207-1209.

44. Su, H.-C.; Chen, C.-H.; Chen, Y.-C.; Yao, D.-J.; Chen, H.; Chang, Y.-C.; Yew, T.-R., Improving the Adhesion of Carbon Nanotubes to a Substrate Using Microwave Treatment. *Carbon* **2010,** *48* , 805-812.

45. Soldano, C.; Mahmood, A.; Dujardin, E., Production, Properties and Potential of Graphene. *Carbon* **2010,** *48* , 2127-2150.

46. Minami, T., Transparent Conducting Oxide Semiconductors for Transparent Electrodes. *Semicond. Sci. Technol.* **2005,** *20* , S35-S44.

47. Datsyuk, V.; Kalyva, M.; Papagelis, K.; Parthenios, J.; Tasis, D.; Siokou, A.; Kallitsis, I.; Galiotis, C., Chemical Oxidation of Multiwalled Carbon Nanotubes. *Carbon* **2008,** *46* (6), 833-840.

48. Liu, L.; Ryu, S.; Tomasik, M. R.; Stolyarova, E.; Jung, N.; Hybertsen, M. S.; Steigerwald, M. L.; Brus, L. E.; Flynn, G. W., Graphene Oxidation: Thickness-Dependent Etching and Strong Chemical Doping. *Nano Lett.* **2008,** *8*, 1965-1970.

49. Zhu, Z.; Wang, M.; Gautam, A.; Nazor, J.; Morneu, C.; Prodanovic, R.; Schwaneberg, U., Directed Evolution of Glucose Oxidase from Aspergillus Niger for Ferrocenemethanol-Mediated Electron Transfer. *Biotechnol. J.* **2007,** *2*, 241-248.

CHAPTER 4

CHARACTERIZING PLANAR SUPPORTED LIPID BILAYER FORMATION USING SUM-FREQUENCY VIBRATIONAL SPECTROSCOPY

4.1 Introduction

Previous chapters of this dissertation have discussed the importance of using model membranes to investigate the biophysical and biochemical processes that occur within cell membranes. Chapter 2 discussed the influence of the structure of cholesterol on phospholipid flip-flop using membranes formed by the Langmuir Blodgett/Langmuir Schaefer (LB/LS) deposition technique. One other widely implemented technique for creating model lipid membranes entails deposition and rupture of vesicles in solution onto a planar support. This method originated in the mid 1980s and has been widely studied and utilized for the past 20 years.[1] Using vesicles as a model for membrane research, as compared to planar membranes, presents a number of unique differences due to the physical and geometrical properties of vesicles. Decreasing the size of a vesicle can impose stresses on the vesicle from an increased radius of curvature. There is also a greater potential energy for rupture as vesicle size is decreased.[2-3] In biological cells varying curvatures of the membrane can be used to help control differing membrane lipid compositions by requiring that lipids inducing curvature be contained on the inner leaflet

of the membrane and more cylindrically shaped lipids be contained on the outer leaflet of the membrane.[4] The effect of varying membrane curvature also can help regulate the placement and function of integral membrane proteins within the cell membrane. Membrane curvature has also been investigated in pure vesicle systems and has been found to influence cholesterol movement, binding of ligands and protein function.[5-8] However, a difficulty in these model systems is that they can be unstable and rupture over the duration of an experiment.[9-10] Planar supported lipid bilayers (PSLBs) are an alternative model used to study lipid components of the plasma membrane and are more stable over time than vesicles or liposomes.[9-10] There are two widely implemented methods of making planar supported lipid bilayers. The vesicle fusion technique uses a solution of vesicles that spontaneously fuses to the substrate to form a lipid membrane, while the other method uses the Langmuir-Blodgett and Langmuir-Schaefer (LB/LS) deposition technique to create lipid membranes allowing for precise control over the packing density and lipid composition.[9-10]

The process of vesicle fusion has been investigated for decades by a number of researchers. For example Nollert *et al.* examined vesicle fusion using fluorescence spectroscopy and concluded that some vesicles fuse and spread whereas others stay adsorbed without fusing.[11] Keller and Kasemo observed that bilayer formation is preceded by initial vesicle adsorption using a quartz crystal microbalance (QCM).[12] Jass *et al.* proposed a mechanism where vesicles adsorbed to a surface then proceeded to flatten out until completely collapsed thereby forming a double bilayer structure. They proposed that this structure transitions to a single bilayer structure with one layer sliding or rolling off the other onto the supporting substrate based on observed results using

atomic force microscopy (AFM).[13] Further work using AFM by Reviakine and Brisson supported the earlier studies by Keller whereby vesicles fuse, then rupture to form bilayers.[1] This work also proposed that rupture would only occur for vesicles with a radius ≤ ~ 75 nm and was defined as the critical radius for fusion.[1] Subsequent research by Reimult *et al.* suggested that larger vesicles than reported by Reviakine and Brisson spread more than small vesicles upon adsorption on silica resulting in rupture and bilayer formation.[3] The work by Reimult also demonstrated a correlation between temperature and bilayer formation with more uniform bilayers being formed at higher temperatures above the phase transition temperature.[3] More recently, Jing *et al.* used QCM with dissipation monitoring (QCM-D) and showed that vesicle fusion will occur independent of vesicle size when heated using vesicles with diameters of 90 and 160 nm.[14] The mechanism hypothesized by Jing and coworkers corresponded to an adsorption event, flattening, and finally rupture. Beyond size and concentration of vesicles in solution impacting the formation of supported lipid membranes, the influence of vesicle curvature,[15-16] and vesicle – substrate electrostatic interactions[17] on membrane formation have been investigated. These studies reported that membrane formation does not occur with highly curved vesicles, at low vesicle solution concentrations, at low temperatures or at low ionic strength.[15-17] The information from these previous studies helped scientists understand what experimental conditions were necessary to create planar supported lipid membranes. These techniques have provided a wealth of information about the overall influence of vesicle size and fusion conditions and their respective influence on bilayer surface coverage but are not able to provide more discrete information of the lipid organization within the inherent bilayer structure.

Information that would benefit lipid studies includes the potential difference in lipid number between the proximal and distal leaflet resulting from the inherent vesicle geometry. Knowing this information would provide an answer to a critical omission in the mechanism of vesicle fusion to form planar bilayers along with providing a better understanding of the interplay of fusing lipids with biological membranes in vivo. Compared with previous techniques, SFVS is advantageous for use in studying the formed planar bilayers through vesicle fusion as it is sensitive to the lipid density and absolute orientation of lipids of each leaflet in the bilayer.[18] By investigating planar bilayers formed through vesicle fusion with SFVS it is possible to discern the lipid distribution in the formed bilayers as may be predetermined by the vesicle sizes in solution.

SFVS has been thoroughly described previously in the literature[19-22] and also in Chapter 2. As a reminder, SFVS possesses inherent symmetry constraints thereby resulting in no measureable signal from bulk isotropic solutions. However, an SFVS signal may be detected when a material is anisotropic or at an interface. SFVS has been utilized to determine the leaflet location of cholesterol in cholesterol rich (60 mol %) lipid membranes[23] as well as the induction of asymmetry when a positively charged polypeptide is associated with a negatively charged membrane surface.[24] The observeable SFVS signal results from a nonzero value of the effective second order nonlinear susceptibility tensor, $\chi_{eff}^{(2)}$, which for a lipid membrane. When considering the methyl symmetric stretch mode (CH_3 ν_3), $\chi_{eff}^{(2)}$ is defined by the following equation:

$$\chi_{eff}^{(2)} = \frac{N_{distal}}{\epsilon_0}\langle\beta_{ijk}^{CH_3\nu_s}\rangle - \frac{N_{proximal}}{\epsilon_0}\langle\beta_{ijk}^{CH_3\nu_s}\rangle + \chi_{NR}^{(2)} \quad (4.1)$$

where N_{distal} and $N_{proximal}$ describe the number of lipids in the distal and proximal leaflets,

respectively, β is the molecular hyperpolarizibility, the bra-ket notation represents the average molecular orientation of molecules with respect to the surface normal and ε_0 is the vacuum permittivity constant. For an ideal bilayer where the lipid composition is the same in both leaflets, it is expected that $\chi^{(2)}$ is zero as oppositely oriented vibrational modes in each leaflet will cancel. However, if there is a population difference between the two leaflets of the membrane, then a measureable amount of signal may be observed. The population difference in a membrane can be quantified in terms of percent asymmetry as calculated from the square root of the measured intensity by the equation:[18, 23-24]

$$\%\, AS = \frac{\sqrt{I_{CH_3\nu_S}}}{\sqrt{I_{max}^{CH_3\nu_S}}} * 100\% \qquad (4.2)$$

where $I_{CH_3\nu_S}$ is defined as the intensity of the terminal methyl symmetric stretch (CH_3 ν_s) and $I_{max}^{CH_3\nu_S}$is the maximum signal intensity obtained from a completely asymmetric bilayer. Equations 1 and 2 describe how SFVS can measure differences in the number of lipid molecules between leaflets allowing for any offset in lipid number between leaflets of vesiclely fused membranes to be quantified.

The scope of these studies is to demonstrate that the geometrical differences between leaflets in phospholipid vesicles in solution correlate to an asymmetrical population difference between leaflets of the formed planar supported bilayers when vesicles fuse and rupture. Sum-frequency is capable of distinguishing differences in leaflet lipid density due to the coherent nature of the technique itself and is highly dependent on the symmetry of the system investigated.

4.2 Experimental

4.2.1 Materials

1,2-Dipalmitoyl-sn-glycero-3-phosphocholine (DPPC), 1,2-dipalmitoyl-d62-sn-glycero-3-phosphocholine (DPPCd62), and 1-palmitoyl-2-{12-[(7-nitro-2-1,3-benzoxadiazol-4-yl)amino]dodecanoyl}-*sn*-glycero-3-phosphocholine (NBD-PC) were purchased from Avanti Polar Lipids, Inc. (Alabaster, Alabama) and were used without further purification. Sodium perchlorate ($NaClO_4$) and ruthenium trichloride x-hydrate ($RuCl_3 \bullet xH_2O$) were obtained from Alfa Aesar (Ward Hill, Massachusetts). *Caution: $RuCl_3 \cdot xH_2O$ causes severe skin burns and eye damage upon contact; proper protection should be used when handling this product*. Deuterium oxide (D_2O), anhydrous chloroform (≥99% $CHCl_3$ with 0.5-1% ethanol as a stabilizer), methyltriethoxysilane (MTES) and silicon tetrachloride ($SiCl_4$) were purchased from Sigma Aldrich (St. Louis, Missouri). *Caution: MTES is a flammable liquid and should be kept away from ignition sources. $SiCl_4$ is extremely toxic when inhaled; handle this material under proper ventilation conditions.* Absolute ethanol (EtOH, 200 proof) was purchased from Decon Laboratories (King of Prussia, Pennsylvania). Sodium chloride (NaCl) and anhydrous dibasic sodium phosphate (Na_2HPO_4) were purchased from Fisher Scientific (Pittsburgh, PA). Monobasic sodium phosphate monohydrate ($NaH_2PO_4 \bullet H_2O$) was obtained from Macron Chemicals (Center Valley, PA). A Nanopure Infinity Ultrapure water system (Barnstead Thermolyne, Dubuque, Iowa) was used for all the reported studies and had a minimum resistivity of 18.2 MΩ cm. Phosphate buffered saline (PBS) was prepared from 100 mM NaCl, 10 mM $NaH_2PO_4 \bullet H_2O$, and 40 mM NaH_2PO_4 in nanopure water and adjusted to a pH of 7.4 ± 0.1 using 4 M sodium hydroxide (NaOH) and 1 M hydrochloric

acid (HCl). Premiere brand microscope slides were purchased from C & A Scientific (Manassas, Virginia) and quartz cover slips were purchased from Esco Optics (Oak Ridge, New Jersey). Ultraviolet grade fused silica prisms were purchased from both Almaz Optics (Marlton, New Jersey) and Crystran Ltd (Dorset, United Kingdom). Equilateral sapphire prisms were obtained from Crystran Ltd (Dorset, United Kingdom). The prism supports underwent a thorough cleaning procedure as previously described in Chapter 2.

4.2.2 Electrode Synthesis

The detailed protocol for forming the RuO_2 working electrode (WE) described in this study has been previously explained in Chapter 3 and will be briefly communicated here. A sol-gel solution was made containing $RuCl_3 \bullet xH_2O$:MTES:$SiCl_4$ in a molar ratio of 24:6:1, respectively. Initially, MTES and $SiCl_4$, were combined in 10 mL EtOH and the solution was constantly stirred for 2 hours. A second solution containing $RuCl_3 \bullet xH_2O$ dissolved in 10 mL of EtOH was made and constantly stirred for 1 hour. The two solutions were then combined together and stirred for an additional hour to create the conductive sol-gel. The sol-gel was allowed to age a minimum of 48 hours before film deposition. A KSV Nima Minitrough (Helsinki, Finland) substrate dipper was used to coat the microscope slides at a speed of 8.5 cm/min. The wet coating was allowed to dry under ambient conditions before being annealed at 450 °C for 15 minutes, at which point the electrode was allowed to slowly cool to room temperature before use.

4.2.3 Bilayer Preparation

Two methods were used to prepare planar supported lipid bilayers in this study. The first method entails vesicle fusion to the surface. The desired phospholipids were first dissolved in $CHCl_3$ at a concentration of 1 mg/mL. For epifluorescence microscopy, 0.5 mol % NBD-PC was mixed with 99.5 mol % DPPC from stock solutions with concentrations of 1 mg/ml. All lipid solutions were evaporated using N_2 gas and dried under vacuum for a minimum of 8 hours. The DPPC lipid powder was rehydrated in 0.1 M $NaClO_4$(aq) solution and was heated above 41 °C for ~1 hour. During heating, the vesicle solutions underwent periodic vortex cycles to ensure even mixing and dispersion. The vesicle solutions were then either subjected to a sonicating water bath (Branson 1510 Ultrasonic Cleaner, Danbury, Connecticut) until clear (10 minutes) or a mini extruder (Avanti Polar Lipids) containing polycarbonate membranes with a pore diameter size of 30, 50, 100, or 200 nm. The extruded vesicles underwent a minimum of 13 passes through the extruder before being used to form a planar bilayer. Vesicle solutions were injected into a custom flow cell containing the bilayer support to form planar bilayers via vesicle fusion. The flow cell setup was heated above the phase transition temperature of DPPC and vesicles were allowed to fuse for approximately 90 minutes before the cell was rinsed with 9x the volume of the flow cell with 0.1 M $NaClO_4$. The bilayer was then cooled at ~ 0.75 °C/min until 23 °C was reached.

The Langmuir-Blodgett and Langmuir-Schaefer film deposition (LB/LS) method was also used to make supported bilayers using a KSV Nima Minitrough. Phospholipid solutions were prepared in $CHCl_3$ at concentrations of 1 mg/mL and were stored at -20 °C and were used within 3 months of preparation. Sodium perchlorate (0.1 M) was used

as the subphase for bilayer preparation. Phospholipid solutions were spread at the air/subphase interface and were allowed to stabilize for 15 minutes, at which point the monolayer was compressed to the desired pressure at a rate of 4 mm/min. The substrate was then withdrawn through the subphase at a rate of 3 mm/min forming the LB monolayer. The second leaflet of the membrane was formed by depositing the lipid solution on the subphase, allowing 15 minutes for stabilization before compressing to the desired pressure and then passing the substrate with the LB monolayer horizontally through the subphase to form the LS layer. The substrate and fully assembled lipid bilayer were mounted on to a custom built Teflon flow cell, which allows for fluid exchange, temperature, electrochemical impedance and SFVS measurements. Careful handling of the cell ensured that the bilayer was maintained in an aqueous environment at all times after preparation and assembly.

4.2.4 Electrochemical Impedance Spectroscopy (EIS)

EIS measurements were conducted using a Bio-logic SP 150 impedance capable potentiostat (Bio-Logic, Claix, France). A custom built Teflon flow cell was used in a three electrode configuration for all impedance measurements, using a platinum wire counter electrode with Ag|AgCl reference electrode and the previously described RuO_2 thin film electrode as the working electrode.[25] The reference electrode was used in conjunction with a Luggin capillary which was placed ~ 3mm from the working electrode. Sodium perchlorate (0.1 M) was used as the supporting electrolyte and was purged with argon gas for a minimum of 30 minutes before being injected into the flow cell. EIS experiments were conducted at a potential of 0.150 V vs Ag|AgCl and the

scanned frequency range was 130 kHz – 10 Hz. A 10 mV sine wave was used in all experiments. The resulting impedance data were fit using EC-Lab software from Bio-Logic. The reported results were collected from a single bilayer and the reported errors are from five scans of a single sample. Initial impedance spectra were recorded for the bare working electrode and were fit using a circuit of a resistor in series with a resistor and capacitor in parallel. The values of the bare working electrode were used to fit the data collected when a bilayer was on the surface where the circuit was expanded to include a resistor in series with two separate resistor and capacitor loops in parallel.

4.2.5 SFVS Experiments

The SFVS setup in this study has been described in Chapter 2 and a brief description will be provided here. A 1064 nm, 10 Hz, 7 ns solid state pulsed Nd:YAG laser (Continuum, Santa Clara, California) was used to pump a custom optical parametric oscillator (OPO) and optical parametric amplifier (OPA) system (LaserVision, Bellevue, WA) to produce a visible beam at 532 nm and a tunable mid-IR beam. The intensities of the incident beams ranged from 5 – 7 mJ/pulse for the visible and 2 – 4 mJ/pulse for the infrared beam. The angles of the incident beams with respect to the surface normal were 62 degrees for the IR and 67 degrees for the visible beams. The polarizations of the output sum-frequency, input visible beam, and input mid-IR beam were s, s, and p, respectively. The sum-frequency signal was collected using a photomultiplier tube (Hamamatsu Photonics, Hamamatsu, Japan) and processed using a Stanford Research Systems boxcar integrator (Sunnyvale, California). Spectra were collected for vesicle fused and LB/LS prepared bilayers after flushing the sample cell with 0.1 M $NaClO_4$ in

D_2O to prevent spectral overlap from the –OH vibrational modes of water. Spectra were collected by scanning the tunable IR in 2 cm^{-1} steps from 2750 – 3050 cm^{-1} with a minimum of a 9 second integration at each step.

4.2.6 SFVS Normalization

The SFVS spectra were normalized according to the following procedure. The intensity of the phospholipid bilayer spectra were divided by the mean intensity of the PBS (150 mM, pH 7.36) spectrum across the frequency region of 3000 – 3100 cm^{-1} steps after the bilayer was completely removed with methanol. The spectra were then baseline corrected by subtracting the mean value from 2750 – 2800 cm^{-1} and then the square root of the intensity was calculated. Each spectrum is normalized to the maximum intensity from a completely asymmetric DPPC:DPPCd62 bilayer with both leaflets compressed to a surface pressure of 30 mN/m.

4.2.7 Epifluorescence Microscopy

Components and setup of the custom built epifluorescence microscope have been described previously.[26] Briefly, a diode pumped solid state (DPSS) laser with a wavelength of 488 nm and an attenuated power of 0.045 mW (CrystalLaser, Reno, Nevada) was used to illuminate the sample. An Olympus 60x objective with a 1.42 numerical aperture was used for image acquisition; this is coupled with a 1.6x magnifier resulting in a final magnification of 96x. Images were recorded with a 512 x 512 pixels Andor iXon DU897 charged coupled device (1 pixel = 16 x 16 μm) using an exposure time of 0.1 seconds with an electronic gain of 80 and a readout rate of 5 MHz. A number

of images were collected over the entirety of the surface of the membrane in a 500 frame video. A minimum of five images were selected from these data.

4.2.8 Image Analysis

Epifluorescence images were analyzed using ImageJ software.[27] There was a substantial diffraction pattern present within the collected images due to refractive index offsets between the immersion oil and quartz coverslips. This pattern was removed by averaging multiple frames where the diffraction pattern did not change. The averaged image was subtracted from each image of interest for a particular membrane preparation. Once the images had been subtracted, a histogram was collected of the intensity across the entire region of interest (ROI) which was 280 x 280 pixels. Threshold values to determine irregularities in brightness and darkness were set at two standard deviations from the mean intensity for each collected image. Defect sites and bright spots (assumed to be adsorbed vesicles) were counted only if larger than 5 pixels, as this is the previously determined point spread function for the microscope setup.[28] Both the defect sites and bright spots were quantified for a minimum of five images across the entire bilayer surface.

4.2.9 Kinetic Examination of the Persistance of Lipid Population Disparity Between Leaflets

DPPC planar bilayers were prepared with differing leaflet pressures for the proximal and distal leaflets using the LB/LS deposition method. Changing the compression surface pressure directly controls the number of lipids in each leaflet. Lipid

bilayers were prepared where the proximal leaflet to the substrate was consistently compressed to a pressure of 40 mN/m. The distal leaflet compression pressure varied with values of 40, 33, 26, and 20 mN/m. Creating bilayers with known population mismatch between leaflets using the LB/LS method effectively mimics the lipid population differences between leaflets in a vesicle. The above pressures were chosen to give a range of population asymmetry within the membrane while staying within the liquid crystalline phase state of the pressure-area isotherm. Switching the order of the proteated and deuterated lipid components while maintaining the described pressure offsets allows for kinetic rate constants to be determined for both the proximal and distal leaflets. The bilayers were created as detailed above.

Once the bilayer was formed, initial spectra were recorded at room temperature (~ 23 °C). The CH_3 ν_s was monitored as a function of time at a temperature of 23 °C for all created bilayers. The loss of SFVS intensity over time at this temperature was used to calculate the rate of lipid flip-flop for these pressure offset bilayers in a similar way as described in Chapter 2.

4.3 Results and Discussion

4.3.1 SFVS Spectra of Planar Membranes

SFVS spectra of planar bilayers formed by LB/LS are shown in Figure 4.1 for both an asymmetric DPPC:DPPCd62 bilayer and a membrane that was made symmetric by heating above the DPPC phase transition temperature of 41 °C. The spectra were normalized to the CH_3 ν_s mode of an asymmetric DPPC:DPPCd62 bilayer formed by LB/LS that was compressed to a surface pressure of 30 mN/m.[29] The vibrational modes

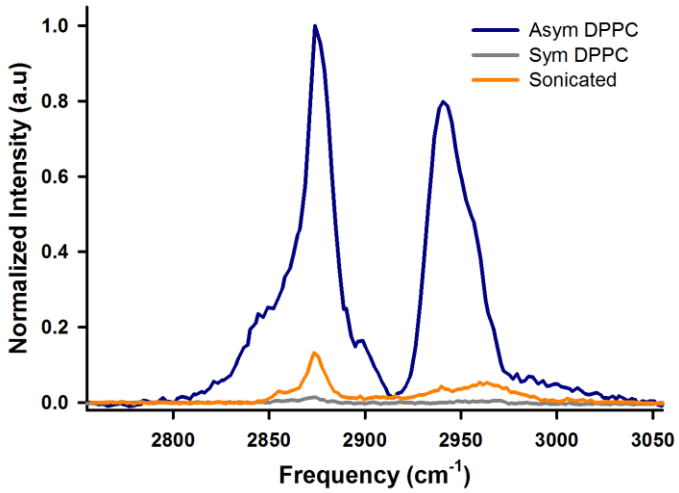

Figure 4.1: SFVS spectra of an isotopically asymmetric bilayer of DPPC and DPPC d62 (blue) and of a completely symmetric bilayer of DPPC (gray) formed by LB/LS.

in Figure 4.1 have been previously identified and are assigned at 2848 cm^{-1} for the CH_2 ν_s, 2875 cm^{-1} for the CH_3 ν_s, at ~2900 cm^{-1} is the CH_2 ν_s Fermi resonance (FR), and a combination of the CH_3 ν_s FR and the CH_3 asymmetric stretch (ν_{as}) is at 2949 cm^{-1}.[30-33] The spectrum of a symmetric bilayer shows a detectable amount of signal at 2875 cm^{-1} which could be explained by differences in lipid number density between leaflets due to bilayer deposition artifacts between formation of the Langmuir-Schaefer layer and the formed Langmuir-Blodgett layer. However, this measured signal is incredibly small compared to that of completely isotopically asymmetric lipid membranes. The amount of signal that is still present is persistent through all prepared membranes and can be neglected as it is systematic artifact originating from the membrane preparation method.

Figure 4.1 also shows the measured spectrum for a planar bilayer created via vesicle fusion from sonicated vesicles composed of DPPC. This spectrum was obtained after the vesicles were allowed to adsorb and fuse with the underlying substrate for at least 1.5 hours above the phase transition temperature (41 °C) of DPPC. The amount of observable signal for membranes formed via vesicle fusion is greater than a purely symmetric membrane formed via LB/LS. This result was unexpected as there is no difference in the isotopic distribution of lipids between the leaflets of the membrane. One possible explanation for the observed response could be a lipid density difference between leaflets of the formed planar membrane. SFVS, unlike traditional optical techniques, is capable of discerning which leaflet contains the greater number of lipids in the formed planar membranes due to the inherent phase and symmetry constraints of this nonlinear optical technique. The results in Figure 4.1 indicate that there may be a discpepancy in the population density of phospholipids in either the proximal or distal

leaflet for planar gel-phase bilayers formed using vesicle fusion. Further methods were implemented to examine the origins of the response observed above.

4.3.2 Determining Lipid Leaflet Location Giving Rise to SFVS Signal

The SFVS spectrum of bilayers formed via vesicle fusion in Figure 4.1 was collected using fused silica prisms as the membrane support. The previous studies of Liu and Conboy have demonstrated that the nonresonant SFVS intensity of fused silica is negligible.[18, 32, 34-35] When a substrate that possesses a substantial nonresonant component is used, it becomes possible to measure phase differences between the orientation of different vibrational modes of a system in relation to the nonresonant signal. A mathematical description of this effect is provided below. The intensity of the sum-frequency response is proportional to the absolute square of the sum of the resonant ($\chi_R^{(2)}$) and nonresonant ($\chi_{NR}^{(2)}$) susceptibility tensors as defined by:[36]

$$I_{sum} \propto \left| \left|\chi_R^{(2)}\right| e^{i\varphi_1} + \left|\chi_{NR}^{(2)}\right| e^{i\varphi_2} \right|^2 \tag{4.3}$$

where φ_1 is the phase of the resonant response and φ_2 is the phase of the nonresonant contribution from the substrate. Expansion of Equation 4.3 is given by:

$$I_{sum} \propto \left|\chi_R^{(2)}\right|^2 + \left|\chi_{NR}^{(2)}\right|^2 + 2\left|\chi_R^{(2)}\right|\left|\chi_{NR}^{(2)}\right| \cos(\varphi_2 - \varphi_1) \tag{4.4}$$

where, the cross term is the product of the nonresonant and resonant susceptibilities scaled by the cosine of the phase difference between them. If a bilayer is prepared on a substrate with a negligible nonresonant signal it is difficult to determine the orientation of the proteated component. However, depositing a bilayer on a substrate with an invariant nonresonant signal allows for the absolute orientation of the molecules contributing to the

SFVS signal to be determined.

The interference between the resonant sum-frequency signal and the nonresonant background intensity of a sapphire prism has been used previously to determine the absolute orientation and distribution of cholesterol in bilayers composed of DSPC and cholesterol.[23] These previous investigations observed that cholesterol is unevenly distributed in a lipid membrane at high concentrations (60 mol %), with an excess of cholesterol residing in the distal leaflet of the membrane.[23] Due to mass balance between the leaflets of the membrane, an excess of DSPC lipids was measured to be on the proximal leaflet of the membrane.[23] Using the applied concepts from Liu and Conboy,[23] sapphire substrates were employed to determine the origin of the population difference in membranes formed via sonicated vesicle fusion that gave rise to the observed signal in Figure 4.1.

Initially, isotopically asymmetric membranes were deposited onto sapphire supports using the LB/LS deposition method to systematically control the location of the proteated component. Figure 4.2 shows the measured spectra for both the nonresonant signal arising from the sapphire support and the asymmetric DPPC:DPPCd62 membrane where the proteated component was located on the distal leaflet with regard to the substrate. From these spectra it is possible to note the destructive interference of the nonresonant signal before the vibrational resonance at 2875 cm^{-1} and the positive interference at frequencies above this resonance. Figure 4.3 also illustrates the measured nonresonant spectrum from the sapphire substrate, and the measured SFVS response when the proteated lipid component is located in the proximal leaflet, closest to the sapphire support. This membrane configuration results in constructive nonresonant

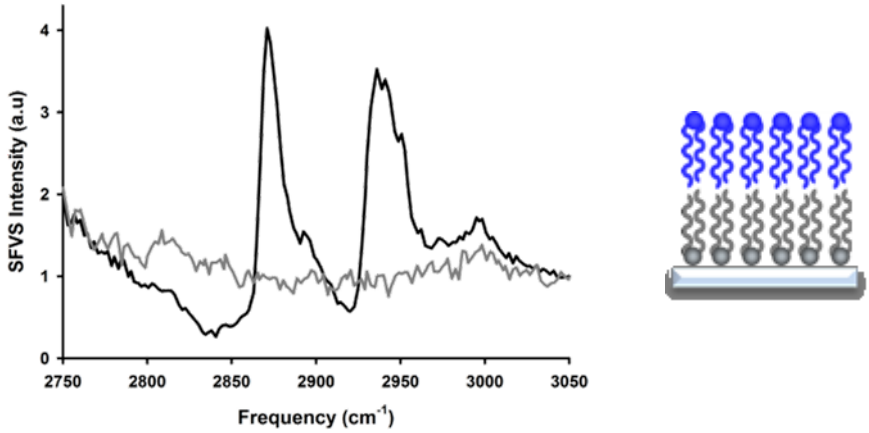

Figure 4.2: SFVS spectra of the D_2O/Al_2O_3 interface (gray) and an asymmetric DPPC – DPPCd62 bilayer (black). The proteated component was located on the distal leaflet as shown in the inset using blue lipids.

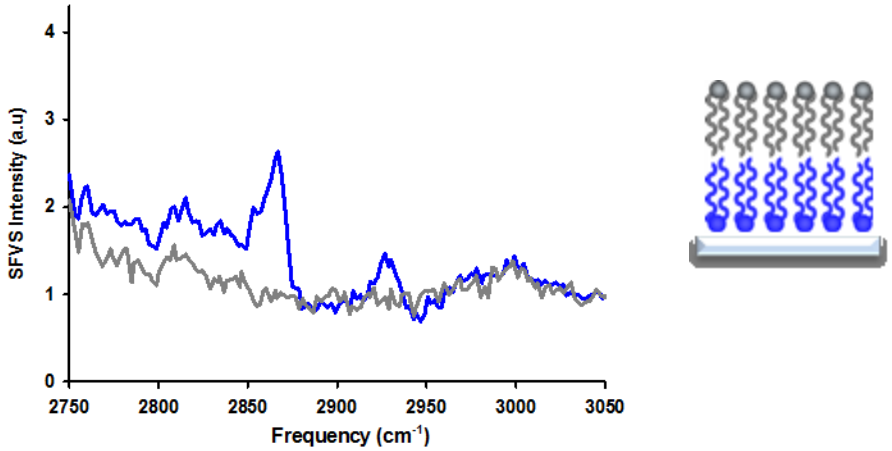

Figure 4.3: An SFVS spectrum for an asymmetric DPPC – DPPCd62 bilayer (blue). The proteated DPPC phospholipids were located on the proximal leaflet. The nonresonant response from sapphire is again shown in gray.

interference before the resonant frequency of 2875 cm^{-1} with destructive interference ocurring at frequencies greater than the resonant. Separately measuring the precise response of the proteated component in the proximal and distal leaflets of a membrane provides an accurate methodology for assigning the absolute orientation of lipids in membranes formed using vesicle fusion.

The vibrational spectrum of a bilayer formed via sonicated vesicle fusion is shown in Figure 4.4. Noticeable interference between the substrate and the bilayer exists and is most similar to the measured response from the membrane where the proteated component was located on the proximal leaflet to the substrate. From these data it can be concluded that membranes formed with sonicated vesicles contain a greater number of lipids on the proximal side of the formed planar membrane. There have been a variety of proposed mechanisms describing the process of forming planar membranes from vesicle fusion.[1, 3, 11-17] The collected data using sapphire substrates indicate that a greater majority of lipids within the bilayer are located on the proximal leaflet of the planar membrane. Scheme 4.1 illustrates a proposed mechanism describing the process of vesicle fusion to create planar membranes.

The proposed mechanism functions under the assumption that lipid proportions within leaflets of the vesicle are maintained in the structure of the formed planar membrane. This result is an indication that the mechanism of vesicle fusion occurs through a rupture and unraveling of the vesicle onto the supporting substrate. The geometry of the vesicles in solution may impact the observed response as the population density distribution may depend on the size of the vesicle. Varying the size of the vesicles in solution to form planar membranes is one way to assess the contribution of

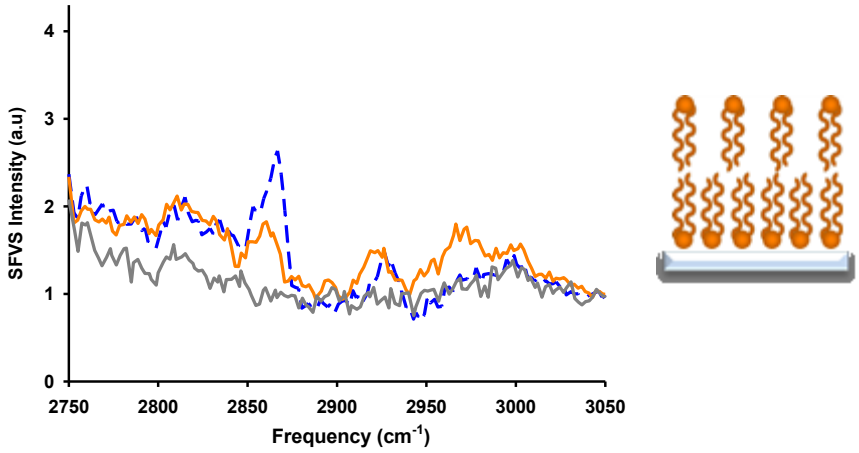

Figure 4.4: An SFVS spectrum for DPPC membranes formed from sonicated vesicles (orange). The collected spectra for an asymmetric DPPC – DPPCd62 bilayer where the proteated component is proximal (blue dashed) and the nonresonant signal of sapphire (gray) are also shown.

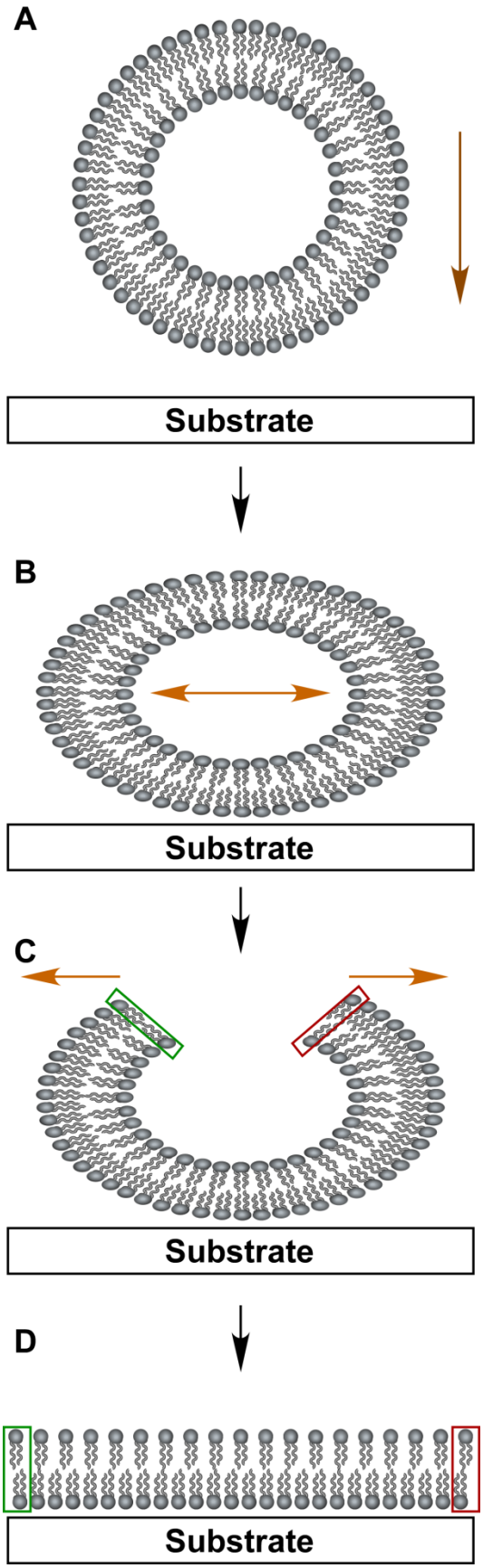

Scheme 4.1: Proposed mechanism for forming planar membranes using vesicle fusion. Initially vesicles begin adsorbing to the substrate (A). B) Adsorbed vesicles compress and pressure is exerted on the exterior of the vesicle. C) The forces exerted on the vesicle reach a critical point when the vesicle ruptures and begins to unravel. Red and green boxes are used as visual guides to bilayer formation. D) A planar membrane is formed due to the unravelling of the vesicle where the lipid densities of the leaflet within the vesicle are maintained in the planar membrane.

vesicle geometry to the measured SFVS response.

4.3.3 Vesicle Radius Impact on Measured SFVS Signal

Considering the geometry of vesicles in solution it is reasonable to assume that a discrepancy between the lipid population in the exterior and interior leaflets of a vesicle could arise based solely on differences in the outer and inner radii of a vesicle. Assuming that the packing pressure remains the same between the leaflets of the vesicle it can be inferred that the outer leaflet would contain a greater number of lipids simply due to the greater surface area of the outer leaflet. If this situation occurs then the resulting SFVS signal would be dependent on the size of vesicle used to form a planar supported bilayer. The concept of outer leaflet lipid population preservation from vesicles to planar bilayers was tested by examining the solution vesicle size dependence on the amount of observable SFVS signal of the corresponding formed planar bilayers. Vesicles were extruded using the methods described above through polycarbonate membranes with pore sizes of 30, 50, 100, and 200 nm in diameter. The results from these experiments are shown in Figure 4.5 as a function of vesicle size and are normalized to the signal generated from an isotopically asymmetry DPPC:DPPCd62 membrane.

The data shown in Figure 4.5 illustrate that as vesicle radii increase, the corresponding SFVS signal decreases. Notably, vesicles with a radius of 100 nm approach the minimum or zero point signal, whereas vesicles with a radius of 15 nm generate a response ~ 5 times greater. As observed above, planar lipid membranes formed from sonicated vesicles containing proteated lipids result in a measureable SFVS response greater than the signal generated from a completely symmetric bilayer formed

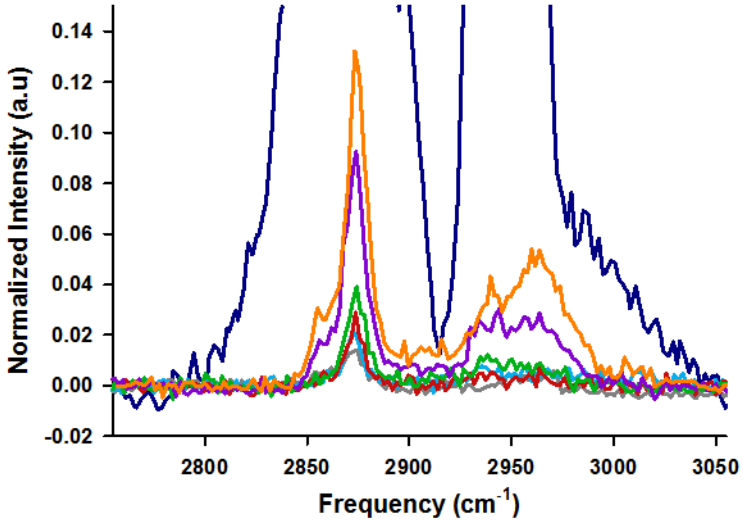

Figure 4.5: Normalized SFVS spectra for membranes formed via vesicle fusion of vesicles varying in radius. Proteated DPPC vesicles with radii of 100 nm (light blue), 50 nm (red), 25 nm (green), and 15 nm (purple) were used. A SFVS spectrum of membranes formed from sonicated vesicles is also shown (orange). The y-axis scale is the same for Figure 4.1 and spectra for symmetric bilayers (gray) and asymmetric bilayers (blue) are shown for reference.

using LB/LS. This signal can be explained by differences in lipid number density between the outer and inner leaflets of the vesicle itself. Quantifying the value of this asymmetry can be done using the simple geometry of two spheres, where one is inside the other representing the inner and outer leaflets of the vesicle. The distance between these two spheres is defined by the the pivotal planes of each leaflet, which is the point where the mean molecular area is invariant upon bending.[37-38] This distance should be fixed for a particular lipid and is mostly depedent on the number of acyl carbons contained within the hydrocarbon chains of glycerophospholipids.[15,39-41] Mathematically, the relationship between the percent asymmetry obtained from the measured SFVS response and the vesicle radii can be defined based on the relationship in Chapter 2 Equation 2.5 as follows:

$$\%\, Asymmetry = \frac{R_{outer}^2 - (R_{outer} - d)^2}{R_{outer}^2 + (R_{outer} - d)^2} * 100 \qquad (4.5)$$

where R_{outer} is the outer radius of a vesicle of spherical shape and solitary fitting parameter, and *d* is the distance between pivotal planes for each leaflet of the vesicle. It is important to note that the values for percent asymmetry were substracted from the minimal signal generated from a completely symmetric bilayer formed via LB/LS as this is the lowest amount of signal observed using the current experimental setup. The signal generated from a completely symmetric membrane made using LB/LS can be subtracted as it theoretically contains equal lipid densities in both the proximal and distal leaflets. The measureable signal is a consequence of inherent experimental error arising from the deposition of the Schaefer layer. The variability of this signal was collected three times and the average value was used as a zero point for the vesicle radii dependence measurements. These calculations are illustrated in Figure 4.6 where the size dependence

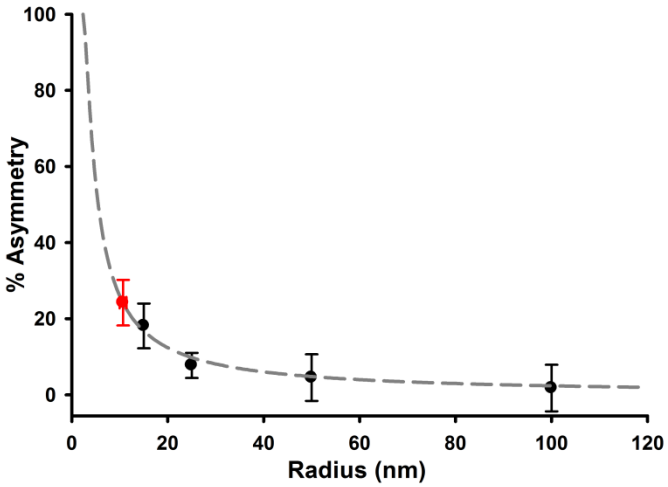

Figure 4.6: Percent asymmetry determined by SFVS as a function of vesicle radius. Shown in black are the data from extruded membranes, the gray dashed line is the fit to the data of Equation 4.5, and the red data point represents the sonicated vesicle radius as determined by the pivotal plane thickness from the fit.

of the SFVS signal of the formed planar membranes is correlated to the solution vesicle radii. The fit line in Figure 4.6 is directly plotted from Equation 4.5 and the distance between pivotal planes of each leaflet is calculated as the parameter *d*. The pivotal plane thickness of DPPC membranes formed by vesicle fusion was determined to be 2.3 ± 0.2 nm. This value is similar to the previously reported value for the hydrocarbon thickness of DPPC membranes determined with X-ray diffraction of 2.6 ± 0.1 nm.[42] The fact that d is slightly less than the measured value using dynamic light scattering stems from the differences in the techniques themselves. DLS measurements rely on the hydrodynamic radius of a particle, which in the case of lipid vesicles includes the phosphate and choline portion of the lipid vesicle and associated water molecules. However, in the assumptions made for the analysis of the SFVS data we use the distance between pivotal planes, which is located ~2 carbons on the interior of the glycerol backbone,[39] thereby resulting in a slightly decreased value for r of sonicated vesicles compared to the DLS value. Using the pivotal plane thickness, the radius of sonicated vesicles was calculated from the measured SFVS percent asymmetry and was determined to be 13 ± 1 nm. Dynamic light scattering (DLS) measurements were collected for a solution of sonicated vesicles resulting in a calculated radius of 14 ± 2 nm. These results demonstrate the ability of SFVS to measure and distinguish population differences in planar membranes due to varying solution vesicle geometries.

Although the results from SFVS and DLS measurements yield comparable values for the value *d,* it is nevertheless perplexing that differences in lipid density between leaflets persist given that the membranes are formed well above the phase transition temperature for the lipid DPPC. An investigation into the kinetics of lipid flip-flop was

undertaken in systems where an initial lipid density was purposefully created to potentially explain the persistence of the observed bilayer asymmetry.

4.3.4 Persistance of Lipid Asymmetry in Bilayers Formed by Vesicle Fusion

Previous research within our group has described the mechanism of lipid flip-flop as a unimolecular mechanism where the rate of translocation of a lipid from the proximal to distal leaflet of a planar membrane is equal to the rate of translocation of a lipid from the distal to proximal leaflet of a planar membrane stemming from the initial description developed by McConnell and Kornberg.[43-44] Work within our research group has previously shown that the substrate does not influence the process of lipid flip-flop by measuring bilayers suspended on a cushion of polyethylene glycol.[31] With this understanding and proposed mechanism it could be possible to establish a population difference in vesicle fused planar membranes if the rate of translocation between the proximal and distal leaflet depends on the lipid density in each leaflet.

The mechanism of lipid flip-flop has been previously described in Chapter 2 as a reversible unimolecular reaction between lipids in the proximal and distal leaflets of a planar bilayer. From Chapter 2,

$$N_{proximal} \underset{k_{dist}}{\overset{k_{prox}}{\rightleftharpoons}} N_{distal}$$

where $N_{proximal}$ and N_{distal} describe the number of lipids in the proximal and distal leaflets of the bilayer, respectively. The rate constants, k_{prox} and k_{dist}, describe the rate of lipid translocation from the proximal to distal leaflet and from the distal to proximal leaflet,

respectively. The change in $N_{proximal}$ and N_{distal} is defined as:

$$\frac{dN_{proximal}}{dt} = -k_{prox}N_{proximal} + k_{dist}N_{distal} \quad (4.6)$$

$$\frac{dN_{distal}}{dt} = k_{prox}N_{proximal} - k_{dist}N_{distal} \quad (4.7)$$

Using the determinant method to solve these differentials as described by Henry Eyring,[45] the time dependent concentrations of $N_{proximal}$ and N_{distal} are:

$$N_{proximal} = \frac{N_{proximal_0}+N_{distal_0}}{1+K} + \frac{(KN_{proximal_0}+N_{distal_0})}{1+K}e^{-(k_{prox}+k_{dist})t} \quad (4.8)$$

$$N_{distal} = \frac{K(N_{proximal_0}+N_{distal_0})}{1+K} - \frac{(KN_{proximal_0}-N_{distal_0})}{1+K}e^{-(k_{prox}+k_{dist})t} \quad (4.9)$$

where, $N_{proximal_0}$ and N_{distal_0} are the initial lipid concentrations in the proximal and distal leaflets, respectively. The equilibrium constant, K, is defined as $K = k_{prox}/k_{dist}$ and t is time. At infinitely long time the above equations simplify to:

$$N_{proximal} = \frac{N_{proximal_0}+N_{distal_0}}{1+K} \quad (4.10)$$

$$N_{distal} = \frac{K(N_{proximal_0}+N_{distal_0})}{1+K} \quad (4.11)$$

Asymmetry within a bilayer is defined as $N_{proximal} - N_{distal}$ and is equal to the following:

$$N_{proximal} - N_{distal} = \frac{N_{proximal_0}+N_{distal_0}}{1+K} - \frac{K(N_{proximal_0}+N_{distal_0})}{1+K} \quad (4.12)$$

which, simplifies to:

$$N_{proximal} - N_{distal} = \frac{(N_{proximal_0}+N_{distal_0})(1-K)}{1+K} \quad (4.13)$$

If $k_{prox}=k_{dist}$, then the above equation is equal to zero meaning that an initial population difference between leaflets in a bilayer is not preserved over long time periods using this mechanism.

Using the Langmuir Blodgett/Langmuir Schaefer deposition method for creating lipid bilayers it is possible to precisely control the lipid number density of each leaflet by

controlling the surface pressure of each layer deposited. This methodology allows for planar membranes to be created where there exists an initial difference in lipid number density between leaflets of planar membranes, allowing for a meticulous way to probe kinetic rates for membranes with offset leaflet populations. Three different bilayers were created where the distal leaflet lipid density varied from the proximal leaflet density as defined by differences between deposited surface pressures of the two leaflets. Scheme 4.2 shows the composition of each of these membranes.

Once formed these offset membranes were allowed to randomly mix over a period of hours while the temperature and SFVS was monitored as previously described. The obtained data were fit to Equation 2.12 where the rate constant can be determined. The calculated fits of the data from three replicated experiments are shown in Figure 4.7 while monitoring the proteated component in the proximal leaflet (Figure 4.7 A) or the proteated distal component (Figure 4.7 B). A complete summary of the measured kinetic rates for these offset membrane experiments is contained in Table 4.1 for the proteated proximal component and proteated distal component, respectively.

The data presented in Figure 4.7 show that decreasing the lipid density in the distal leaflet causes a corresponding increase in the rate of lipid flip-flop for lipids in both the proximal and distal leaflets. Varying the packing density in one leaflet also dictates the overall rate of lipid flip-flop in both leaflets. The results presented in Table 4.1 also illustrate that the rates for unidirectional flip-flop between the proximal to distal leaflet or the distal to proximal leaflet do not statistically vary from one another. Previous lipid flip-flop investigations have reported the rate of lipid flip-flop as a unimolecular kinetic reaction.[35, 43-44] These results present an alternative explanation to the existing

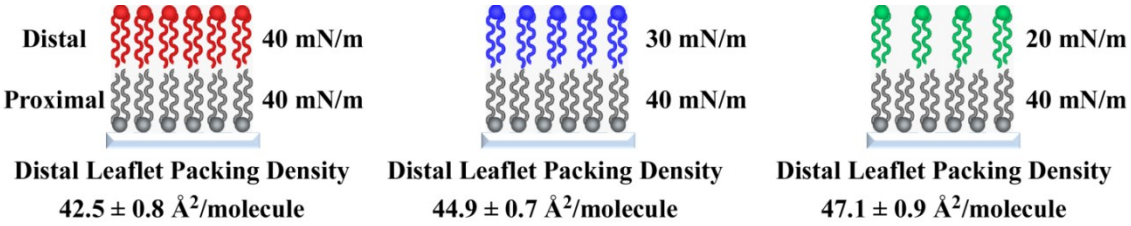

Scheme 4.2: Visual depictions of the bilayers created with differing leaflet pressures and reported packing densities for the distal leaflet.

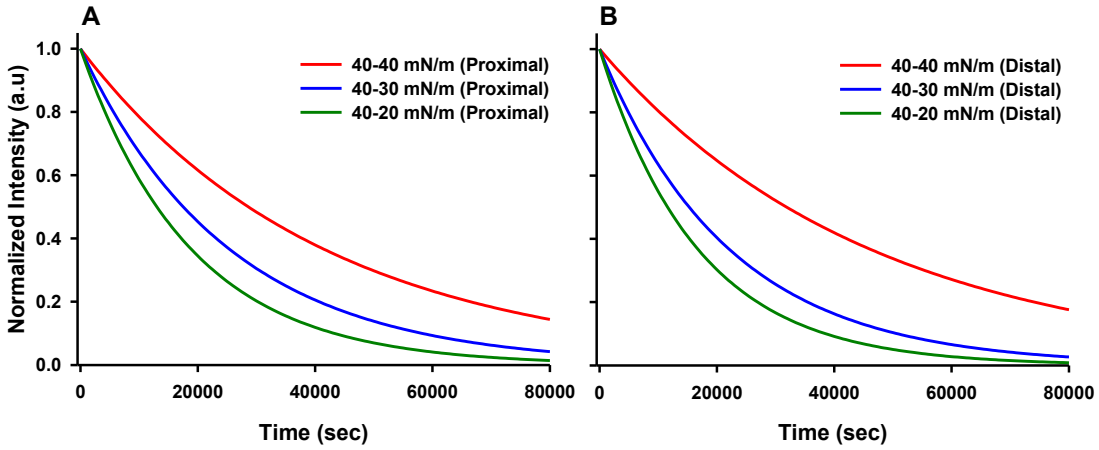

Figure 4.7: Calculated averaged fit lines from Equation 2.12 are shown for clarity using the determined rate constant of signal intensity decay as a function of time for DPPC in leaflet pressure offset bilayers. The average fit is plotted for each bilayer composition of 40 – 40 mN/m (red), 40 – 30 mN/m (blue), and 40 – 20 mN/m (green) and were normalized to the maximum intensity for each experiment. A) depicts when the proteated component was located on the proximal leaflet and B) shows the rate constants when the proteated component was located on the distal leaflet, keeping with the bilayer compositions in Scheme 4.2.

Table 4.1: Summary of rate constants for asymmetric DPPC – DPPCd62 bilayers of varying leaflet surface pressure and location of proteated component.

Pressure (Proximal – Distal)	**k (s^{-1}) x 10^6 (Proximal → Distal)**	**k (s^{-1}) x 10^6 (Proximal ← Distal)**
40 – 40 mN/m	6 ± 1	5 ± 1
40 – 30 mN/m	9.9 ± 0.5	11 ± 2
40 – 20 mN/m	13 ± 3	15 ± 6
20 – 40 mN/m	25 ± 11	10 ± 2

understanding of lipid flip-flop. Given the described experiment design of selectively creating membranes with leaflets of offset packing density it could be assumed that the rates would vary depending on which leaflet was monitored. For example, the leaflet containing more lipids would be expected to have a faster rate of flip-flop due to the more sparsely packed opposing leaflet. The leaflet containing the lower lipid density would be expected to exhibit a slower flip-flop rate due to the greater amount of energy required to expand the leaflet containing the greater number of lipids.

An alternative kinetic explanation for the persistence of a population difference between leaflets after flip-flop has occurred is that the process of lipid flip-flop is a coupled reaction, indicated by the reported rate constants of the leaflet pressure offset membranes. The rate of k_{dist} is statistically similar to k_{prox} for all studied membrane compositions. This suggests that the measured rates are a combination of the ensemble pressure of the membrane instead of the individual leaflet pressures. It also suggests that the rate of the forward and opposite reaction are dependent on the overall number of lipids within the membrane and exhibit characteristics of a bimolecular exchange mechanism instead of a unimolecular reaction mechanism. This explanation would verify the persistence of membrane population asymmetry resulting from the process of vesicle fusion. A coupled reaction would explain why the rate of flip-flop is faster for lower lipid quantities in the distal leaflet and also why a leaflet population asymmetry exists after flip-flop. Coupled kinetic rates of flip-flop mean that the number of lipids that can undergo translocation is equal to the least concentrated leaflet. This also explains that although the bilayers are formed above the phase transition temperature of DPPC, asymmetry persists and is correlated to the initial size of the vesicle. Further

evidence of a coupled reaction for lipid flip-flop is demonstrated by varying the cooling rate after the elevated fusion process.

The cooling rate for all of the reported bilayers created from vesicle fusion was 0.7 °C/min. This cooling rate could potentially be too rapid thereby prohibiting the system from reaching thermal equilibrium as the membrane is cooled down. Although the observed asymmetry at room temperature is reproducible it does not preclude the possibility of potential defects from being essentially locked into the membrane as a result of rapid cooling. A control experiment was conducted, where the cooling rate was slowed to 0.1 °C/min. Under these conditions the system is allowed to reach thermal equilibrium as the temperature is decreased to 23 °C at which point an SFVS spectrum was recorded. Using the same normalization procedure described above for calculating percent asymmetry, the percent asymmetry of the membrane formed from a slow cooling rate was 22 %, which is similar to the measured percent asymmetry of the reported membranes formed from sonicated vesicles of 24.21 ± 0.06 %. Adequately allowing time for the substrate and the membrane to reach thermal equilibrium should prevent thermal gradients from creating defects within the membrane that potentially could contribute to the observeable SFVS signal. The fact that the measured asymmetry for more slowly cooled membranes correlated to membranes cooled at a faster rate indicates that there was not a significant temperature gradient between the membrane and substrate. These results also lend evidence to the possibility of a coupled reaction rate as there was ample time for lipids to undergo the process of flip-flop and reorganization during the cooling process. These results explain how the initial population difference of lipids in each leaflet of vesicles in solution is maintained in the formed bilayers from vesicle fusion.

The initial differences in lipid number between leaflets in vesicles due to the geometry of spheres creates a population disparity between the inner and outer leaflets and potentially persists due to a coupled kinetic mechanism for lipid flip-flop.

The structural integrity of the formed lipid membranes was further investigated using more traditional methods of fluorescence microscopy and electrochemical impedance spectroscopy to verify that the observed SFVS results were not due to physical defects within the membrane.

4.3.5 Fluorescence Imaging of Planar Membranes Formed via Vesicle Fusion

Epifluorescence microscopy was used to examine the surface coverage of model cell membranes formed using vesicle fusion using NBD-tail labeled lipids incorporated at 0.5 mol % into DPPC vesicles. The formed planar supported bilayers containing tail labeled NBD-PC were imaged using a custom built microscopy system with the assistance of Dr. Eric Peterson and Mike Manhart. The collected images are shown in Figure 4.8 for bilayers prepared with 200 nm vesicles (Figure 4.8A), 30 nm vesicles (Figure 4.8B) and sonicated vesicles (Figure 4.8C). A minimum of 5 images collected across the surface of the membrane were used for this analysis. The size of the extruded vesicles was determined from the pore diameter of the membrane used in extrusion. Figure 4.8 also indicates the presence of adsorbed unfused vesicles that appear as brighter spots in the images and defects within the membrane that manifest as dimmer spots in the image. The percent area of both types of these defects was quantified as described in the experimental section and is reported in Table 4.2.

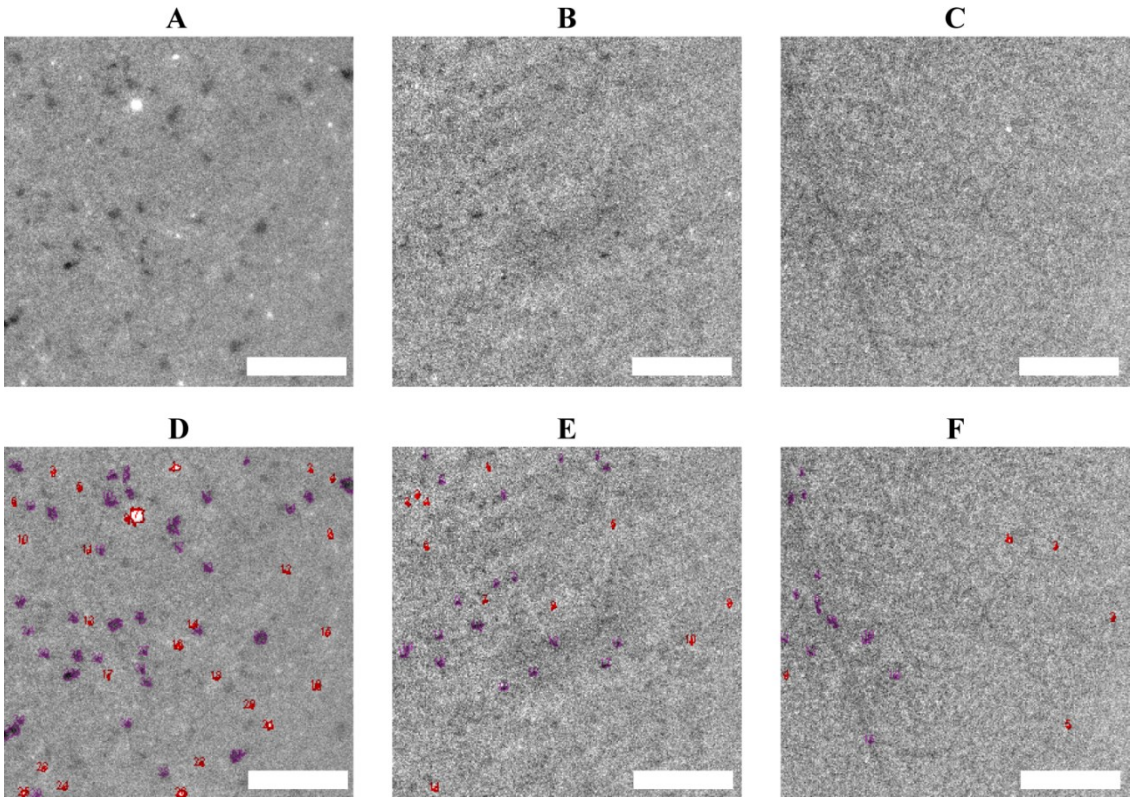

Figure 4.8: Epifluorescence images of NBD tail labeled DPPC membranes formed by A) 200 nm extruded vesicles, B) 30 nm extruded vesicles and C) sonicated vesicles. D), E), F) illustrate the quantification of bright spots(red) and defects (purple) for images A, B, and C, respectively. The scale bar in each image is 80 pixels (13.36 μm).

Table 4.2: Summary of percent area of defects in membranes formed by vesicle fusion for bilayers made with 200 nm, 30 nm, and sonicated vesicles.

Vesicle Type	N (# of image slices)	% area (defects, dark spots) 2σ	% area (vesicles, bright spots) 2σ
200 nm	5	1.0 ± 0.4	0.5 ± 0.1
30 nm	7	0.14 ± 0.07	0.1 ± 0.1
Sonicated	5	0.03 ± 0.05	0.06 ± 0.05

Using this method of analysis it is evident that the collected images are uniform across the surface of the membrane with the largest value of defect area equal to 1.0 ± 0.4 % and the largest value of bright spots equal to 0.5 ± 0.1 %. Both of these values were calculated from membranes formed using vesicles extruded through 200 nm membranes. Contrary to membranes formed from 200 nm vesicles, membranes formed using sonicated vesicles had a defect area equal to 0.03 ± 0.05 % and with an adsorbed, unfused vesicle area equal to 0.06 ± 0.05 %. These data indicate that the observed SFVS signal does not arise from a combination of the observed defects in the actual membranes themselves and the observable trends in the SFVS data do not follow the data obtained by fluorescence imaging. There are a greater number of quantifiable defects between membranes formed from 200 nm vesicles than from sonicated ones. In fact, the membranes formed from sonicated vesicles had the largest measured SFVS signal meaning that if the observed sum-frequency was due solely to the presence of defects or abnormalities then the opposite would have been observed with fluorescence measurements. The reasoning behind doing these studies was to test to see if there was a correlation between the results of SFVS spectra and the amount of defects present in the membrane. In actuality, the membranes with the smallest amount of defects (membranes formed from sonicated vesicles) had the highest amount of SFVS signal. These experiments demonstrate that the signal measured using SFVS does not originate from defects or adsorbed vesicles in the formed planar membranes.

This fluorescent data agree with a recently published study analyzing membranes formed by vesicle fusion using vesicles of varying diameters from 1000 to 30 nm by extrusion.[2] Jackman and coworkers found that larger sized vesicles do not form as

uniform bilayers due to a combination of multilamellar vesicles staying adsorbed to the surface and steric effects that prevent larger vesicles to rupture.[2] They stated that smaller vesicles form better bilayers as there is little chance for multilamellar vesicles and steric hindrance to prevent rupture.[2] The images in Figure 4.8 support the studies by Jackman *et al.* as membranes formed from vesicles with a diameter of 200 nm contained both the largest number of defects and bright spots compared to membranes formed from 30 nm extruded and sonicated (diameter of 27 ± 4 nm) vesicles.

Although there are more defects and bright spots for bilayers made from 200 nm, the percent area that accounts for these irregularities is extremely small compared to the surface area of the membrane. Epifluorescence measurements demonstrated that the observed signal measured using SFVS is not correlated to abnormalities in the formed membranes from vesicle fusion. Fluorescence imaging techniques are limited due to the luminescence of the probe molecules and defects within the membrane can often times be smaller than the imaging resolution. For this reasoning, electrochemical impedance spectroscopy was used to further examine the surface uniformity of the vesicle formed membranes.

4.3.6 Electrochemical Impedance Spectrosopy of Vesicle Fused Planar Membranes

Further investigations into the integrity of the supported bilayer membranes were investigated with potentiostatic electrochemical impedance spectroscopy with assistance from Dr. Shelley Minteer and Tao Wang. A planar membrane is a thin dielectric material that should act as a parallel plate capacitor with capacitance values defined by the

equation:

$$C = \frac{\varepsilon\varepsilon_0}{d} \tag{4.14}$$

where C is the measured capacitance, ε is the effective dielectric of a gel-phase lipid membrane (~ 2 to 4),[46] ε_0 is the vacuum permittivity constant, and d is the thickness of the membrane. Previously reported values of capacitance have been measured to be between 0.4 and1.3 μF/cm^2 for a variety of supported lipid membranes.[47-51] The membrane capacitance can be used to determine structural integrity where a value higher than the upper limit of this range indicates potential defects in the membrane.[47] Defects within the membrane would allow for water to penetrate into the bilayer thereby raising the dielectric constant resulting in a higher capacitance value.

The capacitance of vesicle fused membranes was measured with RuO_2 working electrodes and the circuit diagram describing the chemical setup in these studies is illustrated in Figure 4.9. The ruthenium working electrode circuit is best described by a R1+R2/C1 circuit, where R1 is the solution resistance of the electrolyte, R2 is the resistance of the working electrode and C1 is the capacitance of the working electrode, shown in black in Figure 4.9. Values for the measured electrolyte resistance, electrode resistance and capacitance were calculated from the fit of the circuit diagram to the collected data after 500 Levenberg/Marquardt iterations and are listed in Table 4.3. The capacitance of the ruthenium oxide working electrode is 57 ± 1 nF/cm^2, which is comparable to other metal oxide electrodes used for impedance measurements of lipid bilayers.[52] Bare single crystalline silicon has also been used to measure the capacitance of planar supported lipid bilayers and had a recorded capacitance value of ~ 50 nF/cm^2 at the same potential used in the current study.[52] When a planar lipid bilayer is deposited

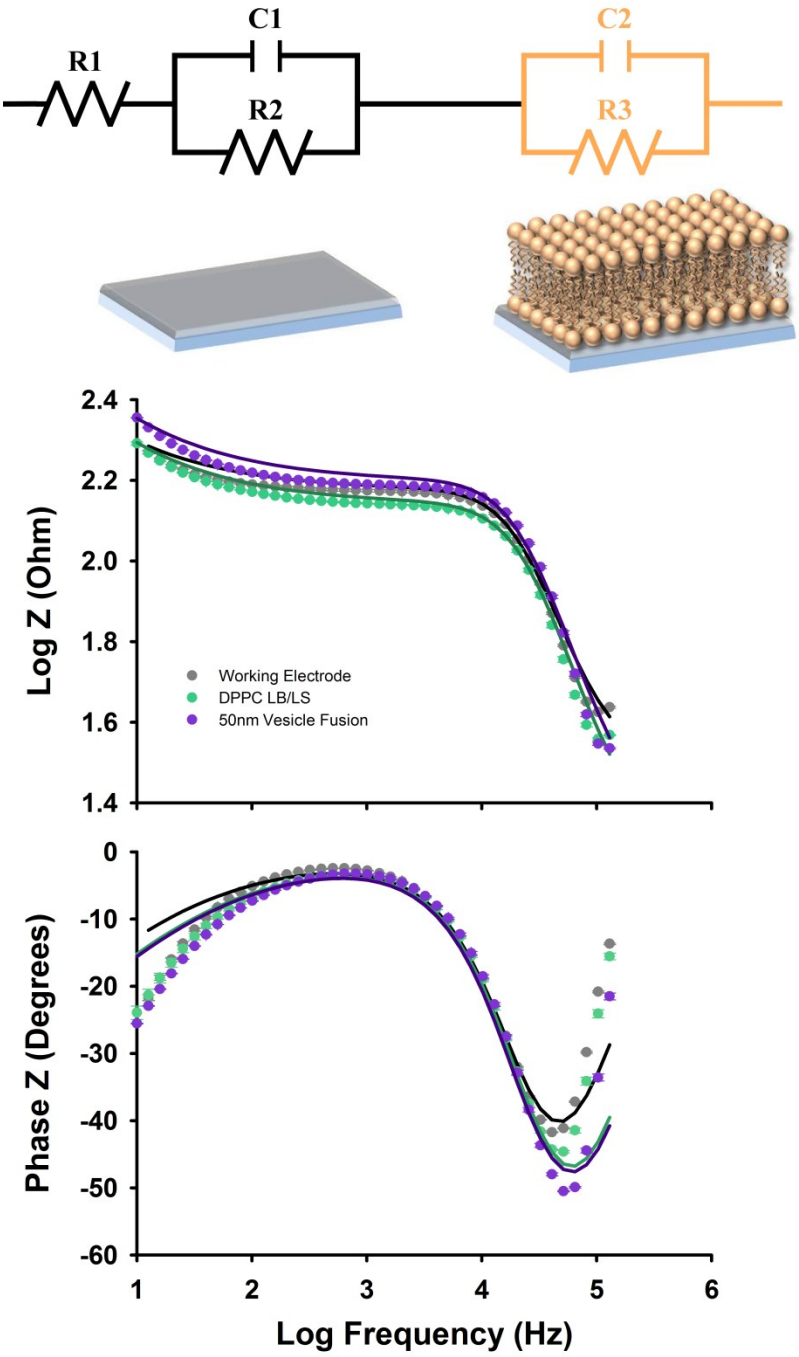

Figure 4.9: Representative electrical impedance data for DPPC membranes on RuO_2 electrodes. Top) Circuit diagram representing the system of the bare RuO_2 electrode (left) and the electrode plus DPPC lipid bilayer (right). Bottom) Representative Bode plots of the working electrode (gray), DPPC bilayer formed via LB/LS (teal), and DPPC bilayer formed by 50 nm vesicles (purple). Fits are shown by the solid lines in each plot.

Table 4.3: Summary of R1, R2, R3, C1, and C2 values for all bilayers studied and the ruthenium WE used.

	R1 (Ω)	**C1 (μF/cm^2)**	**R2 (Ω)**
Bare WE	22.6 ± 0.4	0.057 ± 0.001	126.3 ± 0.3

Bilayer	**C2 (μF/cm^2)**
200 nm Vesicle	0.5 ± 0.3
100 nm Vesicle	0.4 ± 0.2
50 nm Vesicle	0.2 ± 0.1
30 nm Vesicle	0.2 ± 0.1
Sonicated Vesicle	0.87 ± 0.05

onto the RuO_2 working electrode, the circuit diagram for the system becomes R1+R2/C1+R3/C2, shown in orange in Figure 4.9.

The electrochemical impedance spectroscopy data for planar membranes was collected at a fixed potential of 0.150 V vs Ag|AgCl and are represented by the Bode plots in Figure 4.9. As a control, the capacitance of a lipid bilayer formed via LB/LS deposition was measured, resulting in a value of 0.9 ± 0.2 $\mu F/cm^2$. The results of these experiments are comparable to the historically accepted values for membrane capacitance measured using patch clamp or pore spanning techniques.[53-55] This means that the membranes formed via vesicle fusion do not contain measurable defects using electrochemical impedance spectroscopy.

The membranes formed using vesicle fusion were characterized using electrochemical impedance spectroscopy and a novel material developed within our research group. The experiments in this section resulted in calculated capacitance values of the described membranes that are within the previously reported values for membrane capacitance. These measurements, taken with the results and analysis from the fluorescence studies indicate that membranes formed from vesicle fusion are structurally intact and are without significant defects or abnormalities. Further, the observed SFVS results cannot be described due to observeable structural deformities and are best described by differences in lipid density between the proximal and distal leaflets of the formed planar membrane.

4.4 Summary

This chapter continued the exploration of the physical properties of supported model membrane systems. It was demonstrated that SFVS is capable of measuring lipid population differences between leaflets of membranes formed using vesicle fusion. The leaflet containing the greatest number of lipids in these membranes was located on the proximal side of the membrane in relationship to the planar support as determined by exploiting the coherent nature of the SFVS technique. The amount of population asymmetry was correlated with the size of vesicles used to form the planar membranes when the packing density is constant and the pivotal plane radius of each leaflet is considered. This population asymmetry was inversely proportional to the size of the vesicle and approached a minimum at vesicles with radii of 100 nm. Using the previously defined kinetic mechanism of lipid flip-flop it was unexpected that the method of planar membrane formation through vesicle fusion resulted in a measureable amount of SFVS signal. However, through creating a fixed population difference between leaflets of a planar membrane by LB/LS deposition a thorough kinetic understanding of the persistence of this population asymmetry emerged. We found that the most likely explanation of planar membrane population asymmetry is due to the fact that lipid flip-flop is a coupled exchange between both leaflets of the membrane. This new understanding has broader implications in the field of cell biology in that lipids alone are unable to overcome population disparities that may arise due to differences in membrane morphology in the processes of cell budding and vesiculation. As important is the understanding that transport of a singular lipid between leaflets of a membrane may occur through a mediated mechanism via membrane proteins.

Two alternative analytical techniques were employed to examine the structural integrity of the membranes as an explanation of the observed SFVS results. The fluorescent images and electrochemical impedance results were consistent with the known literature and were not correlated to the measured SFVS signal for the investigated membranes. These results indicate that the SFVS results are due to the previously mentioned population disparity between leaflets of the formed planar membranes. The results of this study can not only be used to better understand cell membrane structure and function but also as a guideline in the preparation and formation of model membranes themselves. We allowed the vesicles in solution to fuse for an extended period of time above the investigated lipid phase transition temperature. Through the SFVS results it can be concluded that vesicles of greater size may give more uniform membranes in terms of equal lipid density between leaflets. However, more uniform membranes were created using sonicated vesicle solutions. The reported results demonstrate the sensitivity of SFVS to measure lipid population differences between leaflets of planar membranes that have previously escaped consideration and have provided a potentially missing link in our understanding of lipid dynamics by suggesting that the process of lipid flip-flop is a coupled exchange rather than unimolecular, which greatly impacts the foundations of cell membrane biology.

4.5 References

1. Reviakine, I.; Brisson, A., Formation of Supported Phospholipid Bilayers from Unilamellar Vesicles Investigated by Atomic Force Microscopy. *Langmuir* **2000,** *16* , 1806-1815.

2. Jackman, J. A.; Kim, M. C.; Zhdanov, V. P.; Cho, N.-J., Relationship Between Vesicle Size and Steric Hindrance Influences Vesicle Rupture on Solid Supports. *Phys.*

Chem. Chem. Phys. **2016,** *18* , 3065-3072.

3. Reimhult, E.; Hoeoek, F.; Kasemo, B., Intact Vesicle Adsorption and Supported Biomembrane Formation from Vesicles in Solution: Influence of Surface Chemistry, Vesicle Size, Temperature, and Osmotic Pressure. *Langmuir* **2003,** *19* , 1681-1691.

4. Koller, D.; Lohner, K., The Role of Spontaneous Lipid Curvature in the Interaction of Interfacially Active Peptides With Membranes. *Biochim. Biophys. Acta, Biomembr.* **2014,** *1838* , 2250-2259.

5. Chen, Z.; Rand, R. P., The Influence of Cholesterol on Phospholipid Membrane Curvature and Bending Elasticity. *Biophys. J.* **1997,** *73* , 267-276.

6. Zimmerberg, J.; Kozlov, M. M., How Proteins Produce Cellular Membrane Curvature. *Nat. Rev. Mol. Cell Biol.* **2006,** *7* , 9-19.

7. Edwards, K. A.; Baeumner, A. J., Analysis of Liposomes. *Talanta* **2006,** *68* (5), 1432-1441.

8. Jesorka, A.; Orwar, O., Liposomes: Technologies and Analytical Applications. *Ann. Rev. Anal. Chem.* **2008,** *1* (1), 801-832.

9. Tanaka, M.; Sackmann, E., Polymer-Supported Membranes as Models of the Cell Surface. *Nature (London, U. K.)* **2005,** *437* , 656-663.

10. Castellana, E. T.; Cremer, P. S., Solid Supported Lipid Bilayers: From Biophysical Studies to Sensor Design. *Surf. Sci. Rep.* **2006,** *61* , 429-444.

11. Nollert, P.; Kiefer, H.; Jaehnig, F., Lipid Vesicle Adsorption Versus Formation of Planar Bilayers on Solid Surfaces. *Biophys. J.* **1995,** *69* , 1447-55.

12. Keller, C. A.; Kasemo, B., Surface Specific Kinetics of Lipid Vesicle Adsorption Measured with a Quartz Crystal Microbalance. *Biophys. J.* **1998,** *75* , 1397-1402.

13. Jass, J.; Tjärnhage, T.; Puu, G., From Liposomes to Supported, Planar Bilayer Structures on Hydrophilic and Hydrophobic Surfaces: An Atomic Force Microscopy Study. *Biophys. J.* **2000,** *79* (6), 3153-3163.

14. Jing, Y.; Trefna, H.; Persson, M.; Kasemo, B.; Svedhem, S., Formation of Supported Lipid Bilayers on Silica: Relation to Lipid Phase Transition Temperature and Liposome Size. *Soft Matter* **2014,** *10* , 187-195.

15. Hamai, C.; Yang, T.; Kataoka, S.; Cremer, P. S.; Musser, S. M., Effect of Average Phospholipid Curvature on Supported Bilayer Formation on Glass by Vesicle Fusion. *Biophys. J.* **2006,** *90* , 1241-1248.

16. Hamai, C.; Cremer, P. S.; Musser, S. M., Single Giant Vesicle Rupture Events Reveal Multiple Mechanisms of Glass-Supported Bilayer Formation. *Biophys. J.* **2007,** *92* , 1988-1999.

17. Anderson, T. H.; Min, Y.; Weirich, K. L.; Zeng, H.; Fygenson, D.; Israelachvili, J. N., Formation of Supported Bilayers on Silica Substrates. *Langmuir* **2009,** *25* , 6997-7005.

18. Liu, J.; Conboy, J. C., Asymmetric Distribution of Lipids in a Phase Segregated Phospholipid Bilayer Observed by Sum-Frequency Vibrational Spectroscopy. *J. Phys. Chem. C* **2007,** *111* , 8988-8999.

19. Guyot-Sionnest, P.; Hunt, J. H.; Shen, Y. R., Sum-Frequency Vibrational Spectroscopy of a Langmuir Film: Study of Molecular Orientation of a Two-Dimensional System. *Phys. Rev. Lett.* **1987,** *59* , 1597-600.

20. Shen, Y. R., Surface Properties Probed by Second-Harmonic and Sum-Frequency Generation. *Nature (London)* **1989,** *337* , 519-25.

21. Shen, Y. R., Basic Theory of Surface Sum-Frequency Generation. *J. Phys. Chem. C* **2012,** *116* , 15505-15509.

22. Johnson, C. M.; Baldelli, S., Vibrational Sum Frequency Spectroscopy Studies of the Influence of Solutes and Phospholipids at Vapor/Water Interfaces Relevant to Biological and Environmental Systems. *Chem. Rev.* **2014,** *114* (17), 8416-8446.

23. Liu, J.; Conboy, J. C., Phase Behavior of Planar Supported Lipid Membranes Composed of Cholesterol and 1,2-distearoyl-sn-glycerol-3-phosphocholine Examined by Sum-Frequency Vibrational Spectroscopy. *Vib. Spectrosc.* **2009,** *50* , 106-115.

24. Brown, K. L.; Conboy, J. C., Electrostatic Induction of Lipid Asymmetry. *J. Am. Chem. Soc.* **2011,** *133* , 8794-8797.

25. Allhusen, J. S.; Conboy, J. C., Preparation and Characterization of Conductive and Transparent Ruthenium Dioxide Sol–Gel Films. *ACS Applied Mater. Interfaces* **2013,** *5* (22), 11683-11691.

26. Peterson, E. M.; Manhart, M. W.; Harris, J. M., Single-Molecule Fluorescence Imaging of Interfacial DNA Hybridization Kinetics at Selective Capture Surfaces. *Anal. Chem.* **2016,** *88* (2), 1345-1354.

27. Schneider, C. A.; Rasband, W. S.; Eliceiri, K. W., NIH Image to ImageJ: 25 years of Image Analysis. *Nat. Meth.* **2012,** *9* (7), 671-675.

28. Peterson, E. M.; Harris, J. M., Quantitative Detection of Single Molecules in Fluorescence Microscopy Images. *Anal. Chem. (Washington, DC, U. S.)* **2010,** *82* , 189-

196.

29. Marsh, D., Lateral Pressure in Membranes. *Biochim. Biophys. Acta, Rev. Biomembr.* **1996,** *1286* , 183-223.

30. Anglin, T. C.; Cooper, M. P.; Li, H.; Chandler, K.; Conboy, J. C., Free Energy and Entropy of Activation for Phospholipid Flip-Flop in Planar Supported Lipid Bilayers. *J. Phys. Chem. B* **2010,** *114* , 1903-1914.

31. Liu, J.; Brown, K. L.; Conboy, J. C., The effect of Cholesterol on the Intrinsic Rate of Lipid Flip-Flop as Measured by Sum-Frequency Vibrational Spectroscopy. *Faraday Discuss.* **2013,** *161* , 45-61.

32. Liu, J.; Conboy, J. C., Structure of a Gel Phase Lipid Bilayer Prepared by the Langmuir-Blodgett/Langmuir-Schaefer Method Characterized by Sum-Frequency Vibrational Spectroscopy. *Langmuir* **2005,** *21* , 9091-9097.

33. Allhusen, J. S.; Kimball, D. R.; Conboy, J. C., Structural Origins of Cholesterol Accelerated Lipid Flip-Flop Studied by Sum-Frequency Vibrational Spectroscopy. *The J. Phys. Chem. B* **2016,** *120* (12), 3157-3168.

34. Liu, J.; Conboy, J. C., Phase Transition of a Single Lipid Bilayer Measured by Sum-Frequency Vibrational Spectroscopy. *J. Am. Chem. Soc.* **2004,** *126* , 8894-8895.

35. Liu, J.; Conboy, J. C., Direct Measurement of the Transbilayer Movement of Phospholipids by Sum-Frequency Vibrational Spectroscopy. *J. Am. Chem. Soc.* **2004,** *126* , 8376-8377.

36. Lambert, A. G.; Davies, P. B.; Neivandt, D. J., Implementing the Theory of Sum Frequency Generation Vibrational Spectroscopy: A Tutorial Review. *Appl. Spectrosc. Rev.* **2005,** *40* , 103-145.

37. Leikin, S.; Kozlov, M. M.; Fuller, N. L.; Rand, R. P., Measured Effects of Diacylglycerol on Structural and Elastic Properties of Phospholipid Membranes. *Biophys. J.* **1996,** *71* , 2623-2632.

38. Wang, X.; Deserno, M., Determining the Pivotal Plane of Fluid Lipid Membranes in Simulations. *J. Chem. Phys.* **2015,** *143* (16), 164109.

39. Fuller, N.; Rand, R. P., The Influence of Lysolipids on the Spontaneous Curvature and Bending Elasticity of Phospholipid Membranes. *Biophys. J.* **2001,** *81* , 243-254.

40. Rand, R. P.; Fuller, N. L.; Gruner, S. M.; Parsegian, V. A., Membrane Curvature, Lipid Segregation, and Structural Transitions for Phospholipids Under Dual-Solvent Stress. *Biochemistry* **1990,** *29* , 76-87.

41. Deserno, M., Fluid Lipid Membranes: From Differential Geometry to Curvature Stresses. *Chem. Phys. Lipids* **2015,** *185*, 11-45.

42. Lewis, B. A.; Engelman, D. M., Lipid Bilayer Thickness Varies Linearly with Acyl Chain Length in Fluid Phosphatidylcholine Vesicles. *J. Mol. Biol.* **1983,** *166* , 211-17.

43. McConnell, H. M.; Kornberg, R. D., Inside-Outside Transitions of Phospholipids in Vesicle Membranes. *Biochemistry* **1971,** *10* , 1111-20.

44. Liu, J.; Conboy, J. C., 1,2-Diacyl-phosphatidylcholine Flip-Flop Measured Directly by Sum-Frequency Vibrational Spectroscopy. *Biophys. J.* **2005,** *89* , 2522-2532.

45. Eyring, H.; Lin, S. H.; Lin, S. M., *Basic Chemical Kinetics*. John Wiley & Sons, Inc.: 1980.

46. Heimburg, T., The Capacitance and Electromechanical Coupling of Lipid Membranes Close to Transitions: The Effect of Electrostriction. *Biophys. J.* **2012,** *103* , 918-929.

47. Briand, E.; Zaech, M.; Svedhem, S.; Kasemo, B.; Petronis, S., Combined QCM-D and EIS Study of Supported Lipid Bilayer Formation and Interaction with Pore-Forming Peptides. *Analyst (Cambridge, U. K.)* **2010,** *135* , 343-350.

48. Jeuken, L. J. C.; Connell, S. D.; Nurnabi, M.; O'Reilly, J.; Henderson, P. J. F.; Evans, S. D.; Bushby, R. J., Direct Electrochemical Interaction Between a Modified Gold Electrode and a Bacterial Membrane Extract. *Langmuir* **2005,** *21* (4), 1481-1488.

49. Naumowicz, M.; Petelska, A. D.; Figaszewski, Z. A., Capacitance and Resistance of the Bilayer Lipid Membrane Formed of Phosphatidylcholine and Cholesterol. *Cell. Mol. Biol. Lett.* **2003,** *8* , 5-18.

50. Nikolov, V.; Lin, J.; Merzlyakov, M.; Hristova, K.; Searson, P. C., Electrical Measurements of Bilayer Membranes Formed by Langmuir-Blodgett Deposition on Single-Crystal Silicon. *Langmuir* **2007,** *23* , 13040-13045.

51. Steinem, C.; Janshoff, A.; Ulrich, W.-P.; Sieber, M.; Galla, H.-J., Impedance Analysis of Supported Lipid Bilayer Membranes: A Scrutiny of Different Preparation Techniques. *Biochim. Biophys. Acta, Biomembr.* **1996,** *1279* , 169-80.

52. Lin, J.; Merzlyakov, M.; Hristova, K.; Searson, P. C., Impedance Spectroscopy of Bilayer Membranes on Single Crystal Silicon. *Biointerphases* **2008,** *3* , FA33-FA40.

53. Coster, H. G. L.; Chilcott, T. C.; Coster, A. C. F., Impedance Spectroscopy of Interfaces, Membranes and Ultrastructures. *Bioelectrochem. Bioenerg.* **1996,** *40* , 79-98.

54. Hanai, T.; Haydon, D. A.; Taylor, J., An Investigation by Electrical Methods of Lecithin-in-Hydrocarbon Films in Aqueous Solutions. *Proc. R. Soc. London, Ser. A* **1964,** *281* , 377-91.

55. White, S. H., Formation of "Solvent-Free" Black Lipid Bilayer Membranes from Glyceryl Monooleate Dispersed in Squalene. *Biophys. J.* **1978,** *23* , 337-47.

CHAPTER 5

CONCLUSION

In this dissertation the physical properties of planar supported membrane models were investigated with SFVS. SFVS is a coherent nonlinear optical technique that is highly sensitive to anisotropic solutions or interfaces due to its symmetry constraints. These characteristics of SFVS make it uniquely suited to study changes in planar membrane leaflet symmetry. In Chapter 2 the relevant aspects of SFVS theory were described that enable the study of planar membrane models. SFVS was implemented to study the differences in chemical structure of cholesterol, cholestanol, and cholestene and the resulting effects on the kinetics and thermodynamics of DSPC flip-flop. From these investigations, it was found that the lack of a double bonded sterol ring in cholestanol and the lack of a hydroxyl group in cholestene resulted in lowering the thermodynamic free energy by decreasing the energy needed to expand or compress a membrane. Specifically, incorporation of cholestene and cholestanol had a greater impact on the $\Delta G^{\ddagger}$ for DSPC flip-flop across the studied concentration range than cholesterol at the exact same concentrations. These were the first reported results that correlated the molar elastic compression modulus with the process of lipid flip-flop. The results from this investigation sparked further analysis of the physical properties of planar supported membranes.

In Chapter 3 a novel synthesis method was described for creating conductive metal oxide thin films to investigate the electrochemical properties of planar membrane systems. Metal oxide films are more advantageous than pure metal films for membrane analysis as native lipid structures can be used without modification to create model bilayers. The conductive properties of RuO_2 make it an appealing material for use as a thin conductive oxide film. The sol-gel synthesis procedure was used to create thin conductive films of RuO_2 interspersed in a matrix of SiO_2. This method allows for easily tunable conductive and optical properties simply by varying the solution and deposition parameters. Thorough characterization of the films was conducted using UV-Vis, FTIR, XPS, AFM, and cyclic voltammetry. The distinctive properties of these new materials were demonstrated in the spectroelectrochemical analysis of the reduction and oxidation of ferrocene methanol in aqueous electrolyte. The qualities of these materials lent themselves to be appealing substrates for further analysis of model membrane physical properties.

Chapter 4 described further investigation of model membrane systems with the particular focus of interrogating the mechanism of membrane formation via vesicle fusion. SFVS is capable of discerning minute differences in lipid population between leaflets. This sophisticated ability was used to measure the amount of asymmetry remaining in membranes formed via vesicle fusion. Sonicated and extruded vesicles of 30, 50, 100 and 200 nm were used to make membranes on fused silica supports. Through SFVS measurements it was discovered that the population difference between leaflets of vesicles in solution remains in the formed planar membranes, that the proximal leaflet contains the greater lipid population and that this population offset remains even after the

system is allowed to symmetrically mix through lipid flip-flop. Complementary techniques of epifluorescence microscopy and electrochemical impedance spectroscopy were implemented to investigate the structural integrity of membranes formed from vesicle fusion and found that the membranes were uniform over the deposited area and the capacitance values for the membranes matched the acceptable range of planar supported membranes for vesicles of all sizes. This chapter characterized the differences in membrane asymmetry from vesicles in solution and demonstrated the ability of RuO_2 thin conductive electrodes to be used with phospholipid bilayers.

The studies presented in this dissertation implemented a wide variety of analytical techniques and methods for the study of model phospholipid membranes. SFVS was specifically used to investigate the physical structure between leaflets of the membrane in conjunction with more classical techniques such as electrochemistry. Implementation of SFVS to study model membranes resulted in new experimentally determined pathways of lipid flip-flop and a more comprehensive understanding of the mechanism of vesicle fused bilayers. The studies in this dissertation clearly demonstrate the superior ability of SFVS to investigate biological interfaces and model lipid membranes.